

ESTIMATING AND MITIGATING INDOOR AIRBORNE PATHOGENS TO
SUPPORT HEALTHY BUILDINGS

by

HOOMAN PARHIZKAR

A DISSERTATION

Presented to the Department of Architecture
and the Division of Graduate Studies of the University of Oregon
in partial fulfillment of the requirements
for the degree of
Doctor of Philosophy

March 2022

DISSERTATION APPROVAL PAGE

Student: Hooman Parhizkar

Title: Estimating and Mitigating Indoor Airborne Pathogens to Support Healthy Buildings

This dissertation has been accepted and approved in partial fulfillment of the requirements for the Doctor of Philosophy degree in the Department of Architecture by:

Kevin G. Van Den Wymelenberg, PhD	Chairperson
Siobhan Rockcastle, PhD	Core Member
Mark Fretz, DDS	Core Member
Richard L. Corsi, PhD, PE	Core Member
Carl Brozek, PhD	Institutional Representative

and

Krista Chronister, PhD	Vice Provost for Graduate Studies
------------------------	-----------------------------------

Original approval signatures are on file with the University of Oregon Division of Graduate Studies.

Degree awarded March 2022

© 2022 Hooman Parhizkar

DISSERTATION ABSTRACT

Hooman Parhizkar

Doctor of Philosophy

Department of Architecture

March 2022

Title: Estimating and Mitigating Indoor Airborne Pathogens to Support Healthy Buildings

The global pandemic has caused myriad damages to the lives of millions of people worldwide. Several studies confirm that indoor spaces are the main hotspots of COVID-19 outbreaks resulting in multiple confirmed instances of human-to-human transmission. Therefore, quantifying the impact of indoor environments and human activities on the transmission of infectious disease is key to stopping the spread of COVID-19 and prepare for future outbreaks. This dissertation is a multidisciplinary collaboration between designers, engineering, biologists, and public health experts to answer a question: “what is the airborne viral exposure risk indoors and how can building design and operations help to effectively reduce the risk of disease transmission indoors during the COVID-19 pandemic?”

We aimed to answer these questions through following the projects:

Chapter.II. A quantitative aerosol risk estimation platform.

Chapter.III. Environmental mitigation of aerosol viral load.

Chapter.IV. Respiratory exposure at alternate distances.

In Chapter.II, we describe a quantitative aerosol risk estimation platform that is more mechanistic in nature than traditional risk estimates for airborne infectious disease.

It enables the inclusion of aerosol size distributions and emissions from infected individuals with several predefined assumptions.

In Chapter.III we provide the first real-world evidence that building related interventions described in Chapter.II significantly impact the dispersion and abundance of SARS-CoV-2 virus in the presence of individuals who were diagnosed with COVID-19. We also provide novel insights about the relationships of human and environmental viral loads (aerosols and surfaces) in near and far fields.

In Chapter.IV, we describe a novel gas-tracing technique to quantify the degree of exposure to bioaerosols at alternate distances. Here we provide quantitative data to better explain the application of the well-mixed room assumption as well as insights about the distance from emitter variable that underly aerosol risk exposure estimates.

In this dissertation, we conclude that buildings have a substantial impact on the risk of COVID-19 transmission. We offer an estimation platform for better understanding the risk of infection transmission indoors and provide proof that environmental mitigation strategies substantially reduce the viral load in a controlled study with infected participants.

This dissertation includes both previously published/unpublished and co-authored material.

CURRICULUM VITAE

NAME OF AUTHOR: Hooman Parhizkar

GRADUATE AND UNDERGRADUATE SCHOOLS ATTENDED:

University of Oregon, Eugene
Shahid Beheshti University, Tehran
University of Kashan, Kashan

DEGREES AWARDED:

Doctor of Architecture, 2022, University of Oregon
Master of Science, Architectural Technology, 2018, Shahid Beheshti University
Bachelor's degree, Architectural Engineering, 2015, University of Kashan

AREAS OF SPECIAL INTEREST:

Healthy Buildings
Viral Transmission of SARS-CoV-2 in Indoor Spaces
Environmental Mitigation Strategies
Aerosol Disease Transmission Risk Analysis
Bioaerosol Sampling

PROFESSIONAL EXPERIENCE:

Research assistant, Institute for Health in the Built Environment, University
Oregon, Eugene, 2019-2022

Teaching assistant, Department of Architecture, University of Oregon, Eugene,
2018-2021

GRANTS, AWARDS, AND HONORS:

Pacific Northwest Center for Translational Environmental Health Research
Award, Missing Links in Characterization of Viral Aerosols and Indoor
Transmission Risks, Oregon State University, 2021

University of Oregon 2021 Innovation Award (IHBE group award), COVID-19
response and mitigation, University of Oregon, 2021

Miller Hull Scholarship, University of Oregon, 2021

Nascence and UO Hong Kong Alumni Scholarship in the Department of
Architecture, University of Oregon, 2021

Wm H Stenhjem Jr Scholarship, University of Oregon, 2020

PUBLICATIONS:

Parhizkar H, Dietz L, Olsen-Martinez A, Horve PH, Barnatan L, Northcutt D, Van Den Wymelenberg KG. Quantifying environmental mitigation of aerosol viral load in a controlled chamber with participants diagnosed with COVID-19. *Clin Infect Dis* **2022**; Available at: <https://academic.oup.com/cid/advance-article/doi/10.1093/cid/ciac006/6498295>.

Parhizkar H, Van Den Wymelenberg KG, Haas CN, Corsi RL. A quantitative risk estimation platform for indoor aerosol transmission of COVID-19. *Risk Anal* **2021**; Available at: <http://dx.doi.org/10.1111/risa.13844>.

Horve P, Dietz L, Bowles G, MacCrone G, Olsen-Martinez A, Northcutt D, Moore V, Barnatan L, Parhizkar H, Van Den Wymelenberg KG. Longitudinal analysis of built environment and aerosol contamination associated with isolated COVID-19 positive individuals. 2021; Available at: https://assets.researchsquare.com/files/rs-861942/v1_covered.pdf?c=1630438371.

Parhizkar H, Stenson J, Fretz M, Laguerre A, Gall E, Corsi RL, Van Den Wymelenberg KG. A novel VOC tracer method to evaluate the degree of respiratory exposures at alternate distances. Link to preprint: <https://doi.org/10.21203/rs.3.rs-1437107/v2>. Submitted to *Building and Environment* **2022**.

Parhizkar H, Khoraskani RA, Tahbaz M. Double skin façade with Azolla; ventilation, Indoor Air Quality and Thermal Performance Assessment. *Journal of Cleaner Production* **2020**, 249(119313), 119313.

Parhizkar H, Elzeyadi I. (2020), Investigating the Impact of Plant Phytoremediation on Indoor Air Quality in Work Environments: A Meta-Analysis. *ASHRAE Winter Conference* V 126; February 2020 Orlando (FL)

Parhizkar, H., Khoraskani, R. A. Green façade system for indoor air purification. *Advanced Building Skins Conference*; October 2017 Bern, Switzerland

ACKNOWLEDGMENTS

I wish to express my sincere appreciation to Professor Kevin G. Van Den Wymelenberg for his infinite support during all the stages of my PhD study and beyond. I also thank my committee members Dr. Siobhan Rockcastle, Dr. Carl Brozek, Dr. Mark Fretz, and Dr. Richard L. Corsi for their generous support. I wish to kindly thank Dr. Laura Jacek for all her efforts in making our projects happen successfully. In addition, special thanks is due to Dr. Charles N. Haas for his input and co-authorship on the publication described in Chapter II. I wish to thank all colleagues from Biology and the Built Environment Center at the University of Oregon including Leslie Dietz, Andreas Olsen Martinez, Patrick Horve, Dale Northcutt, and Liliana Barnatan for their contributions as co-authors in publication described in Chapter III. Furthermore, I thank Garis Bowles, Georgia MacCrone, Jackson Mestler, Dan Richards, and Vincent Moore for their contribution in data collection for publication described in Chapter III. In addition, I would like to thank Dr. Elliott Gall, Aurélie Laguerre, and Jason Stenson for their contribution in conducting the pilot project and the publication described in Chapter IV. I wish to thank countless individuals at the University of Oregon for helping make this research design possible, including our participants who spent their times during a challenging time of COVID-19 infections. I would like to thank Thermo Fisher Scientific for funding our project described in Chapter III with award number 4133V. Moreover, I also thank Pacific Northwest Center for Translational Environmental Health Research at Oregon State University for funding Chapter IV under grant number P30ES030287. I would like to thank Mira Zimmerman and Shape Diver Co. for their contribution to launching Safeairspace.com aerosol risk estimation platform.

For my parents Hamid & Shahrzad and my sister Parastoo, who taught me the value of
love

TABLE OF CONTENTS

Chapter	Page
I. INTRODUCTION	1
I.1. History of Pandemics	1
I.2. Infectious Disease and Transmission Routes	4
I.3. Buildings in Support of Health and Vectors for Disease Transmission	5
I.3.1. Buildings Are the Main Hotspots for COVID-19 Transmission	6
I.3.1.2. Environmental Surveillance of Pathogens.....	7
I.3.2. Buildings Can Mitigate the Exposure to Infectious Disease.....	8
I.3.2.1. Ventilation.....	8
I.3.2.2. Filtration.....	9
I.3.2.3. Environmental Factors and other treatments.....	10
I.4. Aims and Scope	11
I.4.1. A Radical Multidisciplinary Collaboration Work	12
I.4.2. The Structure of Dissertation.....	12
I.4.2.1. Summary of A Quantitative Aerosol Risk Estimation Platform	13
I.4.2.2. Summary of Environmental Mitigation of Aerosol Viral Load.....	15
I.4.2.3. Respiratory Exposure at Alternate Distances.....	19
I.4.2.4. Using Disease Transmission Risk as the Guide for Evidence-Based Design.....	21
II. A QUANTIATIVE AEROSOL RISK ESTIMATION PLATFORM	23
II.1. Introduction	23
II.2. Methodology	25
II.2.1. Time-Dependent Particle Number Concentrations	25
II.2.2. Deposition of Particles in the Respiratory System.....	28
II.2.3. Using Guangzhou Restaurant Outbreak to Anchor the Model to an Existing Dose-Response Relationship	30
II.3. Application of the Model to Four Covid-19 Outbreaks	35
II.3.1. Case 1. Bus Riders in Eastern China	35
II.3.2. Case 2. Two Choir Rehearsals in Skagit Valley	36
II.3.3. Case 3. A 10-Hour Flight from London to Hanoi	39
II.3.4. Case 4. Transmission of SARS-CoV-2 by Direct Airflow in a Restaurant in South Korea	42
II.4. Conclusion	44
II.5. Bridge	46
III. ENVIRONMENTAL MITIGATION OF AEROSOL VIRAL LOAD	47
III.1. Introduction	48

Chapter	Page
III.2. Methodology	49
III.3. Results	52
III.3.1. Near and Far Field Aerosol Samples and Paired Human Specimens.....	52
III.3.2. High-Touch Surfaces, Settling Plates, and Paired Human Specimens	55
III.3.3. High Expiratory Activity, Particles, and Aerosol Viral Load	56
III.3.4. The Impact of Ventilation and Filtration on Aerosol and Surface Viral Load	57
III.3.5. Relative Humidity and Aerosol Viral Load.....	61
III.4. Conclusion and Limitations	62
III.5. Bridge	64
IV. RESPIRATORY EXPOSURE AT ALTERNATE DISTANCES	67
IV.1. Introduction.....	68
IV.2. Methodology	69
IV.2.1. Methodology background.....	69
IV.2.2. Participant Recruitment.....	70
IV.2.3. Climate Chamber	70
IV.2.4. Statistical Analyses.....	74
IV.3. Results	74
IV.3.1. Data Normalization	74
IV.4. Discussion	78
IV.5. Conclusion and Limitations	80
IV.6. Bridge	81
V. USING DISEASE TRANSMISSION RISK AS THE GUIDE FOR EVIDENCE-BASED DESIGN	83
V.1. Case Study Simulation.....	83
V.1.1. Simulation Parameters	84
V.1.1.1. Natural Ventilation.....	85
V.1.1.2. Indoor Humidification	85
V.2. Results	86
V.2.1. The Impact of Window Design on the Risk of COVID-19 Infection	86
V.2.2. The Impact of Outdoor Climate on the Risk of Infection in 2 Sites.....	87
V.3. Future Outlook	89
VI. CONCLUSION.....	91
VI.1. Moving Forward	94

Chapter	Page
APPENDIX A	96
APPENDIX B	106
APPENDIX C	107
APPENDIX D	112
APPENDIX E.....	113
REFERENCE CITED	117

LIST OF FIGURES

Figure	Page
FIGURE I.1. ST. LOUIS RED CROSS MOTOR CORPS PERSONNEL IN PREPARATION FOR HOLDING VICTIMS OF INFLUENZA PANDEMIC, COURTESY OF THE WASHINGTON POST[16].	3
FIGURE I.2. SCHEMATIC STRUCTURE OF CHAPTERS.....	13
FIGURE II.1. ARRANGEMENT OF RESTAURANT TABLES AND AIR CONDITIONING AIRFLOW AT SITE OF OUTBREAK OF 2019 NOVEL CORONAVIRUS DISEASE, GUANGZHOU, CHINA, 2020, FOLLOWING[43]	32
FIGURE II.2. TOTAL PARTICLE CONCENTRATION IN RESTAURANT ZONE DURING TIME INFECTOR IS IN THE SPACE.	33
FIGURE II.3. PARTICLE CONCENTRATIONS FOR OUTBREAK ON A 10-HOUR FLIGHT.	40
FIGURE II.4. SEATING LOCATION OF PASSENGERS ON VIETNAM AIRLINES FLIGHT 54 FROM LONDON, UK, TO HANOI, VIETNAM, ON MARCH 2, 2020 FOLLOWING [49].....	41
FIGURE II.5. (A) SCHEMATIC FLOOR PLAN OF THE SOUTH KOREA OUTBREAK RESTAURANT, FOLLOWING[44], AND (B) ESTIMATED PARTICLE CONCENTRATIONS ASSUMING WELL-MIXED CONDITIONS.....	43
FIGURE III.1. RAPID DEPLOYMENT MODULAR UNIT (RDM), A) HIGHER EXPIRATORY TRIALS (S1), B) REGULAR TRIALS (S2)	50
FIGURE III.2. A) THE CORRELATION OF NEAR FIELD (1.2 M) OR FAR FIELD (3.5 M) AEROSOL VIRAL LOADS (RNA) WITH CORRESPONDING HUMAN NASAL SAMPLES DURING ROUTINE TRIALS B) COMPARISON OF NEAR FIELD AND FAR FIELD AEROSOL VIRAL LOADS FOR ROUTINE TRIALS, C) COMPARISON OF MEAN CO ₂ CONCENTRATIONS IN THE NEAR FIELD AND FAR FIELD FOR ROUTINE TRIALS, D) PAIRED T-TESTS FOR ALL PARTICLE SIZE BINS AT NEAR FIELD AND FAR FIELD FOR ROUTINE TRIALS, E) CORRELATION BETWEEN MEAN FAR FIELD AEROSOL VIAL LOADS AND THE CORRESPONDING MEAN CONCENTRATION OF FAR FIELD PARTICLES FOR ROUTINE TRIALS.	53
FIGURE III.3. A) VIRAL LOAD (RNA) ON EACH HIGH-TOUCH SURFACE RELATIVE TO PAIRED NASAL SAMPLES, B) VIRAL LOAD (RNA) ON SETTLING PLATES AT NEAR AND FAR FIELD RELATIVE TO PAIRED NASAL SAMPLES, C) THE CORRELATION OF EACH SAMPLE TYPE (AEROSOL, HIGH TOUCHED SURFACES, AND SETTLING PLATES) TO PAIRED NASAL SAMPLE.....	56
FIGURE III.4. LINEAR CORRELATION BETWEEN C _T VALUE AND PARTICLES FOR A) 0.3-1 μM PARTICLES, B) 1-2.5 μM PARTICLES, C) 2.5-3 μM PARTICLES, D) 3-5 μM PARTICLES, E) 5-10 μM PARTICLES, AND F) 10-25 μM PARTICLES.	58
FIGURE III.5. THE IMPACT OF VENTILATION AND FILTRATION ON C _T VALUE OF AEROSOL SAMPLES, A) MATCH PAIRED COMPARISON BETWEEN TRIALS WITH REMOVAL MECHANISM TRIALS (FILTRATION AND VENTILATION) AND CONTROL TRIALS WITH ~0 ACH, B) LINEAR CORRELATION BETWEEN AEROSOL C _T VALUE AND PAIRED MEAN CO ₂ CONCENTRATION AFFECTED BY ONLY VENTILATION (SAME PHYSICAL ACTIVITIES), C) COMPARISON OF AEROSOL C _T FOR VENTILATION TRIALS OF UNDER ~4.5 ACH AND ABOVE ~9 ACH IN NEAR FIELD AND FAR FIELD, D) MATCH PAIRED COMPARISON OF AEROSOL C _T FOR TRIALS WITH IN-ROOM HEPA FILTRATION AND CORRESPONDING CONTROL TRIALS WITH ~0 ACH.	60
FIGURE III.6. A) CORRELATION BETWEEN AEROSOL C _T VALUE AND MEAN RELATIVE HUMIDITY AMONG DEHUMIDIFICATION, HUMIDIFICATION, AND CONTROL TRIALS B) PAIRED COMPARISON OF AEROSOL C _T BETWEEN DEHUMIDIFICATION AND HUMIDIFICATION TRIALS, C) CORRELATION BETWEEN SURFACE C _T VALUE AND MEAN RELATIVE HUMIDITY AMONG DEHUMIDIFICATION, HUMIDIFICATION, AND CONTROL TRIALS, D)) PAIRED COMPARISON OF SELECT SURFACE (COMPUTER) C _T BETWEEN DEHUMIDIFICATION AND HUMIDIFICATION TRIALS.....	63
FIGURE IV.1. EXPERIMENTAL SETUP, A) CLIMATE CHAMBER, AIRFLOW DISTRIBUTION, AS WELL AS SAMPLING LOCATION FOR EACH UNIQUE TRIAL (MODELED IN RHINOCEROS SOFTWARE), B) EXPERIMENTAL PROCEDURE AND THE NUMBER OF BREATH MINTS CONSUMED BY THE PARTICIPANT FOR EACH TRIAL.	72
FIGURE IV.2. A) CONCENTRATION OF THREE TARGET TRACER COMPOUNDS (MENTHOL, MENTHONE, AND MONOTERPENES) IN THE HEADSPACE OF A 250 mL GLASS CHAMBER AS A FUNCTION THE TIME WHEN A BREATH MINT IS PLACED INSIDE, B) CONCENTRATION OF THE THREE TARGET COMPOUNDS WHEN THE PARTICIPANT EXHALED THEIR BREATH ONCE INTO THE 250 mL CHAMBER WHILE CONSUMING THE BREATH MINT.	76
FIGURE IV.3. COMPARISON OF 2.5, 5, AND 7.5FT TRIALS NORMALIZED BY VOLUME INTEGRATED BACKGROUND.	77
FIGURE V.1. SIMULATION WORKFLOW (ENERGY AND SIMULATION FIGURES ARE COURTESY OF LADYBUG TOOLS[187])	84
FIGURE V.2. THE IMPACT OF NATURAL VENTILATION ON RISK OF COVID-19 INFECTION; A) OUTDOOR AIR EXCHANGE LEVELS FOR DIFFERENT WINDOW CONFIGURATIONS IN A SINGLE DAY OF SUMMER MONTHS AND B) RISK OF INFECTION FOR DIFFERENT WINDOW CONFIGURATIONS IN A SINGLE DAY OF SUMMER.....	88
FIGURE V.3. THE IMPACT OF RELATIVE HUMIDITY ON RISK OF COVID-19 INFECTION; A) RELATIVE HUMIDITY LEVELS ASSOCIATED WITH LOCATION’S CLIMATE DURING WINTERTIME AND B) RISK OF INFECTION FOR THE CITY OF EUGENE AND BOSTON. .	89

LIST OF TABLES

Table	Page
TABLE I.1. EXAMPLES OF WELL-DOCUMENTED COVID-19 SUPER SPREADING OUTBREAKS.	7
TABLE II.1. INPUT PARAMETERS FOR GUANGZHOU RESTAURANT X	31
TABLE II.2. INPUT PARAMETERS FOR BUS RIDERS IN EASTERN CHINA.....	36
TABLE II.3. INPUT PARAMETERS FOR SKAGIT VALLEY CHOIR OUTBREAK.....	37
TABLE II.4. INPUT PARAMETERS FOR OUTBREAK ON A 10-HOUR FLIGHT.	40
TABLE II.5. INPUT PARAMETERS FOR OUTBREAK IN A SOUTH KOREAN RESTAURANT.	44
TABLE III.1. STUDY PLAN FOR PARTICIPANTS THAT WERE DIAGNOSED WITH COVID-19; S1 AND S2 REFER TO EXPERIMENTAL SETUP 1 AND SETUP 2	51
TABLE IV.1. SUMMARY OF EXPERIMENT TRIALS	73
TABLE IV.2. COMPARISON OF THE FIRST AND LAST MINUTE OF BASELINE PERIOD FOR FIVE MAJOR COMPOUNDS (PAIRED T-TEST)	75

LIST OF SUPPLEMENTAL FIGURES

Figure	Page
SUPPLEMENTAL FIGURE III. 1. THE CORRELATION OF BOTH NEAR FIELD (1.2 M) AND FAR FIELD (3.5 M) AEROSOL VIRAL LOADS (RNA) WITH CORRESPONDING HUMAN NASAL SAMPLES DURING ROUTINE TRIALS.	96
SUPPLEMENTAL FIGURE III. 2. DIFFERENCE BETWEEN NUMBER OF PARTICLES OF DIFFERENCE SIZES (0.3 μM-25 μM) FOR ROUTINE TRIALS; A) 0.3 μM – 1 μM, B) 1 μM -2.5 μM, C) 2.5 μM -3 μM, D) 3 μM -5 μM, E) 5 μM -10 μM, F) 10 μM - 25 μM.	97
SUPPLEMENTAL FIGURE III. 3. CORRELATION BETWEEN AEROSOL PARTICLES OF DIFFERENCE SIZES (0.3-25) AND AVERAGE CO2 CONCENTRATION FOR ROUTINE TRIALS AT ~0 ACH; A) 0.3 μM -1 μM, B) 1 μM -2.5 μM, C) 2.5 μM -3 μM, D) 3 μM -5 μM, E) 5 μM -10 μM, F) 10 μM -25 μM.	98
SUPPLEMENTAL FIGURE III. 4. COMPARISON OF SURFACE VIRAL LOAD FOR THREE HIGH TOUCHED SURFACES.	99
SUPPLEMENTAL FIGURE III. 5. COMPARISON OF SURFACE VIRAL LOAD FOR SETTLING PLATES IN NEAR AND FAR FIELD.	99
SUPPLEMENTAL FIGURE III. 6. CORRELATION BETWEEN AEROSOL AND PAIRED NASAL VIAL LOAD FOR HIGHER EXPIRATORY RIALS.	100
SUPPLEMENTAL FIGURE III. 7. COMPARISON OF AEROSOL CT FOR SITTING-SPEAKING AND SITTING-QUIETLY TRIALS IN NEAR FIELD AND FAR FIELD.	101
SUPPLEMENTAL FIGURE III. 8. PHYSICAL ACTIVITY CORRELATIONS, A) PAIRED CT VALUES AND CORRESPONDING AVERAGE CONCENTRATION AFFECTED BY ONLY PHYSICAL ACTIVITY (~0 ACH), B) AVERAGE CO2 OF DIFFERENT PHYSICAL ACTIVITIES.	102
SUPPLEMENTAL FIGURE III. 9. COMPARISON OF AEROSOL CT FOR VENTILATION TRIALS OF UNDER ~4.5 ACH AND ABOVE ~9 ACH IN NEAR FIELD AND FAR FIELD.	103
SUPPLEMENTAL FIGURE III. 10. THE IMPACT OF REMOVAL MECHANISM ON HIGH TOUCHED SURFACE VIRAL LOAD.	103
SUPPLEMENTAL FIGURE III. 11. NUMBER AND TYPE OF SAMPLES COLLECTED FOR EACH PARTICIPANT.	104
SUPPLEMENTAL FIGURE III. 12. NUMBER AND PROPORTION POSITIVE OF NASAL AND SALIVA SAMPLES.	104
SUPPLEMENTAL FIGURE IV. 1. EVALUATING THE IMPACT OF DISTANCE ON BIOAEROSOL EXPOSURE IN A TYPICAL INDOOR ENVIRONMENT.	113
SUPPLEMENTAL FIGURE IV. 2. COMPARISON OF THE CONCENTRATIONS OF BREATH TRACERS FOR EACH DISTANCE TO VOLUME INTEGRATED BACKGROUND WITH EXPANDED UNCERTAINTIES.	115

LIST OF SUPPLEMENTAL TABLES

Table	Page
SUPPLEMENTAL TABLE III. 1. DEMOGRAPHIC DATA OF THE STUDY PARTICIPANTS.	105
SUPPLEMENTAL TABLE III. 2. THE MEAN DIFFERENCE OF REMOVAL MECHANISM TRIALS AND THEIR PAIRED CONTROL TRIALS WITH ~ 0 ACH.	105
SUPPLEMENTAL TABLE IV. 1. EVALUATING THE IMPACT OF DISTANCE ON BIOAEROSOL EXPOSURE IN A TYPICAL INDOOR ENVIRONMENT.....	114
SUPPLEMENTAL TABLE IV. 2. COMPARISON OF SPATIAL PARAMETERS BETWEEN THE PRESENT AND THE CONTROLLED STUDY WITH PARTICIPANTS DIAGNOSED WITH COVID-19[159].	116
SUPPLEMENTAL TABLE IV. 3. COMPARISON OF NEAR- FIELD AND FAR-FIELD IN A RECENT CONTROLLED STUDY ON PARTICIPANTS THAT WERE DIAGNOSED WITH COVID-19.[159]	116

I. INTRODUCTION

Severe Acute Respiratory Syndrome Coronavirus 2 (SARS-CoV-2) is the causative agent of coronavirus disease 2019 (COVID-19) which has caused myriad damage to the lives of millions of people worldwide. As of February 1, 2022, there have been 373,229,380 confirmed cases of COVID-19, including 5,658,702 deaths, reported to the World Health Organization (WHO)[1]. COVID-19 has resulted in infection levels ranging from mild to severe degrees with symptoms commonly reported as fever, fatigue, and dry cough[2]. Several severe cases were associated with pulmonary and extrapulmonary manifestations that resulted in multiorgan failure and death[3,4]. A recent preprint has further characterized the severity of COVID-19 infection outside of respiratory tract and found that SARS-CoV-2 viral RNA copies were detected across the human body, including the brain, and persist for over seven months following symptoms onset, all of which provides more evidence that SARS-CoV-2 causes systemic infection in the human body[5].

I.1. History of Pandemics

Throughout history, the spread of infectious disease among people have caused endemics, epidemics, and pandemics with widespread illness and loss of life. According to the rate and scale of the spread, an endemic is defined by the continuous spread of an infectious pathogen on a regional scale during certain seasons of the year[6]. An epidemic describes a disease spread when its occurrence in a community is in excess of the usual rates[7]. In a pandemic, an outbreak is rapidly spread to different countries, causing widespread infections across populations at an international scale[8].

The “plague” or the “black death” pandemic is believed to have killed up to two thirds of Europe’s population between 1347 and 1351, recording the most devastating impact on human life, as compared with any other known pandemic or war[9]. The spread of Smallpox disease through variola virus with trade routes from 6th century resulted in more than 56 million deaths worldwide[10]. The last cases of Smallpox infection were reported between 1975-1977[10] in Merca, Somalia.

In 1918, a novel variant of influenza virus (H1N1) swept the globe and caused the most severe pandemic in recent history[11]. It is estimated that 500 million people (one-third of the world’s population) acquired infection, resulting in at least 50 million deaths worldwide (Figure I.1). Like SARS-CoV-2, there was no vaccine or antibiotics to treat secondary infections for H1N1 virus, hence- control efforts were limited to non-pharmaceutical interventions such as isolation, quarantine, personal hygiene, disinfections, and limitations of indoor congregations[11].

Public health interventions, antibodies and vaccines have significantly contributed to the control of previous infectious diseases. For example, Smallpox was completely eradicated from human population through vaccination[12]. Despite the vast improvements in public health interventions, nutrition status, and reduced residential crowding, remain a part of human life. In 2003, ~8000 people became sick with a viral respiratory illness caused by severe acute respiratory syndrome (SARS)[13]. In 2015, the largest outbreak of Middle East respiratory syndrome coronavirus (MERS-CoV) in south Korea resulted in 186 infections including 36 deaths[14]. According to centers for disease control and prevention (CDC), 41 countries have been preparing for and managing measles outbreaks in recent years[15].

Figure I.1. St. Louis Red Cross Motor Corps personnel in preparation for holding victims of influenza pandemic, courtesy of The Washington Post[16].



Reviewing the history of infectious disease reveals that pandemics are occurring frequently and are likely to remain a part of human life. The COVID-19 pandemic showed that our societies were vulnerable and not prepared to combat widespread airborne disease transmission, which has resulted in ~6 million deaths as of February 13, 2022[1]. As the vast majority of infection transmission occurs indoors, buildings need to play a major role in the future of public health.

Several scientist have already called for global attention to control the current pandemic and better prepare buildings to help in the fight against viral infectious spread in the future[17,18]. Given all that we have learned from previous pandemics including COVID-19, our strategies to combat infectious disease need to be reimagined to

intentionally include the role of buildings to improve resilience and support a healthier future.

I.2. Infectious Disease and Transmission Routes

The COVID-19 virus (SARS-CoV-2) and other pathogens such as Influenza viruses can be released into the air through respiratory activities such as coughing, speaking, singing, and sneezing[19,20]. Aerosolized viruses do not transport naked, but they are embedded in aerosol particles that vary in size, ranging from nanometers to millimeters [17]. The initial belief was that COVID-19 could only be transmitted through large droplets ($> 100 \mu\text{m}$), almost necessitating that the susceptible person be within 6 ft of the source emitter, thus the CDC and WHO guidance for individual behavior followed suit: wash your hands, stay six feet apart, and wipe down high-touched surfaces[21]. However, further research confirmed what many aerosol scientists proposed; that viruses in smaller particles ($< 5 \mu\text{m}$) can float in the air for hours and deposit in people's respiratory system, even for those individuals that were outside the six foot radius of the infected emitter, and still cause infection[22]. While "social" or spatial distancing can help reduce disease transmission sourced from larger droplets that more quickly fall into the ground [23]. On May 7, 2021, CDC updated their guidelines, stating that inhalation of fine respiratory droplets and aerosol particles is the primary route of human-to-human transmission, beyond 6 ft of the emitter source[24]. WHO also updated their guidelines on Dec 15, 2021[25].

I.3. Buildings in Support of Health and Vectors for Disease

Transmission

Buildings shape our health and wealth. In modern times, humans spend more than 90% of their lifetime indoors and many building-related factors directly influence our health and well-being[26]. “Material health” has become a new focus in building standards that address the essence of controlling many classes of chemicals found in buildings materials, such as volatile organic compounds (VOCs) and semi-volatile organic compound (SVOCs) that cause a wide range of chronic and sub-chronic effects[27]. Indoor surfaces and microbial exposure is another factor by which human health can be affected, when human skin comes into contact with environmental sources of microbes[28].

Most of the air that is breathed by humans on a daily basis is breathed indoors, with a ratio that is thousands of times higher for indoor environments than for outdoor urban air[29]. Indoor environmental pollution can contain a variety of sources including chemicals emitted from indoor material (paint, wax, or disinfections) or furniture (printers, scanners, etc.), outdoor base pollutants such as particulate matters of different sizes or hazardous gases such as ozone that can penetrate indoor air[30]. According to the Institute for Health Metrics and Evaluation (IHME), air pollution was the 1st global burden of disease among environmental factors in 2019, causing a broad range of acute- and chronic impacts on human health such as cardiovascular diseases, chronic respiratory diseases, maternal and neonatal disorders, as well as respiratory infections[31]. The majority of air pollution from both indoor and outdoor origins are transferred into our respiratory system within indoor spaces[32]. Indoor environments are associated with

larger surface to volume ratios[32], changes to the viable bacterial communities because of decreased level of sunlight exposure[33], higher exposures to viable volatile organic compounds (VOCs)[34], and elevated concentrations of human origin bioaerosols[35].

Prior to the COVID-19 pandemic, research confirmed that healthy indoor environments devoid of various organic and non-organic pollutions can significantly improve human health and support a healthy economy[36]. While this was already known, COVID-19 has dramatically increased the scale and urgency with which we should consider the health of buildings.

1.3.1. Buildings Are the Main Hotspots for COVID-19 Transmission

Mounting evidence suggests that COVID-19 is primarily transmitted in indoor spaces[37–39] including well-documented superspreading outbreaks in which a large cluster of indoor occupants acquired infection by a single individual[40]. Moreover, evidence suggests that COVID-19 was transmitted between people in adjacent indoor spaces where there was little to no possibility for direct contact transmission[41]. Table I.1 shows some examples of super spreading outbreaks that were documented by further epidemiological investigations. Section II.3 of this dissertation describes a quantitative assessment of some of the well-known COVID-19 outbreaks, providing more evidence that outbreaks are predictable and thus, more likely to be preventable.

1.3.1.1. Measuring SARS-CoV-2 in Buildings

Bioaerosol pathogen detection technology was previously introduced as a novel concept to combat pandemics[42]. Studies of environmental surveillance of COVID-19 have highlighted the importance of active samplings to detect and quantify the

Table I.1. Examples of well-documented COVID-19 super spreading outbreaks.

Space type	Number of index case(s)	Number of infected people*	Documentation reference
Restaurant 1	1	9	[43]
Restaurant 2	1-2	2	[44]
Choir rehearsal	1-7	52	[45]
Religious services	1	12	[46]
Bus	1	23	[47]
Gym	1-5	117	[48]
Airplane	1	12	[49]

concentration of SARS-CoV-2 in buildings[50–53]. Different sampling methods from surface and air are used to monitor buildings for the presence of SARS-CoV-2[54].

Surface and air samples from various methods such as solid impactors, liquid impactors and impingers, dry filters, and other methods were evaluated by reverse transcriptase polymerase chain reaction (RT-PCR) and the viral RNA of SARS-CoV-2 was detected in surface and air samples from indoor spaces that were occupied by individuals diagnosed with COVID-19 [51,53,55–58]. Moreover, viable SARS-CoV-2 has been successfully detected in indoor air, both in experimental set-ups and real world settings[20,59,60].

These studies provide substantial evidence that indoor environments are prone to contamination by infectious agents such as SARS-CoV-2 when they are occupied by those with a positive diagnosis. Moreover, they suggest that monitoring of air and surfaces in buildings is among the most effective mitigation strategies to safeguard public health by providing early warning regarding environmental contamination and protect occupants from long periods of exposure.

1.3.1.2. Environmental Surveillance of Pathogens

Tracing the residuals of pathogens in buildings has attracted great attention since 2020 and with the spread of COVID-19 worldwide. Companies such as ThermoFisher,

Poppy, and Smith’s Detection offer virus detection technologies which can provide useful data about the potential presence of SARS-CoV-2 in indoor spaces[61,62]. However, the ability to manage the risk in buildings with these data streams would depend on 1) better understanding of room risk levels (Chapter II), and 2) real-world evidence confirmation of effective mitigation measures (Chapter III) to make these data actionable.

1.3.2. Buildings Can Mitigate the Exposure to Infectious Disease

So far, we conclude that buildings can be contaminated by occupants who have acquired an infectious disease (including COVID-19), which inherently poses a risk of infection to other people who live within or occupy adjacent spaces. The purpose of this section is to provide evidence that suggests environmental variables and engineering practices can potentially contribute to combating disease transmission indoors[63].

1.3.2.1. Ventilation

Ventilation is the act of bringing air, including outside fresh air, into spaces through passive flow of outdoor air (natural ventilation) or via mechanical equipment[64]. Prior to the pandemic, several research articles suggested that increased ventilation rates in buildings is associated with improved human health and cognitive function[65–68].

The COVID-19 global pandemic paired with repeated messaging from the building science community has increased public attention to ventilation in buildings[37,69]. While many well-documented super-spreading outbreaks are associated with poorly ventilated indoor spaces (Table I.1), preliminary evidence from epidemiological investigations suggest that increased ventilation is associated with decreased risk of acquiring COVID-19 in elementary schools in the state of Georgia[70].

Moreover, a recent study on COVID-19 isolation dorms (preprint) found that the concentration of SARS-CoV-2 virus in the rooms that had open windows was lower than rooms without windows[53]. Moreover, risk estimation models predict that ventilation can theoretically reduce the viral load and therefore risk of infection to other occupants[71,72]. To date, there is no study that has evaluated the real-world impact of ventilation on the concentration of SARS-CoV-2 virus which makes this subject an important research gap fill.

1.3.2.2. Filtration

Prior to the pandemic, air cleaning technologies received noticeable attention for contributing to clean indoor air, especially when building ventilation rates do not meet minimum requirements. A comprehensive review on the performance of air cleaning technologies such as fan-driven high efficiency particulate air (HEPA), ozone oxidation, photocatalytic oxidation (PCO), plasma, sorption, and ultraviolet germicidal irradiation (UVGI) found that 1) new air cleaning technologies such as PCO, plasma, and ozone related, produce harmful by-products that are harmful to health[73], 2) PCO and plasma technologies typically have low clean air delivery rates (CADR) indicating poor performance in real world settings, 3) traditional air cleaning systems such as HEPA filtration can remove certain types of pollutants from air if sized appropriately, and UVGI systems are can render microbes as non-viable if sufficient power and dwell time are provided [74].

Similar to ventilation, filtration technologies have become more popular for their potential benefits of removing SARS-CoV-2 from indoor environments during the global pandemic. Filtration technologies can reduce the risk of acquiring infection in two ways,

either by removing the biological agents from indoor environment (i.e., HEPA filters), or inactivating the virus[75,76].

According to National Institutes of Standards and Technology (NIST), HEPA filters can theoretically adsorb 99.97% of particles that are larger than 0.3 μm [77]. Given that SARS-CoV-2 virus is believed to be transmitted by bioaerosols in the range of 0.3-100 μm , fan-driven HEPA filters can potentially contribute to removing the vast majority of infectious agents from indoor environments. However, studies conducted in real world field settings show that the efficiency of HEPA air cleaners at removing non-bioaerosol particles (i.e., cigarette smoke) varies between 30-90%[78–80], while some studies reporting significant reduced efficiency for particles of smaller size bins in field settings (<0.5 μm)[81].

The United Kingdom (UK) government published a paper that reviewed the application of filtration technologies to combat COVID-19 transmission[82]. The review concludes that despite the fact that SARS-CoV-2 is transmitted within particles of 1-100 μm and HEPA filters (>MERV 13) can theoretically remove particles of these size ranges[83], there are no direct evidence that use of HEPA filters can reduce the transmission of SARS-CoV-2 and therefore, more research is needed before deploying these systems in large scale[82].

1.3.2.3. Environmental Factors and other treatments

Environmental factors such as relative humidity (RH), temperature, and ultraviolet irradiation (UV) can impact the survival and stability of infectious disease in indoor environments[17,84–87]. Previous studies have characterized the impact of relative humidity on the survival of bacteria (i.e., *Escherichia coli*, *Mycobacterium*

smegmatics, Bacillus. Subtilis, etc.)[88], Phi6 [89], and influenza virus[90,91]. A few laboratory scaled studies have shown that relative humidity and temperature change the viability of SARS-CoV-2 survival on surfaces[92,93] and in aerosols[94], indicating that higher relative humidity and temperature are associated with faster deactivation rates of SARS-CoV-2 virus. In addition to affecting virus infectivity, higher relative humidity can theoretically increase the rate of deposition of bioaerosols to indoor surfaces resulting in physical removal of virus from air, which can help reduce the inhalation risk of virus laden particles indoors[95]. To date, no study has characterized real-world efficacy of relative humidity, temperature, and UV irradiation on viability or deposition rates of SARS-CoV-2 in real world settings. Therefore, testing environmental factors such as relative humidity in real world scenarios can determine whether, and to what extent, that environmental factors can be utilized as additional layers of risk reduction strategies for combating disease transmission indoors.

I.4. Aims and Scope

Here at the University of Oregon, I present my doctoral study in accordance with the Institute for Health in the Built Environment (IHBE) mission, which integrates knowledge from diverse scientific disciplines to support a healthy and thriving community and planet. It is now clear that COVID-19 is an indoor disease that can be worsened or mitigated by how buildings are designed and operated. As a researcher in the architecture field, my goal is to contribute to the body of building science knowledge and explore the capacity of buildings, environmental measures, and design processes to stop the spread of deadly diseases while operating buildings as effectively as possible and reducing energy consumption and associated negative consequences with regards to

climate change. I state that buildings must be reinforced against airborne pathogens in a similar way that earthquakes made us reconsider how to create structurally safe and resilient buildings. Earthquakes may or may not occur during a building's lifecycle, while serious airborne infectious disease risks seem to occur every 10 years and annual influenza (and now maybe COVID) outbreaks are regular. We must prepare our buildings now to help avoid another catastrophic building exodus by 2029 or even 2119.

1.4.1. A Radical Multidisciplinary Collaboration Work

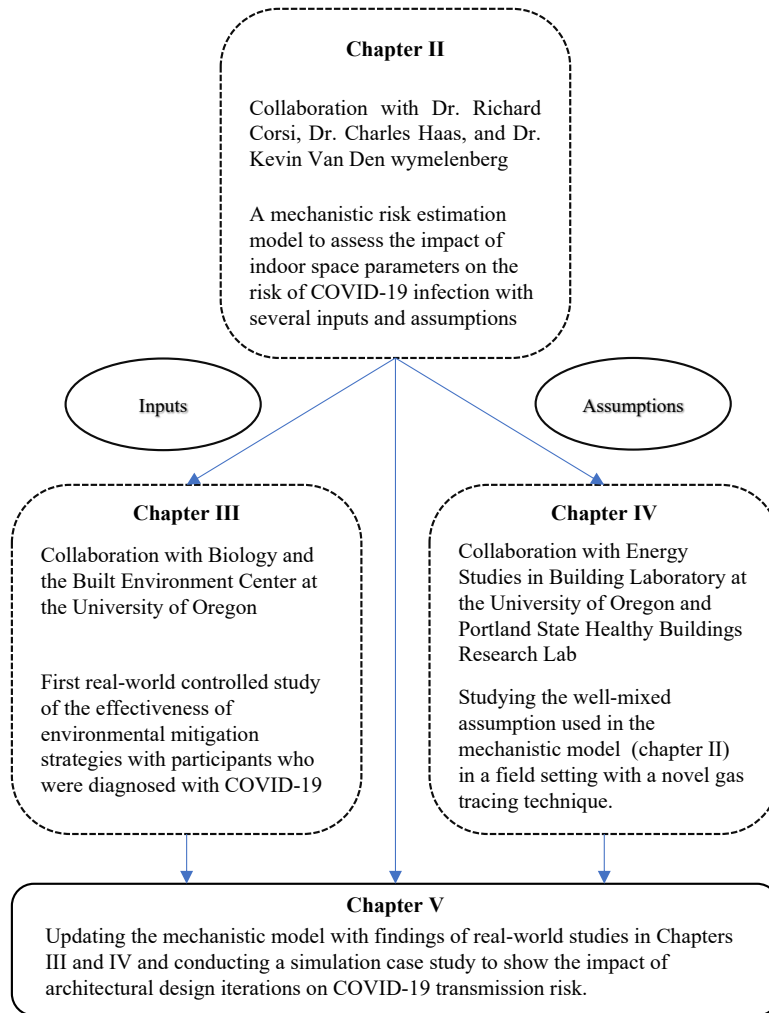
“Designing and operating healthy and energy efficient buildings requires radical interdisciplinary approaches, and so too does unravelling systemic racism and inequality” a quote from my supervisor Dr. Kevin G. Van Den Wymelenebrg. I have had a great privilege to collaborate with world class researchers to answer critical questions regarding the role of buildings in the transmission of COVID-19 disease. In addition to working with my PhD committee, I have directly worked with more than 15 researchers from 5 research institutes all of whom made substantial contributions to this dissertation. Here I clearly state that all the chapters in this dissertation involve co-authored materials. I also indicate that I have had a pivotal role in the conduct of each collaborative work presented in this dissertation that legitimizes using the collaborative content in this dissertation. For each collaborative published and unpublished paper, I have been the first author of the published or publishable content. In addition to this statement, I will provide a statement of my specific contribution at the beginning of each chapter.

1.4.2. The Structure of Dissertation

This dissertation comprises three original research projects and a concluding chapter that also includes original research content but focused on the practical

implications of the three previous research projects. Figure I.2 briefly depicts the organization, relationships, and internal structure of all chapters.

Figure I.2. Schematic structure of chapters.



I.4.2.1. Summary of A Quantitative Aerosol Risk Estimation Platform

In Chapter II, I collaborated with Dr. Richard Corsi, Dr. Charles Haas, and my supervisor, Dr. Kevin G. Van Den Wymelenberg to develop a quantitative bioaerosol disease transmission risk estimation platform that is more mechanistic in nature than traditional risk assessment models for airborne infectious disease. Dr. Corsi first developed the mathematical framework that calculates the concentration of emitted

aerosols based on size distribution characteristics. I worked with Dr. Van Den Wymelenberg to link the inhaled and deposited dose to an estimated attack risk, with input from Dr. Charles Haas. I developed the Safeairspaces.com online risk estimator script in grasshopper, with input from Dr. Van Den Wymelenberg and Dr. Corsi. I further analyzed case studies using simulations and developed the draft of this paper with input from Dr. Van Den Wymelenberg and Dr. Corsi. Here I state that Dr. Corsi drafted a major part of the paper's mathematical methodology, while I provided support upon request with his guidance.

Existing mathematical models can predict a relative risk of infection caused by airborne disease. However, they are based on back calculations of previous outbreaks and as a result they fail to account for particle deposition to indoor materials, filtration, and deposition of particles in the respiratory system of receptors.

Our model features the ability to include exhaled bioaerosol across a range of size distributions from infected individuals as well as particle fate mechanisms indoors. Therefore, insertion of control options (increasing ventilation, application of face masks, in-room filtration, viral inactivation, etc.) can be employed as loss terms in the form of differential mass balance equations, showing the risk of infection via scenarios with different environmental and occupational characteristics.

The novelty of this model relates to the concept of "inhaled and deposited dose" in susceptible individual's respiratory systems. The model predicts particle deposition in three major part of receptor's respiratory system (1= extrathoracic region, 2 = tracheobronchial region, 3 = alveolar region) and converts these to total volume of

particle deposition, summed over all different particle size ranges, and reports the inhaled and deposited volume of rebreathed particles in picoliters.

The dose response relationship for SARS-CoV-2 was not available at the time of publication, therefore, we used a model that was experimentally developed on humans for coronavirus HCoV-229E to convert the volume of inhaled and deposited dose to plaque forming unites (PFUs). In order to adjust the model for SARS-CoV-2, we anchored the resulting infection attack rate to a well-documented superspreading outbreak in a restaurant in Guangzhou, China and developed an interactive online web-tool via Grasshopper with coding script developed in Rhinoceros software. The interactive web-tool is available to use for free at Safeairspace.com.

We used this model to simulate four other well-documented outbreaks. The simulations demonstrate that the risk estimation platform yields results that reasonably predict outbreak attack rates using the available information about the case and reasonable assumptions for missing information. The mechanistic approach will rapidly accommodate updates as soon as new information becomes available, especially with regard to SARS-CoV-2 human dose–response data. Additional updates related to dose–response data associated with SARS-CoV-2 variants and effectiveness of vaccines can also be easily incorporated into future updates of the risk estimation platform.

1.4.2.2. Summary of Environmental Mitigation of Aerosol Viral Load

For this project, Dr. Kevin G. Van Den Wymelenberg performed funding acquisition and managed the investigation team. Dr. Kevin G. Van Den Wymelenberg and I conceived of project scope and methodology with input from UO Biology and the Built Environment team members Leslie Dietz and Patrick F. Horve. Dr. Kevin G. Van

Den Wymelenberg and Leslie Dietz enrolled and consented all study participants. Dale Northcutt worked with all other authors to set up the modular room and all research instrumentation. I collected biological specimen with supports from Liliana Barnatan, Leslie Dietz, and Andreas Olsen Martinez. Similarly, team members Liliana Barnatan, Leslie Dietz, Patrick F. Horve, and Andreas Olsen Martinez performed laboratory analyses. I performed data curation, data exploration, developed final analysis scripts, performed final analysis, and created visualizations with support from all authors. I developed the original manuscript with direction and input from Dr. Kevin G. Van Den Wymelenberg. All authors provided manuscript revisions and edits on subsequent manuscript drafts and approved the final manuscript prior to submission for publication.

We provide the first real world evidence that building related interventions significantly impact the dispersion and abundance of SARS-CoV-2 virus in the presence of individuals who were diagnosed with COVID-19. We obtained approval from the University of Oregon's institutional review board to conduct extensive research on participants who had tested positive for COVID-19 in an environmentally controlled chamber (modular room). We report significant quantitative effectiveness of indoor environmental mitigation strategies useful for selecting effective ventilation rate, quantity of in-room HEPA filtration, and degree of humidification. We also provide novel insight about the relationships of human and environmental viral loads (aerosols and surfaces) from individuals infected with COVID-19 in the immediate field (<1m), near field (1.2 m), and far field (3.5 m). We collected environmental biological samples, human specimen, particulate of different size bins, and carbon and dioxide (CO₂). Together, these results provide novel insight into how buildings and occupant activities can mitigate

the dispersion and abundance of SARS-CoV-2 virus. Below is a summary of our key findings within this research:

1. What is the relationship between human viral load and environmental contamination?

We report a significant coefficient for all nasal and aerosol samples in routine trials whereby an increase in nasal viral load equivalent to $-1 C_T$ is associated with an increase in room aerosol viral load of $-0.362 C_T$. Furthermore, we report quantitative correlations between human viral load and high touched surfaces, as well as settling plates.

2. Is there a difference in aerosol viral load at different distances from the infected participant, and is this affected by room air movement?

We report that an increase in viral load equivalent to $-1 C_T$ in human nasal samples is significantly associated with an increased near field viral load of $-0.326 C_T$ and an increased far field viral load of $-0.40 C_T$ among routine trials.

The difference of means between the aerosol C_T value of near field and far field aerosol samples in routine trials was $1.058 C_T$, whereas far field samples represent lower viral load, however the paired t-test differentiating near field and far field samples was not significant ($P = 0.05955$). Interestingly, CO_2 concentration and the number of fine particles show statistically significant differences between near field and far field.

3. How much ventilation do we need to significantly reduce aerosol viral load, and does this differ by distance from the infected individual?

We observed that the aggregate of ventilation and filtration trials significantly reduced room aerosol viral load and that of select surfaces, when compared to control trials with ~ 0 ACH.

When examining total room aerosol viral load (near field and far field together), we report that trials with less than ~ 4.5 ACH (including ~ 0 ACH trials) were associated with statistically higher viral load, by nearly an order of magnitude, than trials with greater than ~ 9 ACH (mean difference of $-3.2 C_T$). We noticed that CO_2 has been frequently discussed among expert communities as an indicator of appropriate ventilation. Therefore, we provide the first real world correlation between aerosol viral load and CO_2 concentration that is affected by outdoor air exchange rates, where an increase in ~ 128 PPM of CO_2 concentration generated by an individual with COVID-19 corresponds with an increase in aerosol viral load equivalent to $-1 C_T$, thus, approximately a doubling of the viral load.

4. How much in-room filtration is needed to significantly reduce aerosol viral load, and does this differ by distance from the infected individual?

We report that HEPA filtration trials (with ~ 1000 m³/hr) had significantly lower room aerosol viral load, by nearly an order of magnitude, when compared with control trials without filtration (mean difference of $3.240741 C_T$).

5. Does the level of indoor relative humidity significantly alter the aerosol viral load?

We report that increasing relative humidity by $\sim 11.85\%$ is significantly associated with approximately a 50% decrease in aerosol viral load.

6. Which particle size bins best characterize the viral load?

We investigated the correlation of particles and viral load through two different study set-ups and found that aerosol viral load is significantly correlated with particles of smaller sizes ($0.3\ \mu\text{m} - 3\ \mu\text{m}$) in near field and far field. In addition to fine particles, we observed statistically significant correlation between aerosol viral load and droplet size ranges ($10\ \mu\text{m} - 25\ \mu\text{m}$) only during immediate field ($< 1\text{m}$) trials of high expiratory activity, but not during routine trials. For immediate field trials, particles of smaller sizes still best characterize the aerosol viral load. These results provide real world quantitative evidence of the effectiveness of some of the most important mitigation strategies that can be used to reduce COVID-19 disease transmission in built environments and better protect care providers.

1.4.2.3. Respiratory Exposure at Alternate Distances

For this project, Dr. Richard L. Corsi proposed the concept of using breath mints consumed by an emitter as a source of tracer gas and as surrogate for viral particles in exhaled aerosols. I worked with Dr. Van Den Wymelenberg to outline the scope of work and write the grant proposal with input from Dr. Gall, Dr. Fretz and Jason Stenson. Portland State University team members Dr. Elliot Gall and Aurélie Laguerre physically transferred their proton-transfer-reaction time-of-flight mass spectrometry (PTR-TOF-MS) to the Energy Studies in Building Laboratory (ESBL) in Portland, Oregon. I worked with Aurélie Laguerre, Mark Fretz, and Jason Stenson to collect data from a single participant. Dr. Elliot Gall and Aurélie Laguerre extracted raw data from the TOF-MS database. I developed the project's data analysis scripts, visualizations, and drafted the paper with input from Dr. Kevin G. Van Den Wymelenberg, Mark Fretz, and Jason Stenson. This initial draft was shared with all team members, including Dr. Gall, Aurélie

Laguerre, and Dr. Corsi, and follow-on meetings and discussion prompted further refinements to the paper draft. In this chapter we further elaborated on the well-mixed assumption that was previously used in chapter II to better explain the impact of distance from emitter on room bioaerosol exposure. The resultant magnifiers of this chapter were compared to ratios of near- and far-field ratios from Chapter III as a case study. As of February 2, 2022, I have updated the manuscript draft and sent it to all co-authors for their review and feedback.

Social distancing has been frequently recommended as a critical strategy to mitigate the spread of COVID-19 disease. Further evidence suggests that far field transmission (> 6 ft) is the primary route to explain the significant number of superspreading outbreaks worldwide[96]. Therefore, quantifying the relationship of far field exposure risk to near field exposure risk over time is a key to better understand the total risk of airborne infection and implement appropriate mitigation strategies.

Respiratory viruses, including SARS-CoV-2, do not travel naked in the air. Rather, they are embedded in respiratory particles of different sizes emitted from a patient's respiratory system and can be suspended in the air for a long period of time whereby they are inhaled and deposited into other peoples' respiratory systems causing some fraction of susceptible cases to acquire infection.

Risk estimation models, including our SafeAirSpaces aerosol risk estimation platform, rely on an assumption of "well-mixed air". In reality, the fate of particles is heavily dependent on forces acting on particles such as viscous drag, viscosity of air, and gravitational force of particles mass. Therefore, the distance from the infected occupant, the location of ventilation supply and exhaust inlets/outlets, and the velocity and amount

of ventilation supply all implicate the concentration of particles rebreathed by other room occupants.

In this study we measured unique identifiable tracers from breath mints consumed by a healthy participant to serve as a proxy for bioaerosol emissions. Measurements were recorded at 2.5 ft, 5 ft, and 7.5 ft, using PTR-TOF-MS. PTR-TOF-MS measures volatile organic compounds (VOCs) across a mass range of ~30 to >300 amu with <1 second time resolution. We are proposing this research as a novel methodology for the future studies of indoor air quality and microbial risk assessment models.

Our study resulted in a series of quantitative magnifiers that explain the distribution of bioaerosols that may contain viable virus as well as other biological contaminants that are resolved by distance from the source emitter and compared with the volume integrated background concentration. Our findings indicate that aggregated concentrations of human sourced tracers during steady-state periods toward the end of 60-minute trials at 2.5 ft, 5 ft, and 7.5 ft are fairly modest at ~18%, ~11%, and ~7.5% higher than volume integrated background, respectively. We observed that 2.5ft trials have substantially higher concentrations than other distances during the first 20 minutes of data collection with statistically large effect sizes, highlighting the importance of spatial distancing for shorter duration exposures. In this chapter we introduce a series of magnifiers to determine the proportion of near field and far field exposure with respect to well mixed assumption in future studies of indoor air modeling.

1.4.2.4. Using Disease Transmission Risk as the Guide for Evidence-Based Design

This chapter contains co-authored material with Dr. Siobhan Rockcastle, Dr. Mark Fretz, and Dr. Kevin G. Van Den Wymelenberg. For this Chapter, Dr. Siobhan Rockcastle proposed the concept of applying the dissertation findings into an architectural design case study. I conducted simulations in Rhinoceros and Grasshopper, analyzed data, created visualizations, and developed the initial draft with inputs from Dr. Siobhan Rockcastle, Dr. Mark Fretz, and Dr. Kevin G. Van Den Wymelenberg. The findings of this chapter are planned for submission to SIMAUD 2022, a building simulation conference in the near future, and future refinement for submission as a journal article.

In this chapter, we describe an example of how the findings of this PhD dissertation can be applied to support architectural design processes and building operations. Therefore, we simulated the risk of infection for a simple case study with different window configurations and in different geographic locations. In summary, we observed that increasing the fractional opening of a single window from 0% to 75% results in an increased outdoor air exchange from less than 1 ACH (0% operable) to ~6 ACH (75% operable), leading to a 20% decrease in the risk of infection transmission. Moreover, for a single day, a cross ventilation design can increase the outdoor air exchange up to +25 ACH which corresponds to substantially reduced risk of disease transmission. Furthermore, in a cold climate the indoor relative humidity can be significantly lower in winter due to increased mechanical heating through forced air systems, as compared to a moderate climate, and therefore the colder climate indicates increased indoor disease transmission risk.

II. A QUANTITATIVE AEROSOL RISK ESTIMATION PLATFORM

This chapter is published as:

Parhizkar, Hooman., Van Den Wymelenberg, Kevin.G., Haas, Charles.N. and Corsi, Richard.L. (2021), A Quantitative Risk Estimation Platform for Indoor Aerosol Transmission of COVID-19. *Risk Analysis*. <https://doi.org/10.1111/risa.13844>.

Dr. Corsi first developed the mathematical framework that calculates the concentration of emitted aerosols based on size distribution characteristics. I worked with Dr. Van Den Wymelenberg to link the inhaled and deposited dose to an estimated attack risk. I developed Safeairspaces.com online risk estimator script in grasshopper with inputs from Dr. Van Den Wymelenberg and Dr. Corsi. I further analyzed case studies simulations and developed the draft of paper with inputs from Dr. Van Den Wymelenberg and Dr. Corsi. Here I state that Dr. Corsi drafted a major part of paper's methodology.

II.1. Introduction

Globally as of March 4 2021, more than 2.5 M deaths among 114 M confirmed cases have made COVID-19 one of the most severe diseases in history[1] . There have been many debates around the proportional routes of human-human transmission caused by large droplets, e.g., greater than 100 microns, and smaller aerosol particles that remain infectious both on surfaces and air[58]. Aerosols consist of particles less than 100 μm in diameter that follow airflow streamlines among which smaller diameters, e.g., $< 5 \mu m$, can readily penetrate airways all the way down to the alveolar region where gas exchange takes place between the air and blood[97]. Aerosol transmission has been implicated in several large COVID-19 outbreaks, also called “superspreading

events”[45,47,49,98,99]. Among the community outbreaks with well-established environmental and epidemiological analyses, there is evidence that COVID-19 may be transmitted at distances greater than two meters and may be the primary route in some COVID-19 outbreaks[44,99,100]. After many months of not doing so, the Centers for Disease Control (CDC) in the US indicated that aerosol transmission is believed to be a primary mode of transmission infection[101]. The WHO still prioritizes other modes of transmission but recognizes the importance of ventilation, which primarily influences levels of aerosol particles in indoor air. Several researchers have recommended indoor air mitigation strategies for COVID-19[2,102]. Estimating infection risk by aerosol transmission and understanding the interplay of key variables that implicate the inhaled deposited dose of particles containing SARS-CoV-2 virions is important to help reduce transmission risk[103].

Models for airborne infectious disease transmission often rely on a quanta generation rate, which is back-calculated based on outbreaks with sufficient metadata for modeling the event[104]. While this approach has been widely used, the mechanistic behavior of the environmental accumulation, fate and control of virus-laden aerosol particles is limited and largely lumped into empirically derived quanta generation rates. Such models also fail to differentiate the dynamics of different particle sizes, emission modes, and rebreathed respiratory system deposition.

In this paper we present a model based on quantitative microbial risk assessment (QMRA) for transmission of COVID-19 by aerosols in the far field. The model employs an aerosol number balance in a well-mixed indoor space with one or more infectors, mechanistic and size-resolved particle loss mechanisms, volume deposition in the

respiratory systems of susceptible receptors, and infection risk based on a corona-virus dose-response relationship for humans anchored to a well-defined outbreak case in China.

II.2. Methodology

Given current research gaps, we developed the structure for an aerosol infection transmission risk estimation model as detailed in the following sections.

II.2.1. Time-Dependent Particle Number Concentrations

The size-resolved concentration of particles emitted by an infector in a well-mixed, single-zone, indoor space is defined by the following ordinary differential equation.

$$\frac{dC_i}{dt} = \frac{E_i}{V} - \beta_i C_i \quad (1)$$

Where, C_i is the particle number concentration for size range i in air (particles m^{-3}), E_i is the particle emission rate from the infector in size range i (particles h^{-1}), V is the volume of the indoor space (m^3), β_i is a particle removal constant (h^{-1}), and t is time (h).

Particle emissions are assumed to occur from three modes as defined by Equation 2.

$$E_i = \sum_{j=1}^3 f_{em,i,j} \alpha_j E_{i,j} \quad (2)$$

Where, counter and subscript j correspond to mode of emissions (1 = breathing, 2 = speaking, 3 = coughing), $E_{i,j}$ is size (i) specific emission rate for breathing and speaking (particles h^{-1}) and size-specific particles per cough, $f_{em,i,j}$ is the fractional reduction in particle emissions in size range i for emission mode j as a result of the infector wearing a mask (-) ($f_{em,i,j} = 0$ with no mask), and α_j is the fraction of time exhaling ($j = 1$) or speaking ($j = 2$), or the frequency of coughing (coughs h^{-1}) ($j = 3$). Values of $f_{em,i,j}$ have

recently been published for several different types of mask materials, assuming a good fit to face[105–109].

We treat size-resolved particle distributions as being after the rapid evaporation process of the volatile fraction of particles. This process takes place over time scales of seconds, e.g., much shorter than typical exposure events[95]. Emissions are taken as time-averaged over the course of an exposure event, effectively “smoothing” intermittent emissions, e.g., coughs, and treating emissions for each particle size range as constant.

The particle removal constant, β_i , involves four terms as described by Equation 3.

$$\beta_i = \lambda + k_{s,i} + \sum_{j=1}^n f_j \frac{\eta_{i,j} Q_{c,j}}{V} + n_p \left\{ \frac{f_{m,i} Q_b}{V} + \frac{(1-f_{m,i}) f_{dep,i} Q_b}{V} \right\} \quad (3)$$

Each term in Equation 3 has units of inverse time, here taken to be h^{-1} , and is assumed to be constant or time averaged (e.g., term 2) over the exposure period. The first term on the right-hand side is the air exchange rate for the indoor space (h^{-1}), taken to be the volumetric flow rate of outdoor air into the indoor space ($\text{m}^3 \text{h}^{-1}$) normalized by V (m^3). Values of λ can vary in the indoor space over time and significantly between buildings. However, reasonable bounds can be placed on λ based on previous studies for residential e.g.,[110] and commercial e.g., [111] buildings, standards, design, and measurements (e.g., ANSI/ASHRAE Standard 62.1-2019).

The second term, $k_{s,i}$, is the particle decay rate due to deposition to indoor surfaces (h^{-1}) for particles in size range i . The value of $k_{s,i}$ is a function of particle size, surface-to-volume ratio in an indoor space, mixing conditions in bulk room air, air speeds over materials, and the nature of materials in the indoor space. Values of $k_{s,i}$ for various conditions based on theory, chamber, and field experiments have been reported[112,113].

The third term corresponds to removal of particles in size range i due to engineering control devices, e.g., filtration in a mechanical system or a portable air cleaner. The parameter f_j is the fraction of time that air flows through device j (-), $\eta_{i,j}$ is the fractional removal of particles in size range i that are removed during flow through the control device (-), and $Q_{c,j}$ is the volumetric flow rate of air through the control device ($\text{m}^3 \text{h}^{-1}$). The value of each parameter in this term are system specific. The product $\eta_{i,j} \times Q_{c,j}$ for a portable air cleaner is referred to as a clean air delivery rate (CADR) and is often reported in standard cubic feet per minute (scfm) based on certified testing using smoke, pollen, and dust. A range of values have been published in the literature for portable HEPA air cleaners and ion generators, the latter of which typically have much lower values of CADR[114].

The fourth term corresponds to particle removal on the mask and in the respiratory system of the n_p occupants in the indoor space. The parameter $f_{m,i}$ is the fractional removal of particles in size range i by a receptor's mask ($f_{m,i} = 0$ for no mask), Q_b is the respiratory volume intake of occupants in the indoor space ($\text{m}^3 \text{h}^{-1}$), and $f_{\text{dep},i}$ is the fractional deposition of particles in size range i in the respiratory system of each occupant[115]. Values of $f_{m,i}$ have recently been published for a wide range of mask materials, assuming a good fit to face[105–109]. Values of Q_b can vary by over an order of magnitude depending on body size and level of activity, e.g., rest versus heavy aerobic exercise[116]. Values of $f_{\text{dep},i}$ varies by particle size, mode of breathing (mouth versus nose), and level of activity. Several different models have been developed for estimating $f_{\text{dep},i}$ explicitly or by computational fluid dynamics[117,118].

Separation and integration of Equation 1 yields Equation 4.

$$C_i = C_{i0}e^{-\beta_i t} + \frac{E_i}{\beta_i}(1 - e^{-\beta_i t}) \quad (4)$$

Where, C_{i0} is the initial number concentration of particles in size range i in air at the start of the exposure period (particles m^{-3}), t is time (h), and all other variables are as described previously.

II.2.2. Deposition of Particles in the Respiratory System

The number of particles of a specific size range deposited in three regions of a receptor's respiratory system is estimated by Equation 5.

$$n_{i,l} = (1 - f_{m,i})f_{dep,i,l}Q_b \int_0^{t_f} C_i dt \quad (5)$$

Where, $n_{i,l}$ is the number of particles in size range i that deposit in respiratory region l ($l = 1$ extrathoracic region, $2 =$ tracheobronchial region, $3 =$ alveolar region), $f_{dep,i,l}$ is the fractional deposition of particles in size range i in region l of the respiratory system [115], and all other variables are as defined previously. The integration of C_i is taken from initial exposure time (time = 0 h) to final exposure time t_f (h).

The volume of particles of a specific size range deposited in the aforementioned regions of a receptor's respiratory system is estimated by Equation 6.

$$V_{p,i,l} = n_{i,l} \frac{\pi}{6} d_{g,i}^3 \times 10^{-3} \quad (6)$$

Where, $V_{p,i,l}$ is the volume of particles in size range i that deposit in respiratory region l (pL), and $d_{g,i}$ is the geometric mean diameter based on end points of size bin i (μm). The total volume of particles across all particle sizes and regions of the respiratory system is determined by Equation 7.

$$V_{p,total} = \sum_{i=1}^k \sum_{l=1}^3 V_{p,i,l} \quad (7)$$

Where, $V_{p,\text{total}}$ is total volume of all particles deposited in the receptor's respiratory system summed over all k particle size ranges and three respiratory regions (pL).

Many of the parameters described above are building or indoor space specific and can be easily varied in the model, e.g., to model known outbreaks or to draw comparisons between different hypothetical scenarios. The model can incorporate emissions and particle size distributions reported in the published literature or as new data become available. For the purpose of examples presented in this paper, we use data from the study of size-resolved particle emissions associated with speaking[119], and another study of size-resolved particle emissions associated coughing[120], and an approximation that emissions from breathing are 10% of those from speaking with median amplitude. We further assume, for this analysis, the possibility of a “high emitter” and “low emitter” of aerosol particles. Profiles for each described below:

High emitter:

- Coughs eight times per hour
- Each cough emits 54,000 particles
- Size resolved number of cough particles defined by case #8 in Lindsley et al. (2012)
- Emitter spends 20% of the event time speaking at an elevated amplitude with size-specific emissions as per Asadi et al. (2019).

Low emitter:

- Same as high emitter but without cough and median amplitude.

II.2.3. Using Guangzhou Restaurant Outbreak to Anchor the Model to an Existing Dose-Response Relationship

The model was applied to an outbreak in Restaurant X in Guangzhou, China, with significant metadata available for purposes of model application[43,98,121]. A closed-circuit video was used to determine the position of a single infector (index case) as well as receptors who became infected following the event and exposure times. An inert tracer gas was used to study air flow patterns and to quantify air exchange rates[43].

Ten persons from three families (families A–C) who had dined at the same restaurant (Restaurant X) in Guangzhou, China, became infected with COVID-19[98]. A layout of the restaurant and infection zone is provided in Figure II.1. Family A traveled from Wuhan and arrived in Guangzhou. The next day the index case (Case A1) ate lunch with three other family members (A2–A4) at Restaurant X. Two other families, B and C, sat at neighboring tables at the same restaurant. Later that day, Case A1 experienced the onset of fever and cough and went to the hospital. Several days later a total of nine others (4 members of family A, 3 members of family B, and 2 members of family C) had become ill with COVID-19. The only known source of exposure for the affected persons in families B and C was Case A1 at the restaurant.

For the analysis described herein only respirable particles between 0.5 and 4 μm with size ranges (bins) of 0.5 μm were used to estimate total volume of particles deposited in the respiratory systems of those infected (Equation 7). The upper bound of this range can be easily extended in the model. The infector was assumed to speak with high amplitude 20% of the time and cough with a frequency of 8 coughs h^{-1} .

Receptors were assumed to have a respiratory minute volume of $0.6 \text{ m}^3 \text{ h}^{-1}$ and were nose breathers. The exposure period was taken to be approximately 1.25 hours. Particle deposition in the respiratory system for nose breathers was based on the ICRP 66 model[122].

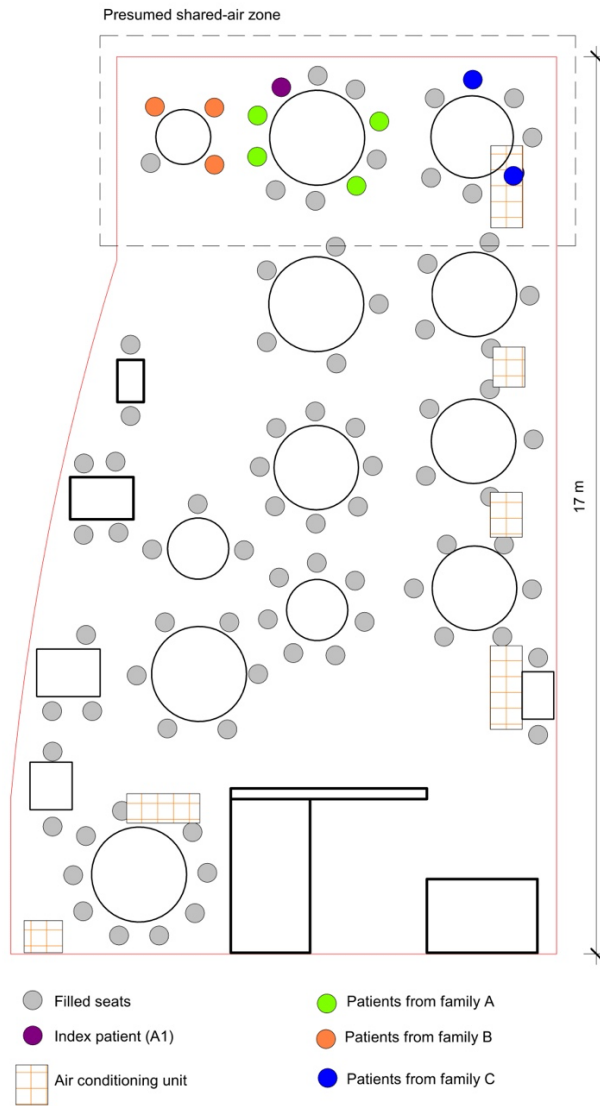
Virus-laden aerosol particles were assumed to be constrained to an infection zone with recirculated air over three tables, including that where the infector was seated. This is a conservative assumption, overestimating the inhaled volume by neglecting dispersion out of the recirculated infection zone. Particle deposition to surfaces was based on values of $k_{s,i}$ as reported by Hussein and Kulmala (2008), but was generally small across particle sizes considered.

Parameters used to simulate the outbreak in Restaurant X are shown in Table II.1. We acknowledge that the aerosol particle emission profile for the infector is hypothetical and based solely on reasonable values in the literature. Other parameters in Table II.1 are those reported for the infection zone in Restaurant X.

Table II.1. Input Parameters for Guangzhou Restaurant X

Guangzhou restaurant physical parameters		Emission parameters (0.5-4 μm)	
Occupants (#)	21	Cough (particles cough ⁻¹)	54,000
Time of event (h)	1.25	# Coughs h ⁻¹	8
Floor area (m ²)	35	Speak (total particles h ⁻¹)	360,000
Ceiling height (m)	3.14	Fractional time speaking	0.2
Outdoor Air Supply (m ³ h ⁻¹)	61.5	Breathing (particles h ⁻¹)	36,000
CADR - filtration (m ³ h ⁻¹)	0	Fractional time not speaking	0.8
High emitter	1	Low emitter	0
Speak multiplier	1.5		

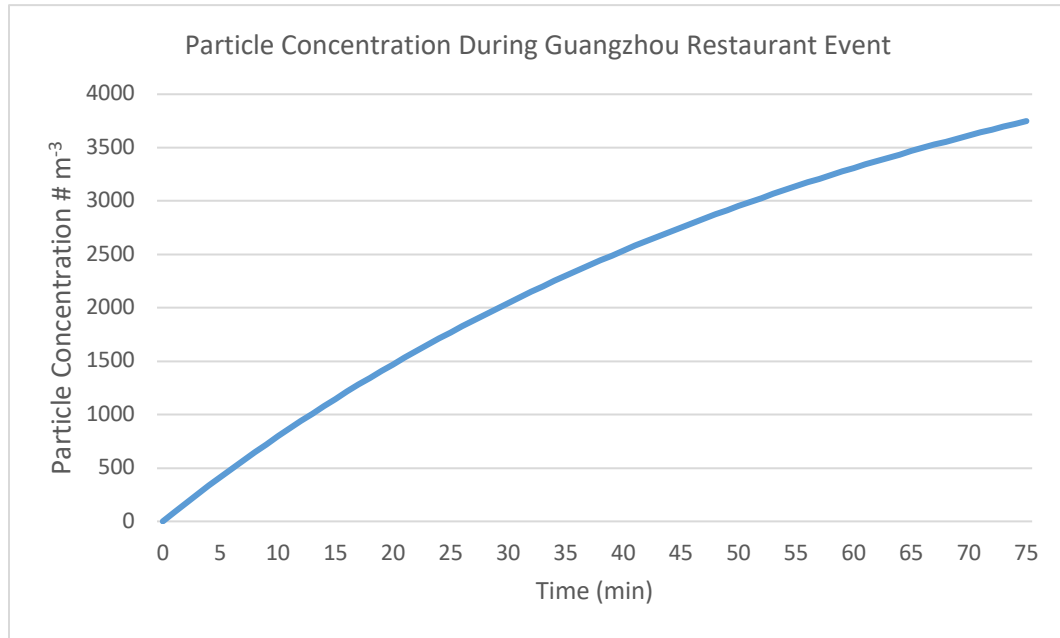
Figure II.1. Arrangement of restaurant tables and air conditioning airflow at site of outbreak of 2019 novel coronavirus disease, Guangzhou, China, 2020, following[43]



An additional speak multiplier function was enabled to count for conditions in which index and susceptible patients' activities involve higher metabolic activities such as speaking loudly, which multiplies the initial 360,000 particles h^{-1} to corresponding values. A model simulation for total particle concentration in the zone of infection in Restaurant X is shown in Figure II.2. The peak concentration for particles in the size range of 0.5 to 4 μm is 3,800 m^{-3} at the time when the infector left the restaurant. A

steady-state condition was not achieved during the infection event, and the average concentration of particles is 2240 m^{-3} .

Figure II.2. Total particle concentration in restaurant zone during time infector is in the space.



For the parameters used in this simulation we estimated that, on average, each individual in the space had 3.6 picoliters (pL) of aerosol particles in the 0.5 to $4 \mu\text{m}$ range deposited in their respiratory system from a high emitter during the infection event. The particle volume was 0.58 pL, 0.25 pL, and 2.78 pL deposited in alveolar, trachea bronchia, and head airways, respectively. Based on a number of simulations with a range of reported particle emission rates for coughing, speaking, and breathing, it seems reasonable that actual volume deposited was in the range of 0.5 to 10 pL. For the remainder of this analysis, we use 3.6 pL for purposes of illustration and comparison.

Once the (average) dose to a receptor is estimated, a dose response curve can be used to assess the risk. At present, no data are available to construct a dose-response

curve for SARS-CoV-2. However prior work has shown that dose-responses for other coronaviruses obey an exponential relationship as described by Equation 8[123].

$$p = 1 - \exp(-kd) \quad (8)$$

Where p is the proportion of exposed individuals adversely affected (probability of infection), and d is the average viral dose that those individuals were exposed to in plaque forming units (PFU). In the absence of data for SARS-CoV-2, the epidemiologic data from the Guangzhou outbreak is used to anchor the dose response relationship in the same sense that has been used in food microbial risk assessment[124]. In this approach, the parameter “ k ” is calibrated to match the attack rate from the exposure observed in the outbreak.

For the outbreak in Restaurant X, there are at least two ways to consider the infection rate, and therefore the response in the dose-response model. One is that the index emitter’s particles resulted in 9 people out of 20 becoming infected with COVID-19, yielding an attack rate of 45%. Another is that 5 out of 11 people that were not at the same table as the index individual were infected via aerosols in the space during the event. There are two justifications for the latter, one being that the infected individual was travelling with two family members and may have spread the virus to them shortly before or after the event at the restaurant, and the other is that the other non-family member at that same table that became infected may have been infected via large droplets or direct contact with the index individual rather than via aerosols. Nonetheless, 5 infected of 11 susceptible individuals results in a similar attack rate of 45%. Therefore, we calculated the probability risk of 45% for this case study.

Using a dose-response model developed by Haas (2021) we calculated a dose of 11 PFUs to yield the observed 45% attack rate in Restaurant X[125]. There is some evidence that this magnitude of viral dose may yield infection based upon previous influenza research [126]. Assuming a volume deposition of 3.6 pL per person within the zone of interest yields an average of ~ 3 PFUs pL^{-1} deposited. We anchored our calculations to the Haas (2021) dose-response curve using 3 PFUs pL^{-1} to extrapolate the risk probability of our SARS-CoV-2 model with a dose in pL. While a broader range of particle sizes can be employed in the model, for this illustrative analysis we assume that the model scales linearly with similar infectious viral load per pL for all particle sizes.

II.3. Application of the Model to Four Covid-19 Outbreaks

Rather than presenting results, per se, we have organized a series of case studies into a discussion with two sections. This is meant to help potential users of the platform to develop a practical understanding of its capabilities and limitations. The section uses the platform to simulate four well-known COVID-19 outbreaks as a means to explore its utility and generalizability.

II.3.1. Case 1. Bus Riders in Eastern China

People who rode one bus to a worship event and back, in which there was at least one confirmed COVID-19 case, had a statistically significant higher risk of SARS-CoV-2 infection than individuals who rode a different bus to the same event. In the first bus, 23 out of 68 passengers tested positive for COVID-19 while none of the passengers in the second bus were diagnosed with COVID-19[47]. Table II.2 summarizes the inputs used in the risk estimation platform.

Table II.2. Input Parameters for Bus Riders in Eastern China.

Bus Riders in Eastern China			
Occupants (#)	68	Outdoor Air Supply ($\text{m}^3 \text{h}^{-1}$)	3.3 - 9.19
Time of event (h)	1.66	Filtration CADR ($\text{m}^3 \text{h}^{-1}$)	0
Volume (m^3)	80	Fractional time speak	0.2
Speak multiplier	1	Coughs h^{-1}	8
High emitter	1	Low emitter	0

The air exchange rate for the bus was not published. Using 4 air changes h^{-1} in the screening model described herein yields the observed 23 infections and 34% infection probability. We were only able to find one published study for which the air exchange rate for a bus was reported. Previously, researchers used sulfur hexafluoride release and decay and reported air exchange rates of 2.6 to 4.6 h^{-1} for a traveling school bus on its normal route [127]. This range bounds the air exchange rate of 4 h^{-1} that yields a model result consistent with disease cases in the outbreak.

II.3.2. Case 2. Two Choir Rehearsals in Skagit Valley

Another outbreak event occurred on the evening of March 10, 2020, in which 32 out of 61 members that attended a weekly rehearsal were confirmed positive for COVID-19 and another 20 were symptomatic but not tested or confirmed positive[45,72]. It is not clear whether all 32 cases (or 52 including unconfirmed and symptomatic) acquired the infection during the event on March 10th or whether some may have acquired the infection during the previous weekly practice on March 3rd. Importantly, three cases were confirmed in less than 24 hours and five more in less than 48 hours after the March 10th event, fairly short periods for symptom onset or positive test, suggesting that some

may have been infected during the March 3rd practice or elsewhere. Therefore, it is conceivable, but not shown, that some or all of these eight individuals could have also been contributing infectors during the March 10th event.

In this outbreak, the major unknown variables are the air exchange rate, how many choir members were emitting viral particles during the infection event, and which susceptible individuals were in contact with potential emitters for what durations during three sub-events on March 10th. The observed attack rate of the event, ranging from 53.3% to 86.7% (32-52 infected) is also in question given the potential number of additionally infected but pre- or asymptomatic choir members. Ventilation rates were estimated to be 0.3 – 1 h⁻¹ based on environmental heat balance estimates[128].

Therefore, we simulated this case in using the risk estimation platform with a range of high and low emitters, as well as three air exchange rates. Our assumptions for evaluating this case are outlined in Table II.3.

Table II.3. Input Parameters for Skagit Valley Choir Outbreak.

Skagit Valley Outbreak			
Occupants (#)	61	Outdoor Air Supply (m³ h⁻¹)	0.7,2.6 (ASHRAE)
Time of event (h)	2.5	Filtration CADR (m³ h⁻¹)	0
Volume (m³)	810	Fractional time speak	0.5
Speak multiplier	1.5	Coughs h⁻¹	8
High emitter	1&4	Low Emitter	0&7

According to the number of potential infectors in the space, we simulated this outbreak as the following three scenarios:

(a) 1 high emitter (the index case).

For a ventilation rate of 0.7 h^{-1} , each individual would have received a deposited respiratory dose of 2 pL. Our estimated simulation and the presence of one super spreader (the index case) would result in an estimated risk of 29%, yielding 18 people being infected during the event. It is possible that emissions from the single infector were higher than our assumed index case, the air exchange rate much lower, or that additional infectors were present during the infection event.

(b) 1 high emitter and 7 low emitters in the space (including those who tested positive on March 11 & 12).

Assuming that COVID-19 qRT-PCR tests after 1-2 days of exposure are not likely to produce positive results (due to virus incubation period), there could have been more than one index emitter in the space, with up to seven additional pre-symptomatic emitters in the rehearsal[129]. Therefore, we also simulated the outbreak with 1 high emitter and 7 low emitters (individuals who were confirmed positive on March 11 and March 12). With these inputs, the model estimates an infection probability of 87%, yielding 53 additional infections (for a total of 61), which is more than the number of reported (confirmed and suspected) cases.

c) 4 high emitters in the space (including those who tested positive on March 11).

In this case, the model estimates 46 additional infected individuals, for a total of 50, representing an infection probability of 75%.

There are a lot of unknowns regarding this Skagit Valley Choir outbreak and the primary intent of this analysis is to show how the model can be used to rapidly assess a range of scenarios or to potentially calibrate to one scenario.

II.3.3. Case 3. A 10-Hour Flight from London to Hanoi

Air travel is commonly judged to have low risk of transmitting SARS-CoV-2 through cabin air due to high ventilation rates and recirculation through HEPA filtration. However, it is conceivable that even relatively low particle concentrations associated with an infector can become an infection transmission concern on long flights[130].

A COVID-19 outbreak was reported to have been associated with a 10-hour flight from London, UK, to Hanoi, Vietnam, in early March 2020[49]. There were 16 crew members and 201 passengers on board. The index case was identified as having symptoms including sore throat and cough that began 3 days prior to the flight. She was confirmed positive after the flight through qRT-PCR test[49]. Among passengers who remained in Vietnam and were traced (all except 30 passengers), 16 positive cases were detected, including 12 (80%) which had travelled in business class with the index case. Additionally, one case was in economy class, and one case was among flight attendants that likely traversed between cabins. The business class section is spatially divided from the economy class with kitchens and bathrooms, and therefore we focused analyses on this discreet zone. We considered the impact of lower ventilation rates (approximately 0 h⁻¹) in the airplane cabin while the plane was on the ground, taxiing on the runway, and at the gate for boarding and deplaning. Then, we estimated a higher air exchange rate of 20 h⁻¹ supplied in the cabin during the flight, whereby 10 ACH of outside air is provided (representing 50% outside air fraction), and the equivalent of 10 ACH of additional clean

air delivery ($1650 \text{ m}^3 \text{ h}^{-1}$) is provided via central HEPA filtration. Business class passengers typically board before the main cabin and therefore experience lower airflow rates for longer periods of time preflight, thus increasing the initial aerosol concentration at the beginning of the event (Figure II.3). Table II.4 and Figure II.4 outline the parameters used in the simulation.

Figure II.3. Particle concentrations for outbreak on a 10-hour flight.

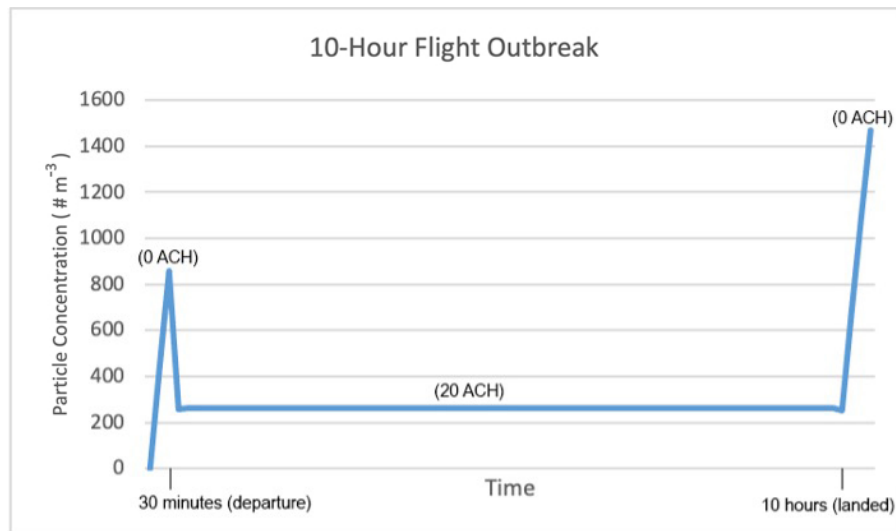
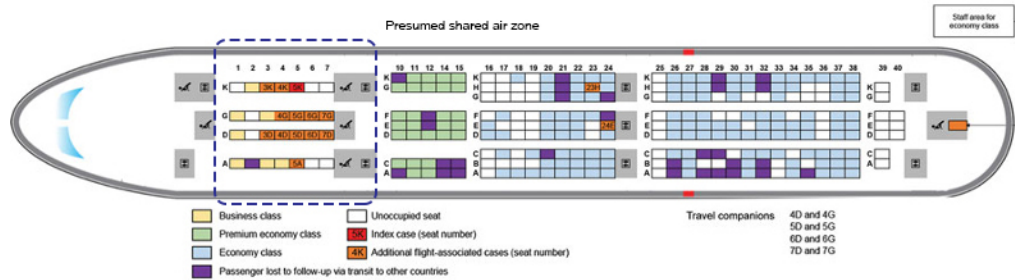


Table II.4. Input Parameters for Outbreak on a 10-Hour Flight.

10-Hour Flight Outbreak			
Occupants (#)	21	Outdoor Air Supply during flight ($\text{m}^3 \text{ h}^{-1}$)	10 ACH
Time of event (h)	0.5 (boarding) 9.5 (flight) 0.5 (departure)	Outdoor Air Supply during boarding & departure ($\text{m}^3 \text{ h}^{-1}$)	0
Volume (m^3)	165 m^3	Filtration CADR ($\text{m}^3 \text{ h}^{-1}$)	1650
Speak multiplier	1	Coughs h^{-1}	8
High emitter	1	Low emitter	0

Figure II.4. Seating location of passengers on Vietnam Airlines flight 54 from London, UK, to Hanoi, Vietnam, on March 2, 2020 following [49]



We created a digital model of the interior business class section of the AIRBUS-A350-900 aircraft and estimated 165 m³ as the volume of the zone. Since the index case had symptoms during the flight, we simulated this event with a high emitter (as explained in methodology section). According to the simulation with these parameters, each passenger was likely to have a respiratory deposited dose of 2.8 pL, which yields an estimated 37% infection probability and 8 additional passengers infected, close to the 10 infections reported. Ten infections (49% attack rate) would require 4 pL of deposited dose from either a higher emitter (15 more coughs h⁻¹) or an air exchange rate of 12 h⁻¹ during the in-flight period, both of which are reasonable values.

It is possible that large droplet, contact transmission, or concentrated aerosol plume transmission occurred between the index case and nearby passengers. According to the seating positions of the index case and the additional confirmed cases during the flight [49], some passengers (especially those sitting in 3K and 4K) may have been infected through large droplets or a concentrated aerosol plume emitted from the index case during coughing. However, infected passengers who were positioned in rows G, D, and A are more likely to have been exposed to the virus through only aerosol transmission. It is also possible that some transmission may have occurred prior to the flight, in the airport, boarding areas, or while boarding or deplaning. Still, even given

these possible alternate scenarios, the model reasonably estimates the number of reported cases likely to have occurred via aerosol transmission.

II.3.4. Case 4. Transmission of SARS-CoV-2 by Direct Airflow in a Restaurant in South Korea

According to a well-characterized epidemiological study for an event on June 17, 2020, a confirmed COVID-19 case was identified to have been infected in a restaurant in Jeonju, South Korea where indoor air circulation may have transmitted the SARS-CoV-2 virus 6.5 m away from the infector[44]. Case A and C were reported to be infected after 5 minutes and 20 minutes, respectively. According to floor plans (Figure II.5A), these cases were downstream of aerosols likely to contain SARS-CoV-2 virions expired by Case B and potentially Case D. Case D was travelling with index Case B but did not have symptoms during the event. The restaurant had a total floor area of 97 m² and reportedly had no windows or ventilation systems[44]. For event evaluation purposes, we assumed 77 m² of this space (excluding the kitchen area) is a shared-air zone and was used as an input to the risk estimation platform. Note that the available evidence suggests that this space may not have represented a well-mixed air volume, thus presenting a challenging case to the risk model. We simulated this event with one high emitter in one scenario and one high emitter and one low emitter (including case D) in an alternate scenario. The event duration is also unique in that there are important time overlaps between cases as outlined in Figure II.5B, presenting another challenge to the risk model. Case A only overlapped with Cases B and D for 5 minutes. Case C overlapped for 20 minutes, but also remained in the space for another 27 minutes after Cases B and D departed and would still be inhaling particles emitted by B & D for that duration. Thus,

the particle concentration over time ($\# \text{ m}^{-3}$) was expanded to account for the decay of expired particles for a period of 28 minutes after the emitter(s) had departed (Figure II.5B). The event duration was estimated to be 55 minutes (0.92 h) for the primary scenario. Simulation inputs are summarized in Table II.5.

Figure II.5. (A) Schematic floor plan of the South Korea outbreak restaurant, following[44], and (B) estimated particle concentrations assuming well-mixed conditions

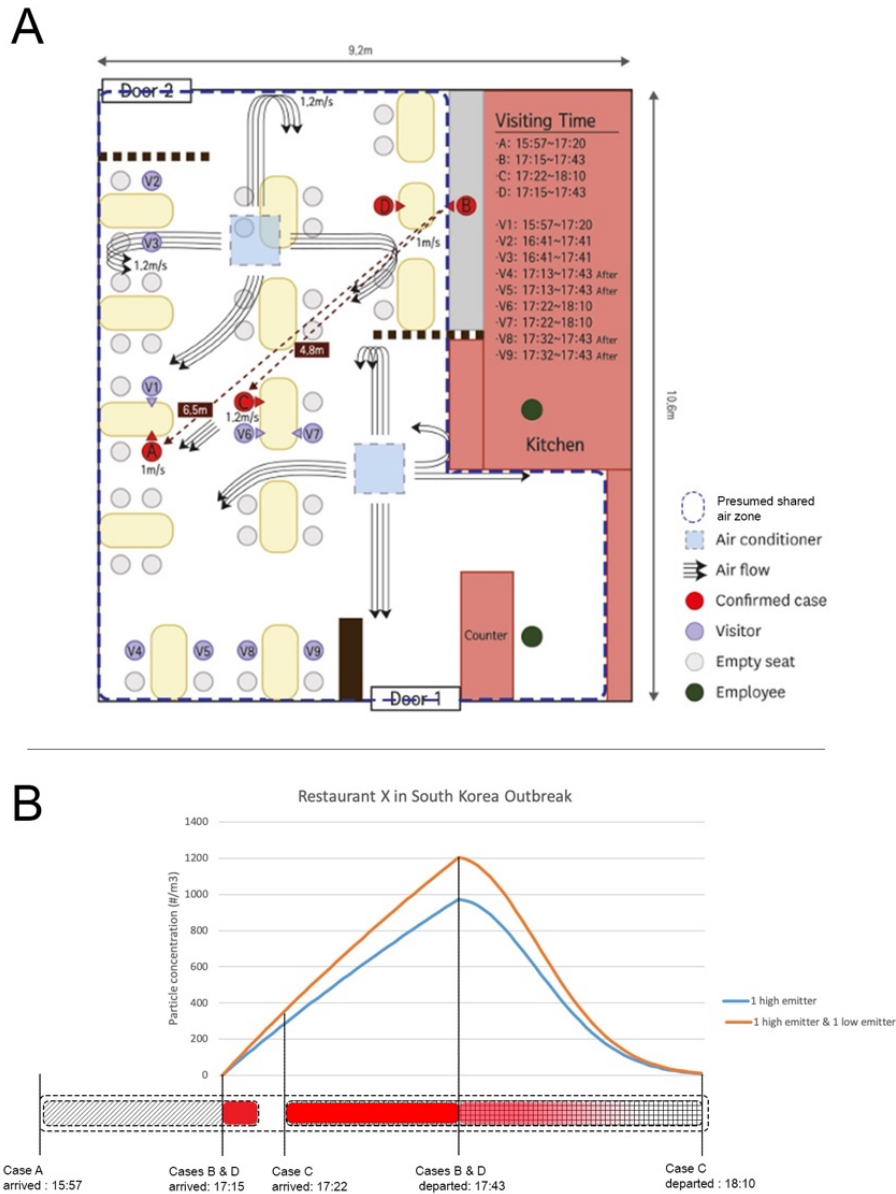


Table II.5. Input Parameters for Outbreak in a South Korean Restaurant.

South Korea Restaurant Outbreak			
Occupants (#)	13	Outdoor Air Supply (m³ h⁻¹)	0.2
Time of event (h)	0.92	Filtration CADR (m³ h⁻¹)	0
Volume (m³)	~185	Fractional time speak	0.2
Speak multiplier	1.5	Coughs h⁻¹	8
High emitter	1	Low emitter	0 & 1

The model estimated an infection probability of 9% for the entire (55-minute) event assuming Case B was emitting aerosols into the shared-air zone for a total duration of 27 minutes, and these aerosols containing SARS-CoV-2 virions remained in the air for additional 28 minutes following a decay curve presented in Figure II.5B. This 9% attack rate would lead to one infected person. Assuming that Case D contributed particles containing virions as a low emitter, the probability of infection increases to 13.5%, leading to approximately 2 persons being infected, similar to the 15.4% (2 infections) observed. Given what is reported in this case, it is probable that the directional airflow patterns contributed to a higher concentration of particles in the specific region within the restaurant where the rapid 5-minute exposure resulted in infection. However, despite this challenging event profile, the model reasonably estimates the event outcome.

II.4. Conclusion

There is compelling evidence that shows aerosol transmission has played an important role in the spread of COVID-19 globally. We have developed a mechanistic aerosol transmission risk estimation platform that incorporates the best available information regarding respiratory particle dynamics, viral viability, human respiratory

physiology, and viral dose-response proxies, to estimate infection probability based on a list of critical inputs. A demo version of the platform is available at

<https://safeairspaces.com/>.

In addition to the Restaurant X outbreak in Guangzhou, China, which provided a basis for anchoring the volume of inhaled and deposited dose into probability of infection, four other outbreaks that occurred prior to vaccinations or extensive mask wearing were simulated using the platform in conjunction with the best available data from epidemiological investigations. The simulations demonstrate that the risk estimation platform yields results that reasonably predict outbreak attack rates using the available information about the case and reasonable assumptions for missing information.

Therefore, users interested in managing risk, and estimating the effectiveness of layered risk reduction strategies can use the platform to guide decision-making. For example, users can explore which combination of risk reduction strategies estimate a risk profile below a specified transmission risk threshold, such as 5% or 2% likelihood of infection. Furthermore, users can explore risk reduction associated with specific strategies such as universal mask wearing, increased ventilation, or the addition of in-room filtration.

Although it is based on several assumptions, including a dose-response curve from a different coronavirus (HCoV-229E), we believe the platform is useful now, and the mechanistic approach will rapidly accommodate updates as soon as new information becomes available, especially with regard to SARS-CoV-2 human dose-response data. Additional updates related to dose-response data associated with SARS-CoV-2 variants and effectiveness of vaccines can be easily incorporated into the estimation platform.

II.5. Bridge

Aerosol transmission has played a significant role in the transmission of COVID-19 disease worldwide. In Chapter II we documented a COVID-19 aerosol transmission risk estimation platform that aimed to better explain how key parameters associated with indoor spaces and infector emissions affect inhaled deposited dose of aerosol particles that contain the SARS-CoV-2 virus. The model uses a mechanistic approach, accounting for particle emission dynamics, particle deposition to indoor surfaces, ventilation rate, and single-zone filtration. This chapter provides a quantitative assessment of some of the most important environmental mitigation strategies. However, the effectiveness of these strategies needs to be studied in real-world settings before they can be applied as recommendations in codes and national guidelines.

To do so, in Chapter III, we aimed to provide the first real-world evidence that environmental mitigation strategies such as ventilation, filtration, and humidification substantially reduce the aerosol viral load. In addition to ventilation and filtration, we studied humidification impact on aerosol viral load. Humidification is not currently added as an input parameter in our aerosol risk estimation platform because the data were not available. The findings from Chapter III will contribute to developing future versions of the SafeAirSpaces risk estimation platform.

Moreover, Chapter III aimed to test assumptions that fine aerosol particle counts of less than 4 μm represent critical sizes for the characterization of the variance of aerosol viral load in participants who were diagnosed with COVID-19.

III. ENVIRONMENTAL MITIGATION OF AEROSOL VIRAL LOAD

This chapter is published as:

Hooman Parhizkar, Leslie Dietz, Andreas Olsen-Martinez, Patrick F Horve, Liliana Barnatan, Dale Northcutt, Kevin G. Van Den Wymelenberg. Quantifying environmental mitigation of aerosol viral load in a controlled chamber with participants diagnosed with COVID-19, *Clinical Infectious Diseases*, 2022; ciac006, <https://doi.org/10.1093/cid/ciac006>

For this project, Dr. Kevin G. Van Den Wymelenberg performed funding acquisition and managed the investigation team. Dr. Kevin G. Van Den Wymelenberg and I conceived of project scope and methodology with input from Leslie Dietz and Patrick F. Horve. Dr. Kevin G. Van Den Wymelenberg and Leslie Dietz enrolled and consented study participants. Dale Northcutt worked with all other authors to set up modular room and all research instrumentation. I collected biological specimen with supports from Liliana Barnatan, Leslie Dietz, and Andreas Olsen Martinez. Liliana Barnatan, Leslie Dietz, Patrick F. Horve, and Andreas Olsen Martinez performed laboratory analyses. I performed data curation, data exploration, developed final analysis scripts, performed final analysis, and created visualizations with support from all authors. I developed the original manuscript with direction and input from Dr. Kevin G. Van Den Wymelenberg. All authors provided manuscript revisions and edits on subsequent manuscript drafts and approved final manuscript. The supplemental document associated with this article including supplemental figures & tables are presented in Appendix A-D. The project of this chapter was funded by ThermoFisher Scientific under award number 4133V.

III.1. Introduction

Severe acute respiratory syndrome coronavirus 2 (SARS-CoV-2), the causative agent of Coronavirus disease 2019 (COVID-19), has resulted in 274,472,724 confirmed cases with more than 5,012,337 deaths globally, as of 03 November 2021[131]. There is substantial evidence that inhalation of aerosol particles containing viable SARS-CoV-2 virions is the primary route of human-to-human transmission[102,132–138]. Modeling of the impact of non-pharmaceutical interventions on the probability of COVID-19 infection and mortality rate [96,139–142] suggests that indoor congregation is the primary driver for COVID-19 disease transmission[143]. Moreover, recent comprehensive reviews highlight the importance of airborne transmission pathway via fine aerosols [17,144,145]. Therefore, better understanding and quantifying the relationship of human factors, design, and building operation practices on the abundance and dispersion of viral load in indoor spaces is necessary to combat disease transmission [23].

Breathing and talking are some of the human expiratory activities that have been studied to determine how these activities are associated with concentrations of viral pathogens[19,146]. These studies have contributed valuable information about the viral load of size fractionated aerosols[2,135]. In addition to human expiratory factors, indoor space design and engineering practices such as ventilation, filtration, and humidity control may influence the abundance and infectious fraction of the environmental viral load, and therefore reduce inhalation dose[2,59,87,92,147–149]. However, these indoor environmental interventions need to be studied independently through controlled

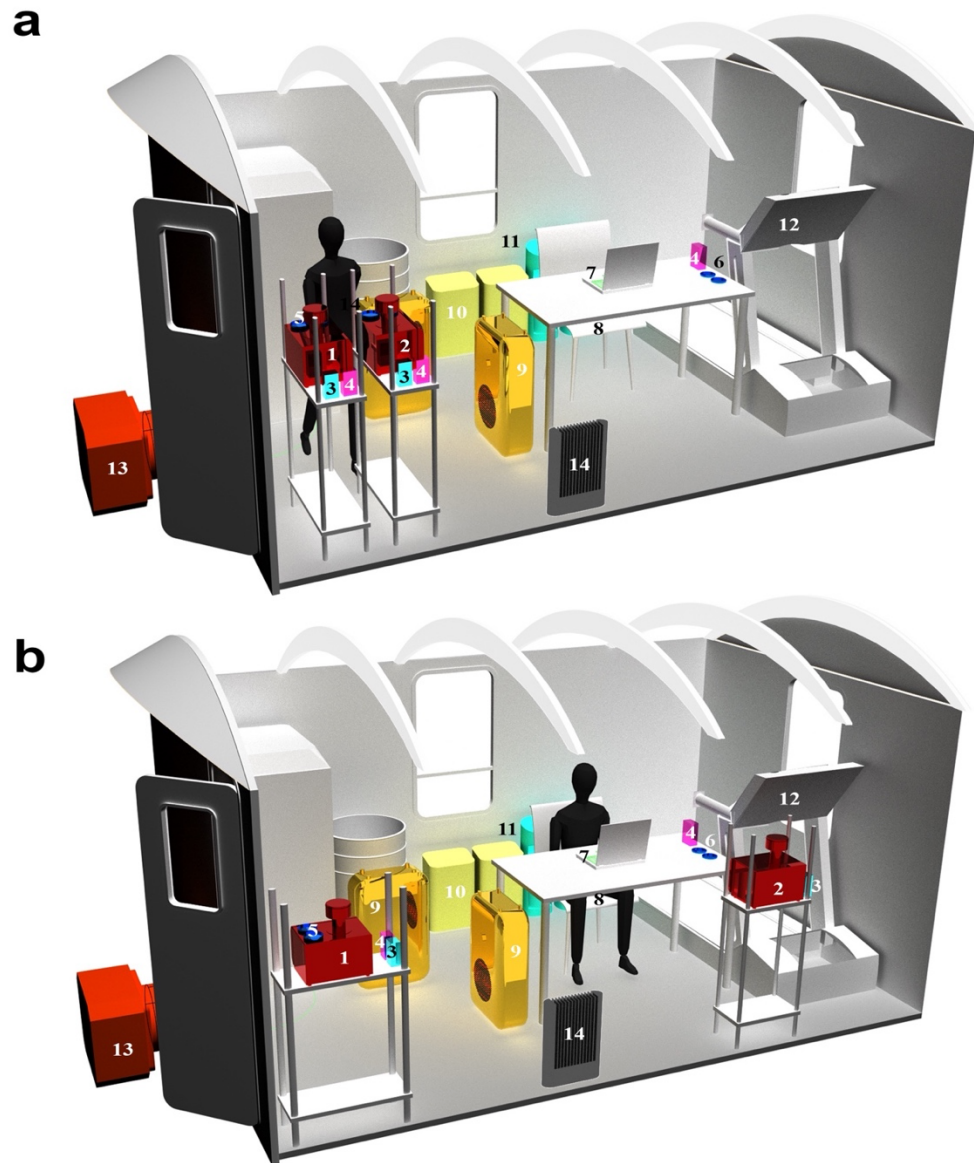
experiments to quantify their impacts, while minimizing confounding variables, especially with regard to aerosols that may contain SARS-CoV-2.

In this research, we sought to better understand viral abundance and dispersion associated with differing degrees of expiratory activity, ventilation, filtration, and humidification through controlled experiments in a quasi-field setting. We measure viral RNA of SARS-CoV-2 using quantitative reverse-transcription polymerase chain reaction (qRT-PCR) techniques as a proxy of viral load in humans and environmental aerosols and surfaces. We studied 11 human participants that were diagnosed with COVID-19 in a controlled chamber measuring 4.3 m in length, 2.8 m in width, and 2.5 m in height (28.04 m³). Our research protocol comprised a 3-day study for each participant in which human activity and environmental factors (ventilation rate, in-room filtration, humidity control) were studied as independent variables.

III.2. Methodology

A rapid deployment modular unit (RDM) was used as an environmentally controlled chamber (Figure III.1) for this human participant study during Winter and Spring 2021. The study population included 11 participants between the age of 18 and 24 (Supplemental table III.1). Two high-flow (200 L/min) AerosolSense air samplers (Thermo Fisher Scientific) were placed approximately 1.2 and 3.5 meters from the participants. At the end of each study period, samples from the air samplers (near, far), high-touch surfaces (phone, computer, chair), settling plates (near, far), and human specimens (shallow nasal) were collected and transported to a BSL-2 laboratory on the University of Oregon campus in Eugene, Oregon, for further molecular analysis.

Figure III.1. Rapid deployment modular unit (RDM), a) higher expiratory trials (S1), b) regular trials (S2)



Legend

- | | | | |
|------------------------------|--------------------------------|----------------------|---------------------------|
| 1- Far field AerosolSense | 2- Close field AerosolSense | 3 - Particle counter | 4 - CO ₂ onset |
| 5 - Far field settling plate | 6 - Close field settling plate | 7 - Computer | 8 - Chair |
| 9 - In room HEPA filters | 10- Dehumidifiers | 11- Humidifiers * | 12 -Treadmill |
| 13 - HEPA exhaust | 14 - Heaters * | | |

* Only one object of this kind is visible in this figure

Trials were conducted in two different set-ups over three days (Table III.1). Trials with a S1 suffix indicate Setup-1 where both air samplers were placed next to each other

for short duration and higher expiratory tests (Figure III.1a). During cough trials, participants were instructed to conduct 10 uncovered coughs into an area over the air samplers, particle counters (TSI AeroTrak 9306), and CO₂ (Onset HOBO MX1102A) sensors. During speak tests, participants were instructed to conduct continuous vocalization using a standardized CDC defined passage[150] (Appendix B) for 5 minutes with normal and higher amplitude at their discretion, respectively[151]. A S2 suffix indicates trials where air samplers were located at 4 ft (near field) and 11 ft (far field) of participant’s sitting position (Figure III.1b). During S2 trials, participants conducted routine activities at a desk, including sitting and standing, sitting silently, sitting and participating in an online conference meeting, or were invited to walk on treadmill (physical activity day) (Figure III.1b). Institutional approvals, data availability, and methods related to RDM layout, participant recruitment, sample collection, molecular analysis, and statistical analysis are described in Appendix C.

Table III.1. Study plan for participants that were diagnosed with COVID-19; S1 and S2 refer to experimental setup 1 and setup 2

Set-up	1. Physical activity	2. Removal mechanism	3. Relative humidity (RH)
S1	10 coughs in <u>1 minute</u>	10 coughs in <u>1 minute</u>	10 coughs in <u>1 minute</u>
S1	Speak for <u>5 minutes</u>	Speak for <u>5 minutes</u>	Speak for <u>5 minutes</u>
S1	Speak loudly for <u>5 minutes</u>	Speak loudly for <u>5 minutes</u>	Speak loudly for <u>5 minutes</u>
S2	<u>1-hour</u> regular sitting	<u>1-hour</u> regular sitting	<u>1-hour</u> regular sitting
S2	<u>1-hour</u> standing	<u>1-hour</u> sitting at ~9 ACH	<u>1-hour</u> sitting at low RH
S2	<u>30-min</u> sitting silently	<u>1-hour</u> sitting at ~3 ACH	<u>1-hour</u> sitting at low RH
S2	<u>30-min</u> sitting speaking	<u>1-hour</u> sitting at ~9 ACH	<u>1-hour</u> sitting at high RH
S2	<u>15-min</u> walking on treadmill	<u>1-hour</u> sitting at ~4.5 ACH	<u>1-hour</u> sitting at high RH
S2		<u>1-hour</u> sitting with HEPA filtration	

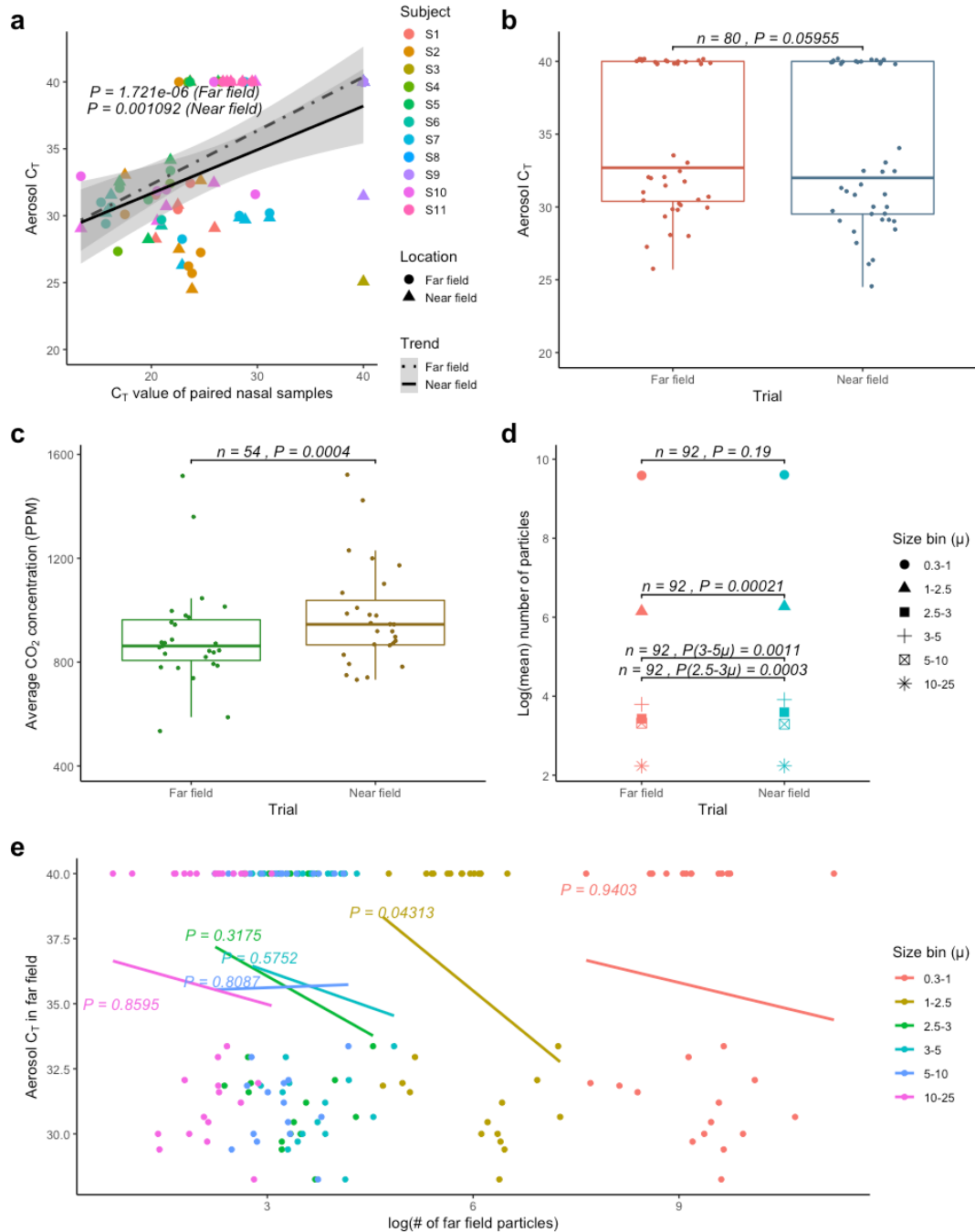
III.3. Results

III.3.1. Near and Far Field Aerosol Samples and Paired Human Specimens

To quantify the relationship between viral loads (RNA copies) in human nasal and aerosol samples, we paired the outcome of each aerosol sample collected with its corresponding shallow nasal sample for both near and far AerosolSense samplers during trials when participants were sitting or standing for one hour at ~ 0 ACH under typical ambient conditions without environmental interventions. We defined routine trials according to following conditions: 1) participants conducted typical office activity while sitting or standing for 1-hour, 2) ambient environmental conditions were maintained using only electric resistance heaters without ventilation at ~ 0 ACH, and 3) participants could have spontaneously coughed because of their symptoms but were not instructed to conduct any expiratory activity during routine trials. Figure III.2a shows the relationship between nasal viral load and near field and far field aerosol viral load for all routine trials. Note that negative samples are defined with a C_T value of 40.

The coefficients associated with significant regression models presented in Figure III.2a indicate that an increase in viral load equivalent to $-1 C_T$ in human nasal samples is associated with increased near field viral load of $-0.326 C_T$ ($R^2 = 0.2276$, $P = 0.001092$) and increased far field viral load of $-0.40 C_T$ ($R^2 = 0.4026$, $P = 1.721e-06$). The difference of means between the aerosol C_T value of near field and far field aerosol samples was $1.058 C_T$, indicating lower viral load for far field samples; however, the paired t-test differentiating near field and far field samples was not significant ($P = 0.05955$) (Figure III.2b, note that black solid horizontal line represents median in all box plots).

Figure III.2. a) The correlation of near field (1.2 m) or far field (3.5 m) aerosol viral loads (RNA) with corresponding human nasal samples during routine trials b) comparison of near field and far field aerosol viral loads for routine trials, c) comparison of mean CO₂ concentrations in the near field and far field for routine trials, d) paired t-tests for all particle size bins at near field and far field for routine trials, e) correlation between mean far field aerosol viral loads and the corresponding mean concentration of far field particles for routine trials.



Therefore, we also report the significant coefficient for all nasal and aerosol samples in routine trials which indicates that an increase in viral load equivalent to -1 C_T in nasal samples is associated with an increase in room aerosol viral load of -0.362 C_T ($R^2 = 0.3119$, $P = 1.675e-08$, Supplemental figure III.1). Based upon qRT-PCR theory, a -1 C_T difference is approximately equivalent to double the viral load[152]; thus, a doubling of viral load in nasal samples corresponds to a ~35% increase in aerosol viral load for samples collected in the room. To our knowledge this is the first reported relationship between environmental aerosol viral load and human viral load in a controlled environment (28,040 L3 room, ~0 ACH, one-hour trials, single COVID-19 positive individual).

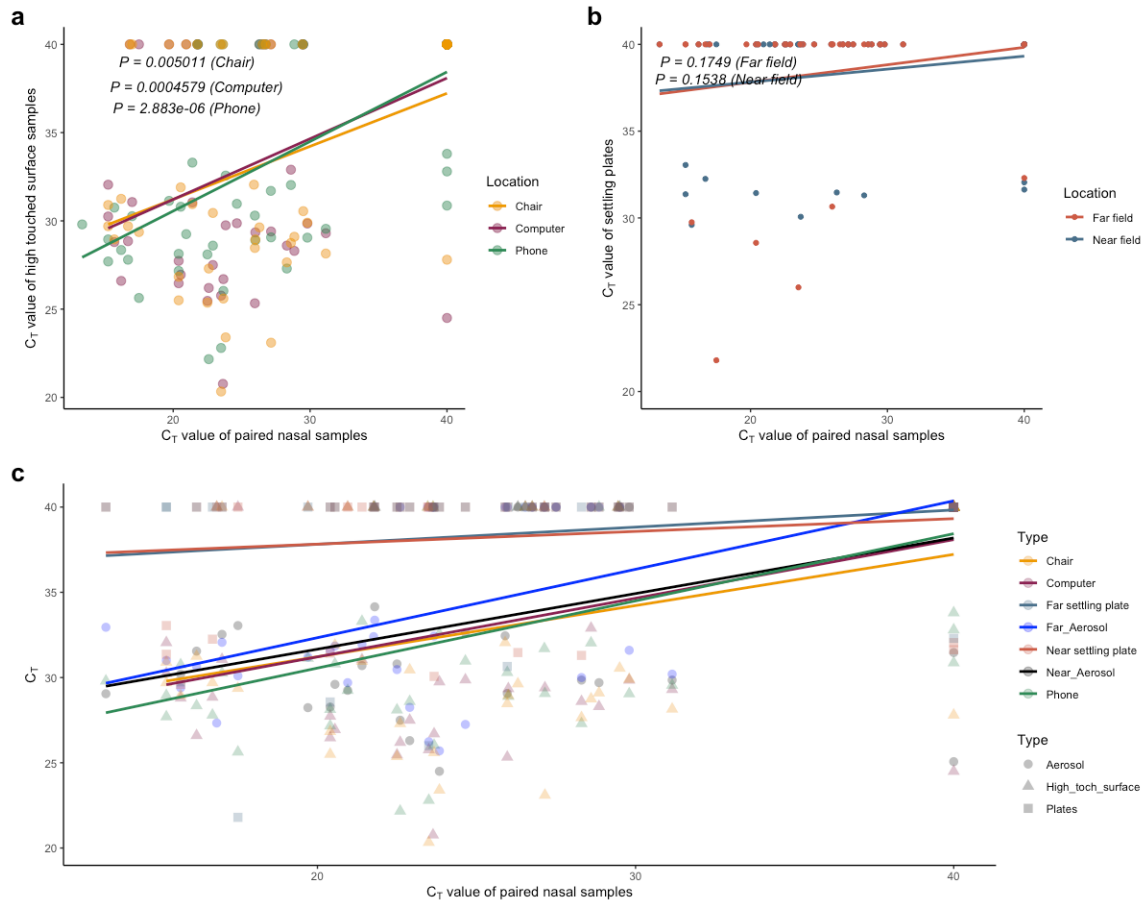
Furthermore, we found a statistically significant difference between the mean CO₂ concentration recorded at near field and far field, where CO₂ concentrations of near field was 80 PPM higher than in the far field ($P = 0.0004009$) (Figure III.2 C). Analysis of particles for routine trials indicates that there is a statistically significant difference between the number of particles collected in the range of 1 μm -5 μm within the near field versus the far field, as summarized in Figure III.2 d (expanded in Supplemental figure III.2). As shown in Figure III.2 e, we identified a significant relationship between aerosol viral load and far field particle counts within the size bin 1 μm - 2.5 μm where increased number of particles within this size bin is associated with higher aerosol viral loads ($R^2 = 0.1112$, $P = 0.04313$). The relatively low reported R^2 is likely due to the reality that there are many particles in the room that are not human-sourced bioaerosols, and therefore this regression should not be interpreted as an absolute prediction model. We also report a statistically significant positive correlation between the average far field

CO₂ concentration and the number of particles of 0.3 μm -3 μm in far field for routine trials (Supplemental figure III.3) which lends more confidence in the interpretation that the observed correlation between aerosol viral load and the number of particles of 1 μm – 2.5 μm is related to bioaerosol emissions. These results provide further evidence of the importance of fine aerosols in the potential for COVID-19 disease transmission in both near and far fields.

III.3.2. High-Touch Surfaces, Settling Plates, and Paired Human Specimens

Human specimens were compared to paired samples collected from the participants' phone (screen), computer (adjacent to keyboard), and chair (described as high-touch surfaces), and from near field settling plates (on participant's desk) and far field plates (adjacent to far field air sampler). Figure III.3a illustrates the significant linear regressions for the viral load (RNA) on each high-touch surface relative to paired nasal samples. Figure III.3b illustrates the significant linear regressions for viral load in settling plates (near and far) relative to paired nasal samples. There are no significant differences between the viral loads found in near field and far field setting plates, nor are there significant differences between any of the high-touch surfaces (Supplemental figures 4 & 5). Figure III.3c illustrates the significant regressions for all sampling types relative to human nasal samples within a single figure and indicate that high-touch surfaces and aerosol samples have stronger correlations to human viral loads than settling plate surfaces. This lends more evidence that emitted virions are present in indoor spaces within smaller particles that remain as aerosols for long time periods.

Figure III.3. a) viral load (RNA) on each high-touch surface relative to paired nasal samples, b) viral load (RNA) on settling plates at near and far field relative to paired nasal samples, c) The correlation of each sample type (Aerosol, high touched surfaces, and settling plates) to paired nasal sample.



III.3.3. High Expiratory Activity, Particles, and Aerosol Viral Load

We find a significant correlation between aerosol viral load associated with high expiratory activities and paired nasal samples where an increase in viral load equivalent to -1 C_T in human nasal samples is associated with increased immediate field (<1m, Figure III.1a) aerosol viral loads as follows: $-0.189 C_T$ ($R^2 = 0.09058$, $P = 0.0225$) for 1-minute cough tests, $-0.271 C_T$ ($R^2 = 0.1979$, $P = 0.00115$) for 5-minute speaking tests, and $-0.229 C_T$ ($R^2 = 0.1796$, $P = 0.00141$) for 5-minute speaking loudly tests (Supplemental figure III.6). Furthermore, we find a significant positive relationship between the mean number of immediate field particles during high expiratory activities

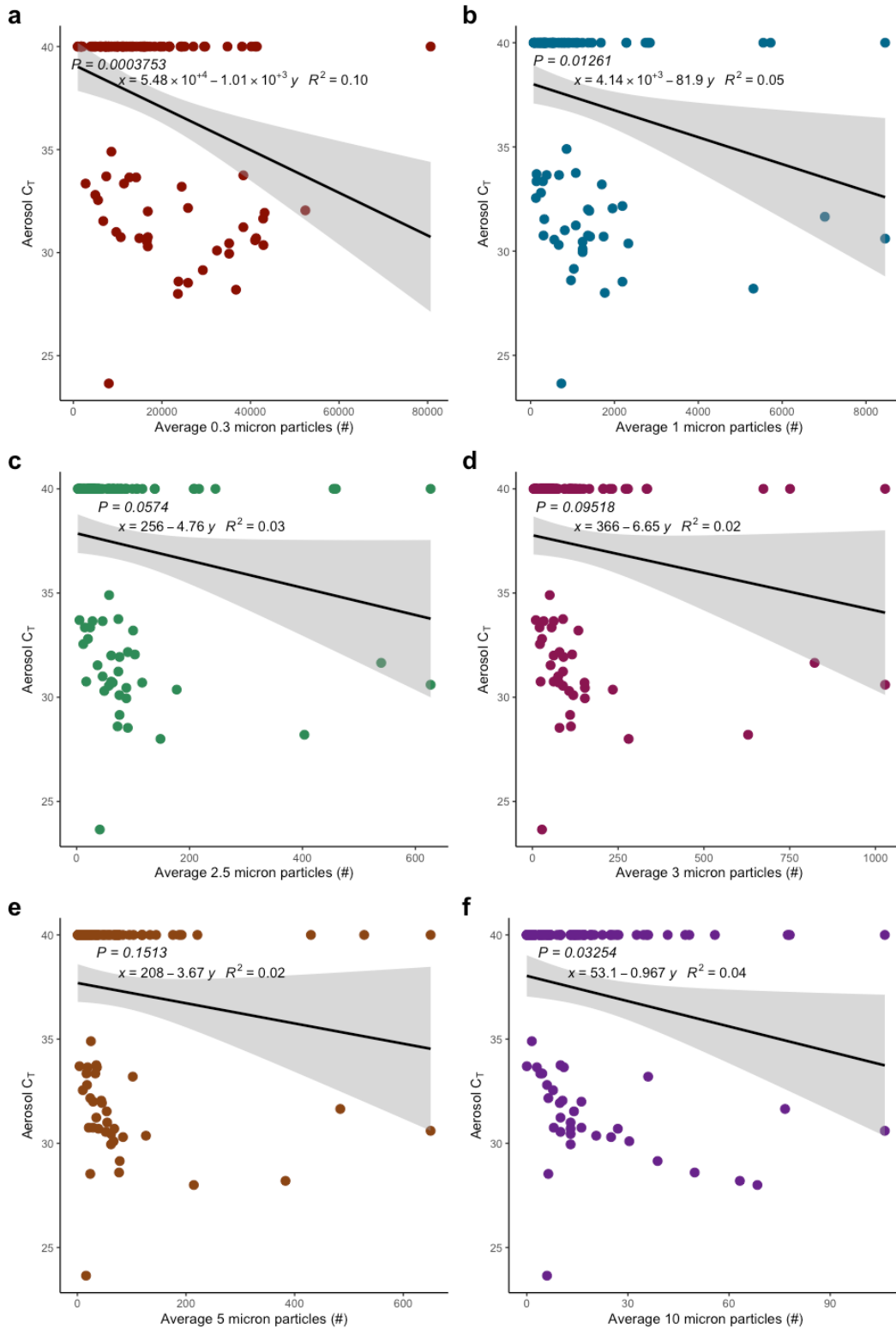
(Setup 1) in the size ranges 0.3 μm -1 μm (Figure III.4a), 1 μm -2.5 μm (Figure III.4b), and 10 μm -25 μm (Figure III.4e) and the viral load in the immediate field aerosols, while the other particle size bins are not significant (Figure III.4). We provided further analysis of the relationship between different respiratory activities and viral loads in Supplemental figures III.7 & III.8. Further discussion about the relationship between aerosol viral loads and particles of different size bins are provided in the, Appendix D.

III.3.4. The Impact of Ventilation and Filtration on Aerosol and Surface Viral Load

Indoor air exchange rate, measured in Air Changes per Hour (ACH), has previously been demonstrated to reduce indoor particles and therefore hypothesized to reduce the concentration of viral aerosols, corresponding inhalation dose, and consequently the probability of indoor occupants acquiring infection[17,153–155]. Few studies have measured the relationship between ventilation, filtration and aerosol viral load[53]. Therefore, we investigated the impact of alternate air exchange rates, using 100% outside air (OSA) and filtration levels during removal mechanism trials.

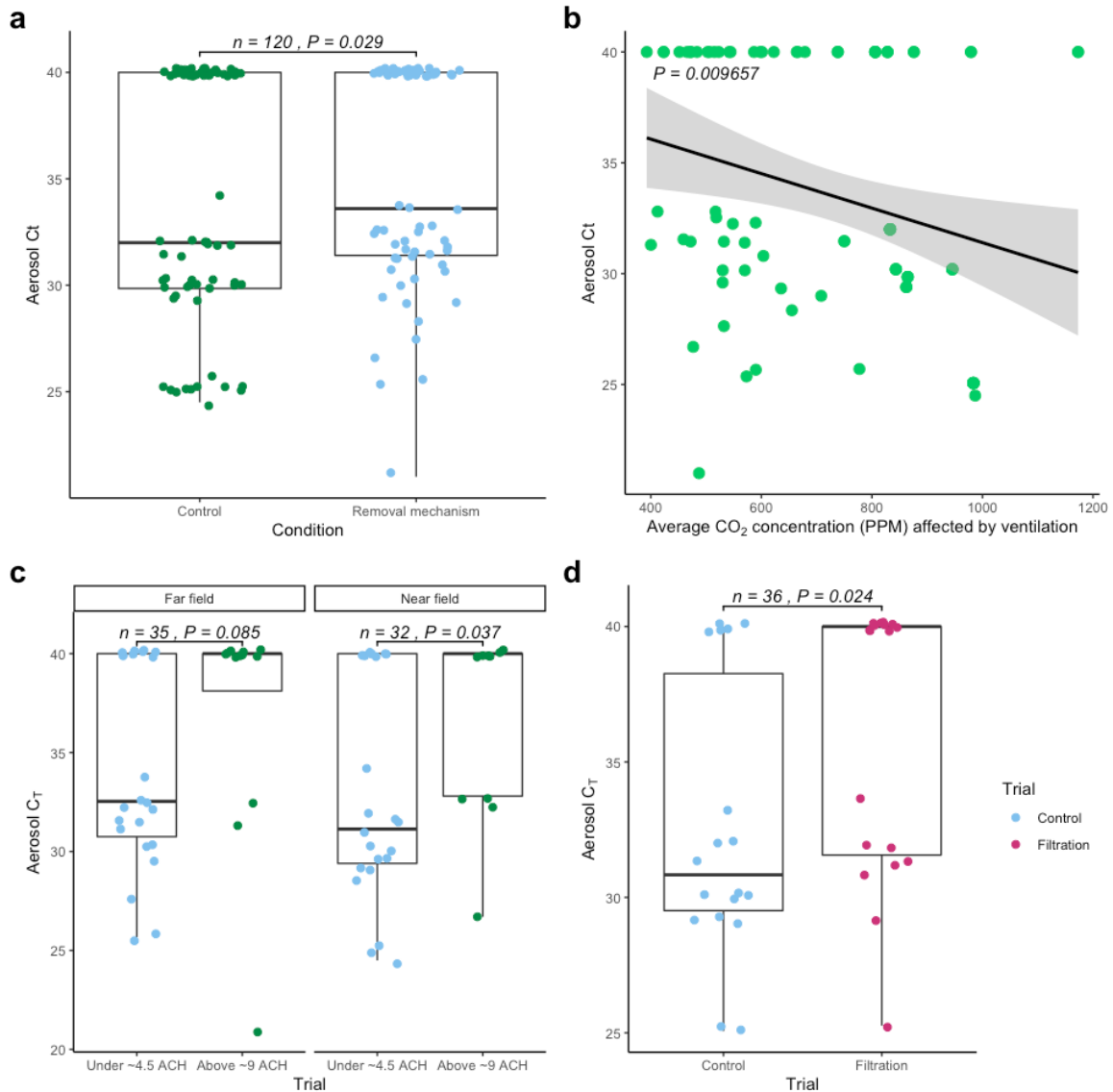
As shown in Table III.1, each removal mechanism day began with a baseline ~ 0 ACH trial, followed by four 100% OSA ventilation trials (two at ~ 9 ACH and two at $\sim 3 - 4.5$ ACH) provided by an exhaust fan (fitted with HEPA filter for infection control). Thereafter, a single trial with two in-room HEPA filters (without OSA) was conducted. All removal mechanism trials and the ~ 0 ACH control trials were conducted for a duration of one hour. We found a significant difference between control trials and all removal mechanism trials ($P = 0.029$, Figure III.5a).

Figure III.4. Linear correlation between C_T value and particles for a) 0.3-1 μm particles, b) 1-2.5 μm particles, c) 2.5-3 μm particles, d) 3-5 μm particles, e) 5-10 μm particles, and f) 10-25 μm particles.



In Figure III.5a we show a significant difference between control trials and paired removal mechanism trials, while in Figure III.5b we show a significant correlation for all control trials at ~ 0 ACH and all ventilation trials with 100% OA organized by mean CO_2 concentration. Trials with less than ~ 4.5 ACH (including ~ 0 ACH trials) were associated with significantly higher aerosol viral loads in the near field when compared with trials greater than ~ 9 ACH, with a mean difference of $-3.6 C_T$ ($P = 0.037$, unpaired t-test, Figure III.5c). Even though the mean difference of aerosol viral load in the far field for trials with less than ~ 4.5 ACH (including ~ 0 ACH trials) was higher than trials with greater than ~ 9 ACH, we did not observe a statistically significant difference for far field aerosol viral load ($P = 0.085$, unpaired t-test, Figure III.5c). When examining total room aerosol viral load (near field and far field together), we report that trials with less than ~ 4.5 ACH (including ~ 0 ACH trials) were associated with statistically higher viral load than trials with greater than ~ 9 ACH, with a mean difference of $-3.2 C_T$ ($P = 0.01153$, unpaired t-test, Supplemental figure III.9). Our research provides further evidence that improved ventilation and filtration is beneficial for both near field and far field aerosol viral load (Supplemental table III.2). Given these relationships within this room (Figure III.5b), ventilation trials indicate that an increase in ~ 128 PPM of CO_2 concentration corresponds with an increase in aerosol viral load equivalent to $-1 C_T$, thus, approximately a doubling of the viral load. Moreover, filtration trials indicate that there is a significant difference between trials with only in-room HEPA filtration ($\sim 1000 \text{ m}^3/\text{hr}$) and paired control trials at ~ 0 ACH, where HEPA trials have lower viral load equivalent to $3.240741 C_T$ ($P = 0.029$), thus, approximately an order of magnitude reduction (Figure III.5d).

Figure III.5. The impact of ventilation and filtration on C_T value of aerosol samples, a) match paired comparison between trials with removal mechanism trials (filtration and ventilation) and control trials with ~ 0 ACH, b) linear correlation between aerosol C_T value and paired mean CO_2 concentration affected by only ventilation (same physical activities), c) Comparison of aerosol C_T for ventilation trials of under ~ 4.5 ACH and above ~ 9 ACH in near field and far field, d) match paired comparison of aerosol C_T for trials with in-room HEPA filtration and corresponding control trials with ~ 0 ACH.



Our results provide evidence that increased air exchange (~ 9 ACH with 100% OSA) or in-room HEPA filtration (~ 1000 m^3/hr) yields reduced aerosol viral load, and reason therefore suggests these measures are likely to reduce inhalation dose and the

probability of infection in indoor spaces. We found no statistical difference between aerosols captured during control trials with ~ 0 ACH and those with $\sim 3 - 4.5$ ACH; however, this may be related to limitations in sample size. Among three types of high-touch surfaces collected in this study, increased ACH was associated with lower viral load on participant's computers, with a mean difference of $4.033 C_T$ ($P = 0.002323$) whereas phone and chair samples showed no significant difference with air exchange rate (Supplemental figure III.10).

III.3.5. Relative Humidity and Aerosol Viral Load

Relative humidity is hypothesized to impact aerosol pathogens and disease transmission in three ways; (1) improved human immune response[154] (2) reduced viability in aerosols at RH between 40-60%[87,143], and (3) increased particle deposition[17,156]. The structure and behavior of aerosol pathogens, specifically particle size, settling rate, and diffusion, are each affected by RH[95,156]. In this study, we aimed to measure environmental viral load at different RH conditions. Two dehumidifiers and two humidifiers were used to regulate RH to low (22.2% - 38.9%, mean = 28.8%) and high (44.83 % - 61%, mean = 53.9%) levels during the "relative humidity" trials. Each participant's relative humidity day started with a 1-hour control trial with ~ 0 ACH and RH at ambient conditions, followed by two 1-hour dehumidification trials and two 1-hour humidification trials. Room aerosol C_T values were paired with mean RH values (ranging from 20-70%) recorded for each trial.

Relative humidity trials indicate that an increase of $\sim 11.85\%$ in RH corresponds with a decrease in aerosol viral load equivalent to $1 C_T$ ($P = 0.008$), thus, approximately a 50% reduction in aerosol viral load, as shown in (Figure III.6a). Similarly, an increase of

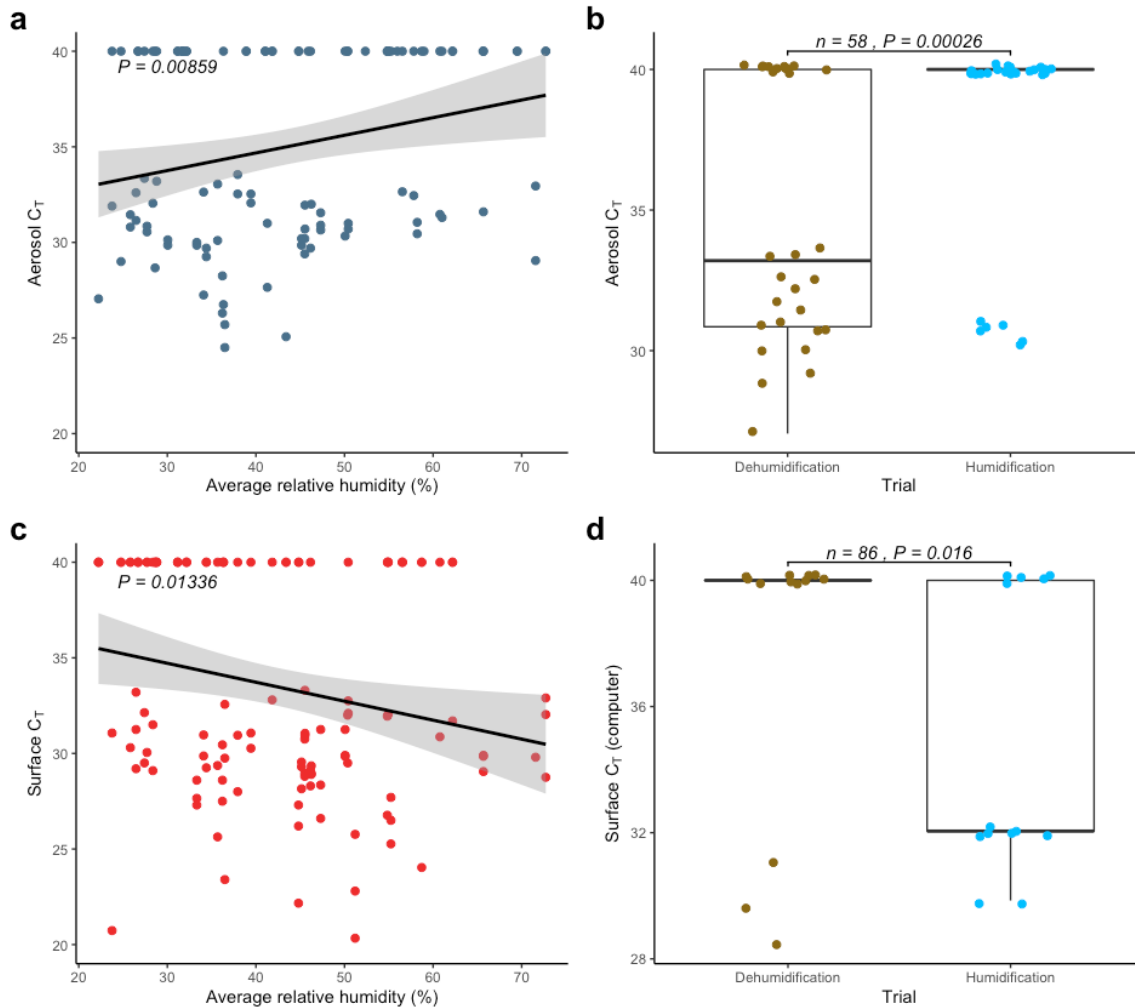
~10.02% in RH corresponds with an increase in surface (chair, computer, phone) viral load equivalent to $-1 C_T$ ($P = 0.01$) as shown in Figure III.6c, consistent with increased particle deposition. Figure III.6b shows the significant decrease in aerosol viral load equivalent to $3.289 C_T$ (paired t-test, $P = 0.0002643$) for humidification trials as compared to dehumidification trials. Conversely, Figure III.6d shows the significant increase in computer surface viral load equivalent to $-2.873 C_T$ (paired t-test, $P = 0.01593$) for humidification trials as compared to dehumidification trials.

This is one of the first studies that investigated the role of relative humidity on viral RNA in aerosols and surfaces in a realistic setting. Our results suggest that increased RH corresponds with decreased viral load in aerosols and increased viral load on select indoor surfaces, consistent with an increased rate of particle deposition. Since several studies have demonstrated that there is a substantially higher risk for aerosol mediated transmission than fomite mediated transmission[157], active humidity control (including humidification, or reduced dehumidification) could be implemented to reduce aerosol mediated COVID-19 transmission risk reduction in indoor spaces. Of course, humidification controls must be properly maintained and managed to avoid condensation and mold propagation.

III.4. Conclusion and Limitations

All participants were given the opportunity to opt out of the study at any time, thus two subjects only completed the first day of study. There were some modest inconsistencies between trial durations in order to accommodate participants' needs. Not all participants walked on the treadmill, and some walked at different speeds or for different durations.

Figure III.6. a) Correlation between aerosol C_T value and mean relative humidity among dehumidification, humidification, and control trials b) paired comparison of aerosol C_T between Dehumidification and Humidification trials, c) Correlation between surface C_T value and mean relative humidity among dehumidification, humidification, and control trials, d) paired comparison of select surface (computer) C_T between Dehumidification and Humidification trials.



Participants may have presented inconsistent symptoms (such as coughing) during the course of the experiments; however, the control trial at the beginning of each day addresses a substantial part of this limitation. While this was an extensive study design, conducted over three days per participants (Supplemental figures III.11 & III.12), the total number of unique participants ($n=11$), and limited age range (18-24 years of age) of

participants, presents some limitations to generalizability. RNA samples were not assessed for viability.

In summary we found statistically significant:

- 1- positive relationships between viral load (RNA) found in human specimens and paired aerosol and surface samples at ~0 ACH and ambient conditions for sitting and standing trials (routine trials) as well as trials with high expiratory activities (coughing, speaking, and speaking loudly);
- 2- positive relationship between viral load in near field aerosols captured during periods of higher expiratory activity and near field particles of 0.3 μm - 1 μm , 1 μm - 2.5 μm , and 10 μm - 25 μm in size, but no statistical significance for 2.5 μm - 10 μm particles;
- 3- increased CO₂ concentrations and particle counts in the range of 1-5 μm measured in the near field as compared to the far field for routine trials;
- 4- positive relationship between aerosol viral load in the far field and the number of corresponding far field particles detected in the range of 1-2.5 μm ;
- 5- inverse relationships between viral load found in aerosols and degree of ventilation, as well as in-room filtration;
- 6- relationships between viral load and degree of relative humidity; whereby higher RH is associated with lower viral load in aerosol samples and higher viral load in select surface samples, consistent with increased particle deposition on surfaces.

III.5. Bridge

In Chapter III we recruited 11 participants diagnosed with COVID-19 to individually occupy a controlled chamber and conduct specified physical activities under a range of environmental conditions; we collected human and environmental samples over a period of three days for each participant. We found that aerosol viral load in the far-field is correlated with the number of particles within the range of $1\ \mu\text{m}$ - $2.5\ \mu\text{m}$, providing real-world support for the use of particles ranging from $1\text{-}4\ \mu\text{m}$ for the risk estimation platform described in Chapter II.

We also found that increased ventilation and filtration significantly reduced aerosol and surface viral loads, while higher relative humidity resulted in lower aerosol and higher surface viral load, consistent with an increased rate of particle deposition at higher relative humidity. According to Supplemental table III.2, trials with outdoor air exchange rates of 9ACH were associated with $2.57\ C_T$ lower viral load in aerosol samples, compared to trials with 0ACH. Based upon qRT-PCR theory, a $-2.57\ C_T$ difference is approximately equivalent to ~ 5.7 reduction in the concentration of SARS-CoV-2 in the air. Using the SafeAirSpaces aerosol risk estimation platform (Chapter II), we simulated the RDM described in Chapter III experiments with assumptions of having one infected person in the room and the total duration of 60 minutes. The results of simulation indicated that increasing air exchange rate from 0 to 9 ACH in RDM corresponds to ~ 5.4 times lower inhaled and deposited dose in human's respiratory system, which agrees with values measured in a real-world case study. This comparison provides more confidence that the mechanistic risk estimation platform is an effective tool for reevaluating the design and operation of buildings during and after COVID-19 pandemic. However, questions about the reliance on an assumption of “well-

mixed rooms” remain. Specifically, Figure III.2 and Supplemental figure III.2 in Chapter III explores potentially important differences between near-field and far-field exposure zones within the RDM. While Chapter III identifies significant differences for particles and CO₂, it technically did not identify a statistically relevant difference for aerosol viral load. Thus, we aimed to further explore the potential differences of near- and far-field exposure risks during a 60-minute trial in Chapter IV using a novel volatile organic compound (VOC) gas tracer methodology.

IV. RESPIRATORY EXPOSURE AT ALTERNATE DISTANCES

This chapter is published (preprint) as:

Hooman Parhizkar, Mark Fretz, Aurélie Laguerre, Jason Stenson, Richard L. Corsi, Kevin G. Van Den Wymelenberg*, Elliott Gall. A novel VOC breath tracer method to evaluate indoor respiratory exposures in the near- and far-fields, 11 March 2022, PREPRINT (Version 2) available at Research Square [<https://doi.org/10.21203/rs.3.rs-1437107/v2>]

For this project, Dr. Richard L. Corsi proposed the concept of breath mint tracer gas. I worked with Dr. Van Den Wymelenberg to outline the scope of work and write the grant proposal, with input from Dr. Gall, Dr. Fretz and Jason Stenson. Dr. Elliot Gall and Aurélie Laguerre transferred TOF-MS to Energy Studies in Building Laboratory (ESBL) in Portland, Oregon. I worked with Aurélie Laguerre, Mark Fretz, and Jason Stenson to collect data. Dr. Elliot Gall and Aurélie Laguerre extracted raw data from TOF-MS. I developed the project's analysis script, visualizations, and drafted the paper with inputs from Dr. Kevin G. Van Den Wymelenberg, Mark Fretz, and Jason Stenson. In this chapter we further elaborated on the well-mixed assumption that was previously used in chapter II to better explain the impact of distance on bioaerosol exposure. The result of this chapter was further paired with chapter III. As of February ,2 2022, I have developed the manuscript draft and sent it to all co-authors for their review and feedback. The project presented in this chapter was funded by Pacific Northwest Center for Translational Environmental Health Research at Oregon State University with award number P30ES030287. Supplemental figures associated with this chapter are presented in APPENDIX E.

IV.1. Introduction

The spread of COVID-19 has caused extensive damage to the lives of millions of people worldwide. Severe acute respiratory syndrome coronavirus 2 (SARS-CoV-2), the causative agent of COVID-19, is transmitted from human to human via bioaerosols particles that are released during respiratory activities such as breathing, talking, singing, and coughing[19,158,159].

Substantial evidence supports that indoor spaces are hotspots where COVID-19 transmits beyond 6 ft of the source emitter[17,20,53,60,159]. Furthermore, epidemiological studies, public health, and engineering risk assessment models indicate that the majority of well-documented superspreading outbreaks can be explained by bioaerosols beyond 6 ft from the source emitter[96,102,160]. Therefore, quantifying the degree of exposure to bioaerosols according to distance from the emitting source is critical to more accurately characterize disease transmission risk, to determine the most effective risk reduction strategies such as ventilation, filtration, and spatial distancing, and ultimately to reduce disease transmission.

A well-mixed air space is a conventional assumption that has been used in most studies of indoor air pollution and infectious disease transmission modeling[161]. For a well-mixed condition, indoor air contaminants, including virus laden aerosol particles, are assumed to be uniformly distributed by appropriate ventilation, interior mixing fans, buoyancy driven flows, and infiltration, immediately after being emitted from the source[162]. However, thermal stratification, inadequate ventilation, and some environmental conditions can cause a non-uniform distribution of bio-aerosols in indoor

spaces[163,164], where the probability of susceptible occupants inhaling virus-laden aerosol particles will rely, at least to some extent, on the distance from the source emitter.

Few studies have considered the importance of spatial parameters such as room height into measurements of indoor pollutants[165–168]. A study of temporal and spatial scales suggests that chemical compounds as well as particles in the range of 1-10 μm with persistent residence time exhibit spatial gradients that are significantly controlled by ventilation rates[169]. Additionally, controlled experiments on participants who were diagnosed with COVID-19 were used to study the abundance of SARS-CoV-2 viral RNA copies in room aerosols. The authors found that the near-field was associated with a higher number of virus RNA copies, and statistically higher carbon dioxide (CO_2), and particle counts of 0.3 μm – 2.5 μm than in the far-field[159]. Differences between near-field and far-field were also examined through ΔCO_2 and $\Delta\text{particles}$ with patients receiving high-flow nasal cannula therapy (HFNC), where the CO_2 concentration was statistically higher at a distance 0.5 m (~1.6 ft) from the source emitter compared to background levels[170].

The goal of the present study is to better characterize the impact of distance from source on distribution of exhaled bioaerosols in an indoor environment. A novel trace gas approach is proposed where a participant consumed breath mints and released known compounds in exhaled breath.

IV.2. Methodology

IV.2.1. Methodology background

A previous study has shown that chewing peppermint flavored gum is associated with release of unique volatile organic compounds (VOCs) such as menthone and

menthol, with source strength dependent on oral activity and chewing frequency[171]. Real-time measurements of VOCs can provide useful information for studying pollutant dynamics of indoor environments[172]. We used proton transfer reaction - time of flight - mass spectrometry (PTR-ToF-MS) to measure volatile organic compounds (VOCs) associated with breath mints across a mass range of 17-490 amu with 1 second time resolution. The principles of the PTR-ToF-MS measurements have been well-described previously[173–175]. This approach allows for a real-time measurement of VOCs with a proton affinity greater than that of H₂O. In theory, ionization is soft, allowing for little fragmentation, and compound identification can be made by observation of the [M+H]⁺ ion (i.e., molecular mass + the mass of the transferred proton). Our study used breath mints instead of chewing gum to trace three specific compounds (menthone, monoterpenes, and menthol).

IV.2.2. Participant Recruitment

Human subjects protocols were reviewed and approved by the University of Oregon Institutional Review Board (IRB) (Protocol #20210509). One human subject participated in this study. The participant was instructed to:

- 1- not use cologne or body sprays during the day preceding and during the study period;
- 2- wear clothes that were not recently washed with detergents;
- 3- follow a consistent diet during the course of three data collection days;
- 4- maintain a constant breath mint consuming rate during all trials.

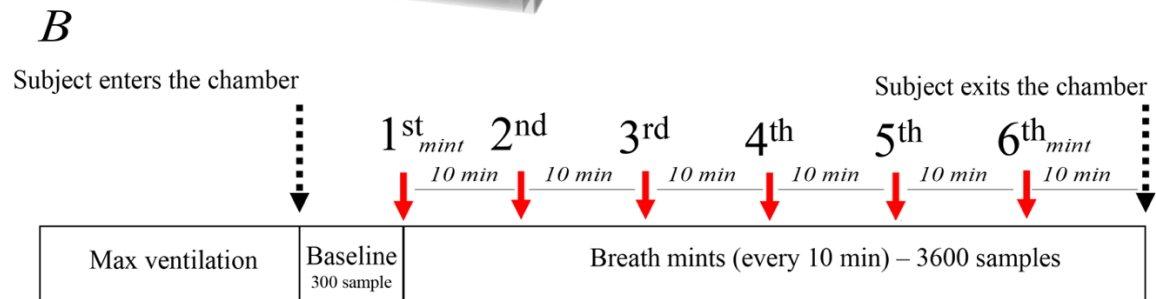
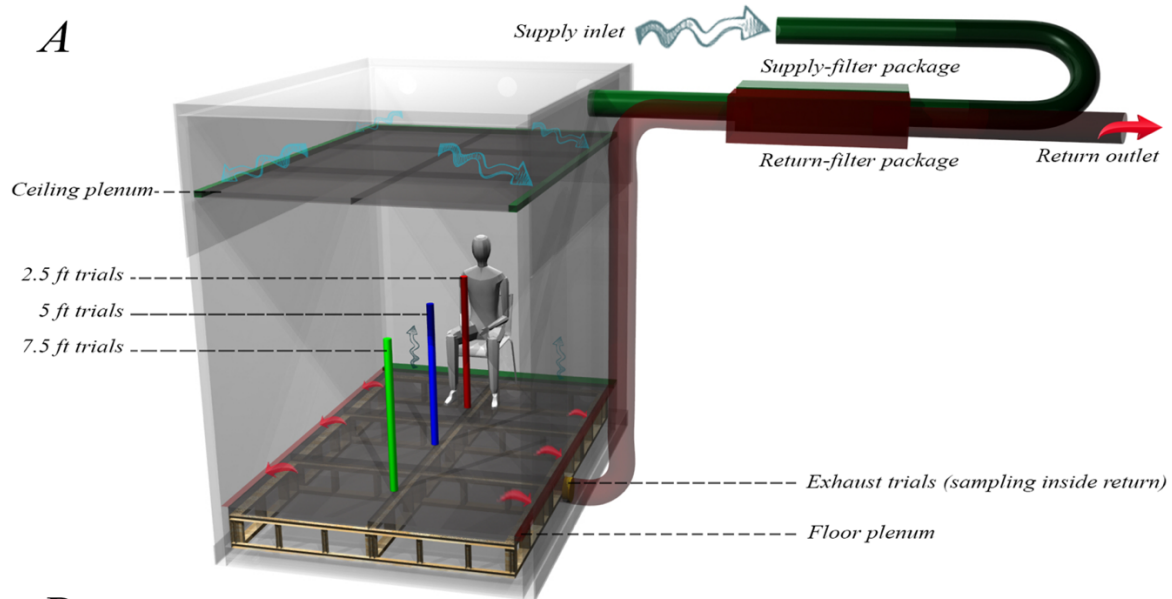
IV.2.3. Climate Chamber

Experiments were conducted at the Energy Studies in Buildings Laboratory, Portland, OR, USA, using a custom environmentally-controlled climate chamber with an interior volume of 27 m³ (Figure IV.1A). Filtered air was supplied through a ceiling plenum and exhausted through a floor plenum. Air was exchanged at ~3 air changes per hour (ACH) during test periods and flushed at > 20 ACH for a minimum of 20 minutes between trial periods. We observed the concentration of breath tracers during the experiment as a distinct VOC that is associated with breath mints to confirm the removal of previous residuals before the beginning of each trial.

Ambient indoor air was supplied through a MERV-13 prefilter and high-flow activated carbon filters (Air Box 4 Stealth; AirBox Filters, Laval, Quebec, CA) and exhausted through an identical filtration system (shown as supply filter package and return filter package in Figure 1A). Air exchange rates were monitored throughout the experiments by balancing supply and exhaust air velocities measured at center-of-duct locations using a thermal anemometer and multi-function ventilation meter (#964 and #9565-P, respectively; TSI Incorporated, Shoreview, MN, USA).

Each trial began with adjustment of the climate chamber's ventilation rate to the maximum value (20 ACH) for a minimum duration of 20 minutes without the presence of the participant in order to evacuate detectable residuals of prior trials (Figure IV.1B). We monitored the concentration of menthone to assure it reached a negligible steady-state background concentration. Next, the participant was instructed to enter the chamber, sit in a chair, and breathe normally for five minutes without consuming any breath mints. These 5-minute periods provided a baseline reference for each trial and were included in the study protocol to identify certain compounds that are exclusively associated with

Figure IV.1. Experimental setup, A) climate chamber, airflow distribution, as well as sampling location for each unique trial (modeled in Rhinoceros software), B) Experimental procedure and the number of breath mints consumed by the participant for each trial.



natural human breath and not breath mint flavoring, and to additionally provide a baseline to observe any exhaled compounds that may have remained in the participant’s mouth from previous trials. After 5 minutes, the participant was visually informed to begin consuming one breath mint every 10 minutes (Figure IV.1B), resulting in 6 breath mints consumed during each 1-hour trial (minutes 0, 10, 20, 30, 40, and 50). All breath mints were carried into the chamber by the participant in an air sealed plastic bag. To keep emissions relatively constant, the participant was instructed to remain silent and minimize body movement during the entire course of study. The participant also took care to

maintain a resting activity level between trials to avoid emission irregularities while inside the chamber during the trials.

A summary of all trials conducted in this study is presented in Table IV.1. We used a single sampling line attached to a portable tripod and moved the probe to designated spots on the floor, measuring 2.5 ft, 5 ft and 7.5 ft from the participant’s mouth (Table IV.1, Trials A-C). Additionally, we placed another sampling line of equal length inside the floor plenum exhaust duct (called exhaust trials) to measure exhaust air as a “well-mixed” approximation of the volume -averaged concentration (Table IV.1, Trial D).

In addition to trials A-D (Table IV.1) within the climate chamber (Figure IV.1A), we conducted two other experiments to confirm the presence of unique tracer compounds associated with the exhaled breath of the participant consuming breath mints (Table IV.1, Trials E&F). In trial E, we placed one single breath mint in the headspace of a 250 mL glass container for ~1 minute and monitored the concentration of VOCs over a 20-minutes period. In trial F, the participant was instructed to consume one breath mint while breathing normally into the same 250 mL glass container for ~1 minute. Similar to trial E (Table IV.1), we monitored the concentration of VOCs over a 20-minute period. For trials E and F (Table IV.1), PTR-ToF-MS sampled at a flowrate of ~100 cc/min during both experiments and three minutes of background (BCK) measurements are shown prior to the start of the experiment.

Table IV.1. Summary of experiment trials

Trials	Sampling probe distance from the participant’s mouth	Number of replicates	Sampling frequency (Hz)	Sampling duration (minutes)	Number of samples
--------	--	----------------------	-------------------------	-----------------------------	-------------------

A	2.5 ft	2	1	60	3600
B	5 ft	2	1	60	3600
C	7.5 ft	2	1	60	3600
D	Exhaust	2	1	60	3600
E	Breath mint in a 250 ml glass container	1	1	20	1200
F	Breath mint exhaled into a 250 ml glass container	1	1	20	1200

IV.2.4. Statistical Analyses

Analyses were performed using the statistical programming environment R. The Taylor expansion[176] procedure was applied using the propagate package[177] to calculate the expanded uncertainties associated with VOC measurements (Supplemental table IV.1). The ratio of samples collected at 2.5, 5, and 7.5 ft were normalized by the volume-averaged concentration resulting in a series of magnifiers for each distance expressed in percentage values. The effect size associated with each magnifier was assessed using the Cohen’s D test[178,179].

IV.3. Results

IV.3.1. Data Normalization

Menthone, menthol, monoterpenes, isoprene, and acetone were selected for further analysis. We conducted paired t-test analyses between the first and last minute of baseline periods during which the participant did not consume breath mints in the chamber (n = 60). Table IV.2 presents the results of paired t-tests between the first and

last minute of the baseline periods for each distance. The concentration of menthone, menthol, and monoterpenes did not change ($p > 0.05$) during baseline periods when the participant did not consume breath mints, while the concentration of isoprene and acetone changed during the baseline periods. This indicates that acetone and isoprene were detected in the participant's natural breath. Upon further review, the changes were inconsistent with breath sources only, suggesting other indoor sources such as the participant's skin and climate chamber interior materials may have contributed to the variability. Therefore, we summed the concentrations of menthone, menthol, and monoterpenes as unique breath tracer for the comparison of different distances in this study.

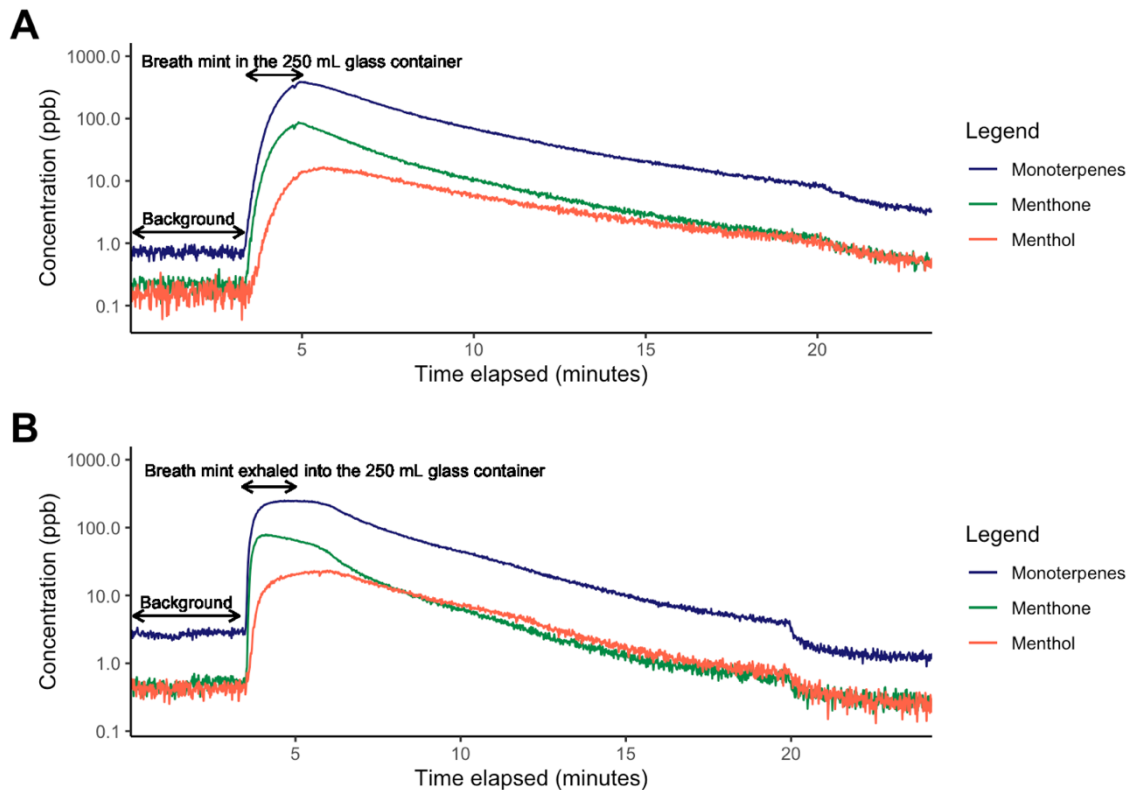
Table IV.2. Comparison of the first and last minute of baseline period for five major compounds (paired t-test)

<i>Compounds</i>	<i>Sampling distance from human source emitter (n = 60)</i>		
	2.5ft	5ft	7.5ft
<i>Menthone</i>	0.0005(p = 0.92)	-0.005 (p = 0.32)	0.0107 (p = 0.1)
<i>Menthol</i>	0.0086(p = 0.46)	0.0189 (p = 0.35)	-0.0191 (p = 0.07)
<i>Monoterpenes</i>	0.0015(p = 0.78)	0.0015 (p = 0.76)	-0.0015 (p = 0.79)
<i>Isoprene</i>	0.0704(p < 0.005)	-0.0556 (p < 0.001)	-0.04940 (p < 0.001)
<i>Acetone</i>	0.5982(p < 0.001)	-0.5913 (p < 0.001)	-0.3421 (p < 0.001)

In addition to the analysis of baseline periods presented in Table IV.2, the presence of menthone, menthol, and monoterpenes in the exhaled breath of the participant while consuming breath mints was additionally confirmed through trials E & F (Table IV.1). Figure IV.2 indicates that the concentrations of menthone, menthol, and monoterpenes substantially increase when the breath mint was placed in the headspace of

a 250 ml container (Figure IV.2A), or when the participant breathed naturally into the 250 ml container (Figure IV.2B).

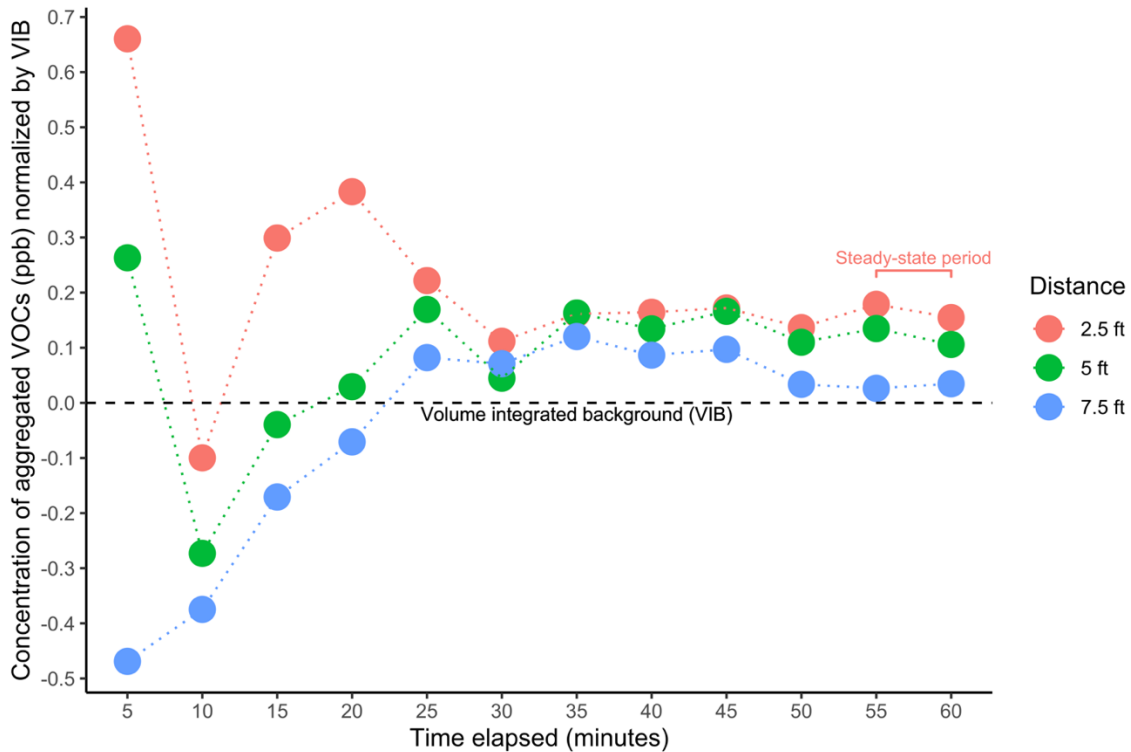
Figure IV.2. **A)** Concentration of three target tracer compounds (menthol, menthone, and monoterpenes) in the headspace of a 250 mL glass chamber as a function the time when a breath mint is placed inside, **B)** Concentration of the three target compounds when the participant exhaled their breath once into the 250 mL chamber while consuming the breath mint.



Furthermore, Supplemental figure IV.1 shows the concentration of major VOCs during ventilation and baseline periods, indicating low but not necessarily zero concentrations for trials A-D (Table IV.1). We hypothesize that baseline concentrations are associated with residual VOCs that were adsorbed by climate chamber or ventilation filter surfaces and slowly re-emitted into the chamber air. To make a consistent starting point for all trials, we subtracted the average concentration of each compound detected during baseline periods from the 60-minute sampling period measurements.

The concentration of each compound for duplicate trials at each sampling location was averaged to produce a single data set for each of the distance trials (2.5 ft, 5 ft, 7.5 ft, and exhaust trials). Thereafter, the modified concentrations of menthone, monoterpenes, and menthol were summed to create a single value as breath tracer for each distance. A comparison of summed breath mint VOC concentrations normalized by the volume-averaged concentration is shown for each distance in Figure IV.3.

Figure IV.3. Comparison of 2.5, 5, and 7.5ft trials normalized by volume integrated background.



Supplemental table IV.1 reports on the magnifiers, expanded uncertainties associated with each value, as well as Cohen’s D effect size statistics for each distance. Supplemental figure IV. 2 demonstrates the uncertainties associated with the values presented in Figure IV.3.

IV.4. Discussion

We used PTR-ToF-MS to trace the concentration of select VOCs associated with a consumed breath mint as a proxy for bioaerosol emissions from a healthy participant during each 60-minute trial. We summed the concentrations of menthone, monoterpenes, and menthol in each trial as a unique breath tracer since they were only detected only when the participant consumed breath mints. The summed tracer concentrations detected at 2.5, 5 ft, and 7.5 ft from the participant were normalized by volume-averaged concentration (VAC), which indicates the magnifier of each location compared with an approximate well-mixed condition. As shown in Figure IV.1, the concentration of VOCs at 2.5 and 5 ft rise above volume-averaged concentration during the first 5 minutes of the study, while the concentration at 7.5 ft begins to rise below the VAC level after minute 10 (Figure IV.3). We observed a steep increase in the concentration of breath tracers at 2.5, 5, and 7.5 ft during the first 5 minutes, which show that signals were first detected at closer range distances compared to the exhaust plenum due to a concentrated exhaled plume that had not mixed extensively throughout the chamber. At minute 5, the concentration of breath tracers also began to rise in the exhaust plenum, resulting in decreases in the ratios of indoor sampling locations normalized by the VAC (Figure IV.3). It took approximately 10 minutes for the concentration of breath tracers to become mixed in the chamber. At minute 10, the concentration of human tracers begins to increase in 2.5 ft trials against VAC, resulting in a higher concentration at 2.5 ft during minutes 5-20 compared to all other locations, with a 36-44% higher concentration than VAC. This finding suggests that the risk of exposure to virus-laden aerosol particles during the first 20 minutes is relatively higher for close contact distances (less than 3ft)

when compared with other distances. Meanwhile, the concentration of breath mint tracers at 5 and 7.5 ft also rise above VAC during minutes 20-25, with the greatest magnifier having a value of 17% higher than VAC at 5 ft. After 25 minutes, tracer concentrations at 2.5, 5, and 7.5 ft maintained a relatively consistent trend in the ratio of distance-specific concentration normalized by VAC was observed. The magnifiers during this approximate steady-state period were ~18% ($\pm 25%$, *Cohen's d estimate = Large*), ~11% ($\pm 21%$, *Cohen's d estimate = Large*), and 7.5% ($\pm 18%$, *Cohen's d estimate = Large*) above VAC at 2.5, 5, and 7.5 ft, respectively. The expanded uncertainties associated with values reported in Supplemental table IV. 1 are in agreement with previous studies that measured VOCs using PTR-ToF-MS[180]. Despite the fact that Cohen's d statistics show large effect size values when the concentration of breath tracers at 2.5, 5, and 7.5 ft were compared to VAC[181], the uncertainty associated with our measurements suggest that reported magnifiers presented in Supplemental table IV.1 should be studied further with more replicates to improve the accuracy of and confidence in the near-field to far-field multipliers. Meanwhile, these findings highlight the importance of both near-field and far-field exposure events and emphasize the importance of exposure duration in consideration of near-field and far-field prioritization. In this study, given these room characteristics and airflow rates the 20-25-minute event threshold helps to differentiate the dominance of near-field exposure risks, whereas longer events suggest dominance of far-field exposure (minutes) risks.

Appendix E describes two case studies that present results of near- and far-field magnifiers for a recent controlled study on individuals that were diagnosed with COVID-19[159], as well as a study of patients undergoing high-flow nasal cannula therapy[170].

Specifically, as shown in Supplemental table IV.2, the concentration of CO₂ and the particles of 1 μm – 2.5 μm in a recent study with participants diagnosed with COVID-19[159] were ~8 % and ~12 % higher in the near field (4 ft from the participants), compared to the far field (11 ft from the participants), respectively[159]. The present study provides confirmatory results in that the concentration of targeted VOCs in the near-field (2.5 ft) was ~10% higher than the far-field (7.5ft) during steady-state periods, thus- providing greater confidence for the concept of breath tracers as a proxy for virus laden bioaerosols.

IV.5. Conclusion and Limitations

Our study provides a series of magnifiers that could be used to estimate the concentration of bioaerosols at 2.5, 5, and 7.5ft from a human emitter in a reasonably well-mixed indoor space with ~ 3ACH over a 60-minute exposure event duration. These multipliers can be used in future studies of microbial risk assessment models to superimpose near-filed exposures and inhalation dose on far-field exposures estimated using a well-mixed assumption. Here we demonstrated that the concentration of detectable respiratory VOCs at 2.5, 5, and 7.5 ft were approximately ~18% , ~11%, and 7.5% higher, respectively, than volume-averaged concentration during steady-state periods. These magnifiers are reasonably consistent with values reported for a controlled study on participants diagnosed with COVID-19 in which near-field (4 ft) was associated with 8% -17% higher concentrations for CO₂ and particles (0.3 μm – 3 μm), resulting in 1 cycle threshold (C_T), or two times, difference between the viral load detected in the near-field and far-field (Appendix E). Our findings indicate that the concentration of bioaerosols in the far-field is relatively close to the well-mixed assumption at a steady-

state period, while close range distances are associated with relatively higher exposure levels during the first 20 minutes of an emission exposure event.

Our study was a pilot project with several limitations. Our data were limited to replicated trials and a constant ventilation rate of ~ 3 ACH. There are several other environmental variables that can be studied through the same methodology such as the impact of relative humidity, temperature, mixing fan, facial masking, and room volume. Ventilation strategies other than overhead (used in this experiment) should be considered with different ACHs in future efforts. We seek to study several other distances & positions from the source emitter (vertical and horizontal distribution) to improve the accuracy of magnifiers with the intention of developing a comprehensive heterogeneous air space model for indoor air quality research.

IV.6. Bridge

We paired the result of this experiment with findings of Chapter III where the difference between aerosol viral load measured with active air samplers and qPCR wet lab methods, size-resolved particles, and CO₂ were described as ratios between near- and far-field. The values of near- and far-field ratios in Chapter III are in close agreement with the near-field magnifiers reported in Chapter IV, thus increasing confidence in the results of both Chapters III and IV. Moreover, the magnifiers that explain the difference between the concentration of bioaerosols in far-field and volume integrated background in Chapter IV provide further evidence for use of the well-mixed assumption in Chapter II for exposure events longer durations, while also indicating future refinement would be warranted for short-term near-field exposure events or early periods of long exposure events.

Chapters II, III, and IV represent fundamental research needed to support improved architectural design and building operations with the aim of reducing disease transmission and supporting human health. While the fundamental science is essential to improve design, it does not complete the process of discovery to support improved design decisions. Therefore, Chapter V is included to provide a framework for how the proceeding chapters can be incorporated into the design process to impact design decision-making.

V. USING DISEASE TRANSMISSION RISK AS THE GUIDE FOR EVIDENCE-BASED DESIGN

This chapter contains co-authored material with Dr. Siobhan Rockcastle, Dr. Mark Fretz, and Dr. Kevin G. Van Den Wymelenberg. For this Chapter, Dr. Siobhan Rockcastle proposed the concept of applying the dissertation findings into an architectural design case study. I conducted simulations in Rhinoceros and Grasshopper, analyzed data, created visualizations, and developed the initial draft with inputs from Dr. Siobhan Rockcastle, Dr. Mark Fretz, and Dr. Kevin G. Van Den Wymelenberg. The findings of this chapter may be submitted for publication in an upcoming building simulation journal or conference presentation.

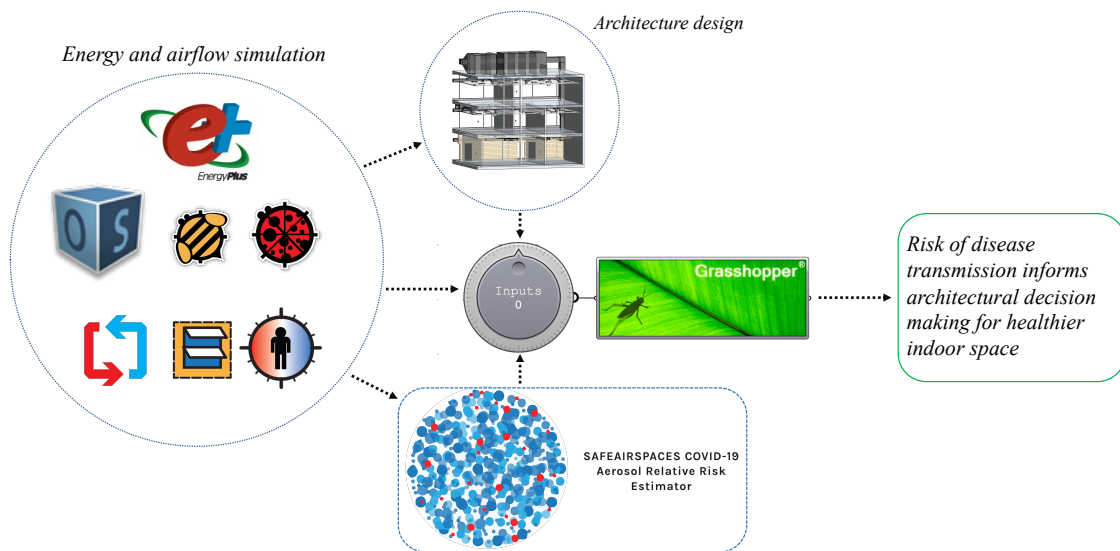
V.1. Case Study Simulation

As an architectural researcher, this chapter intends to demonstrate how the findings of this PhD dissertation can be incorporated into architectural design processes, providing novel insights about the role of architectural design variables in identifying the risk of disease transmission in buildings; **a guideline that is currently missing**. As mentioned in both Chapters II and III, ventilation and humidification are among environmental mitigation strategies that can substantially reduce the aerosol viral load and the risk of infection indoors. Passive design strategies such as natural ventilation are among well characterized methods to improve indoor thermal comfort and reduce buildings' energy consumption[182–185]. Moreover, natural ventilation can result in increased outdoor air intake, contributing to the combat of disease transmission indoors[2,96,159,186].

Therefore, we hypothesize that architectural parameters such as the configuration of windows and percentage of operability can be specifically designed with the intention of decreasing risk of infection and creating healthier indoor spaces.

Moreover, building design specifications such as opening size, material, and site location determine the levels of indoor relative humidity and UVB intake, respectively, which directly translates to alternate risk of infection. To better understand how architectural decision makings can determine the risk of COVID-19 infection in indoor spaces, we created a bridge between building energy plus & open studio simulation engines and SafeAirSpaces risk estimation platform, which was explained in Chapter II. The workflow is visually presented in Figure V.1. Using this workflow, we simulate the risk of infection for a simple case study with different window configuration, and in different site locations.

Figure V.1. Simulation workflow (energy and simulation figures are courtesy of Ladybug tools[187])



V.1.1. Simulation Parameters

The case study is a one-story building that measures 7 m (~23 ft) long, 5 m (~16 ft) wide, and 2.7 m (~9 ft) high, with total volume of 95 m³ (~1022 ft³). Simulations were conducted in Rhinoceros 7.0. and Grasshopper plug-in.

V.1.1.1. Natural Ventilation

According to window size, orientation, and fraction of openings, the following cases were considered for the study of natural ventilation on COVID-19 transmission risk in a building:

- 1- One southern window closed;
- 2- One southern window, 25% operable;
- 3- One southern window, 50% operable;
- 4- One southern large window (2X), 50% operable;
- 5- 2 southern windows, 50% operable with cross-ventilation (both located on one side);
- 6- 2 windows, 50% operable with cross-ventilation on south and west façades (located on two sides).

For all simulations listed above, a minimum mechanical ventilation of ~0.5 ACH was provided for all cases to assure thermal comfort satisfaction. To emphasize the impact of natural ventilation on the risk of COVID-19 infection, the impact of indoor relative humidity and UVB irradiation were neglected in this simulation. The outdoor air exchange was calculated by summing natural ventilation through windows, mechanical ventilation, as well as infiltration from open studio simulation outputs in Honeybee.

V.1.1.2. Indoor Humidification

As mentioned in Chapter III.3.5, we observed that higher relative humidity results in lower aerosol and higher surface viral load, consistent with increased rate of particle deposition. In addition to affecting bioaerosols deposition rates, higher relative humidity is shown to affect virus deactivation rate[188]. During winter and especially in colder climates, indoor spaces often suffer from excessive dryness which is attributed to the correlation between temperature and humidity: warming the environment results in higher absorption of moisture[189]. Therefore, we attempted to simulate a building in two scenarios: the building located in Eugene, Oregon, and the building located in Boston, Massachusetts. To observe the impact of relative humidity, a minimum mechanical ventilation of ~0.5 ACH was provided to keep the temperature at comfort level and windows were considered closed for all time in both locations.

We updated SafeAirSpaces risk estimation platform with a feature to include relative humidity as an input parameter using available information regarding SARS-CoV-2 viral deactivation at different relative humidity levels[188]. Therefore, the half-life of SARS-CoV-2 can be expressed as decay rate as explained in section II.2.1.

V.2. Results

V.2.1. The Impact of Window Design on the Risk of COVID-19 Infection

Simulation of different window design iterations shows that the size and fraction of openings can substantially increase the outdoor air exchange rate during moderate and warm seasons in the city of Eugene, Oregon (Figure V.2A). Using temperature setpoint values in ventilation control component, we determined a minimum and maximum threshold for indoor and outdoor spaces between which windows can be opened to enhance natural ventilation. The ventilation control component automatically closes the

windows during excessively warm or cold temperatures to avoid extra loads on mechanical ventilation system, and to keep indoor temperature at comfort levels.

According to Figure V.2A, increasing the fraction of an opening of a single window from 0% to 75% results in an increased outdoor air exchange from ~1 ACH (0% operable) to ~6 ACH (75% operable), leading to 20% decrease on the risk of infection (Figure V.2B).

One important take away from Figure V.2A is the impact of cross ventilation through two adjacent windows, when the air exchange rate was compared to having a single large window with same size and operable fraction (50%).

For a single day, the cross ventilation can increase the outdoor air exchange up to +25 ACH which corresponds to substantially reduced risk of infection (Figure V.2B).

While providing 25 ACH for a space with +1000 ft² floor area comes with extensive energy use, natural ventilation can provide sufficient air exchange rate with significantly reduced risk of infection.

V.2.2. The Impact of Outdoor Climate on the Risk of Infection in 2 Sites

As previously discussed, building location can impact the risk of infection in various ways. Warmer climates provide more opportunities to activate natural ventilation in buildings which according to the previous section, could significantly reduce the risk of infection. In colder climates, buildings have become more airtight to support indoor thermal satisfaction as well as energy use. Figure V.3A shows that for the same building located in a cold climate (Boston), the indoor relative humidity can be significantly dry in winter due to the increased rate of warming adjustments through mechanical ventilation, when compared to a moderate climate such as the city of Eugene in Oregon. This results in a relatively lower risk of infection in the winter for the city of Eugene (Figure V.3B).

Figure V.2. The impact of natural ventilation on risk of COVID-19 infection; A) Outdoor air exchange levels for different window configurations in a single day of summer months and B) Risk of infection for different window configurations in a single day of summer.

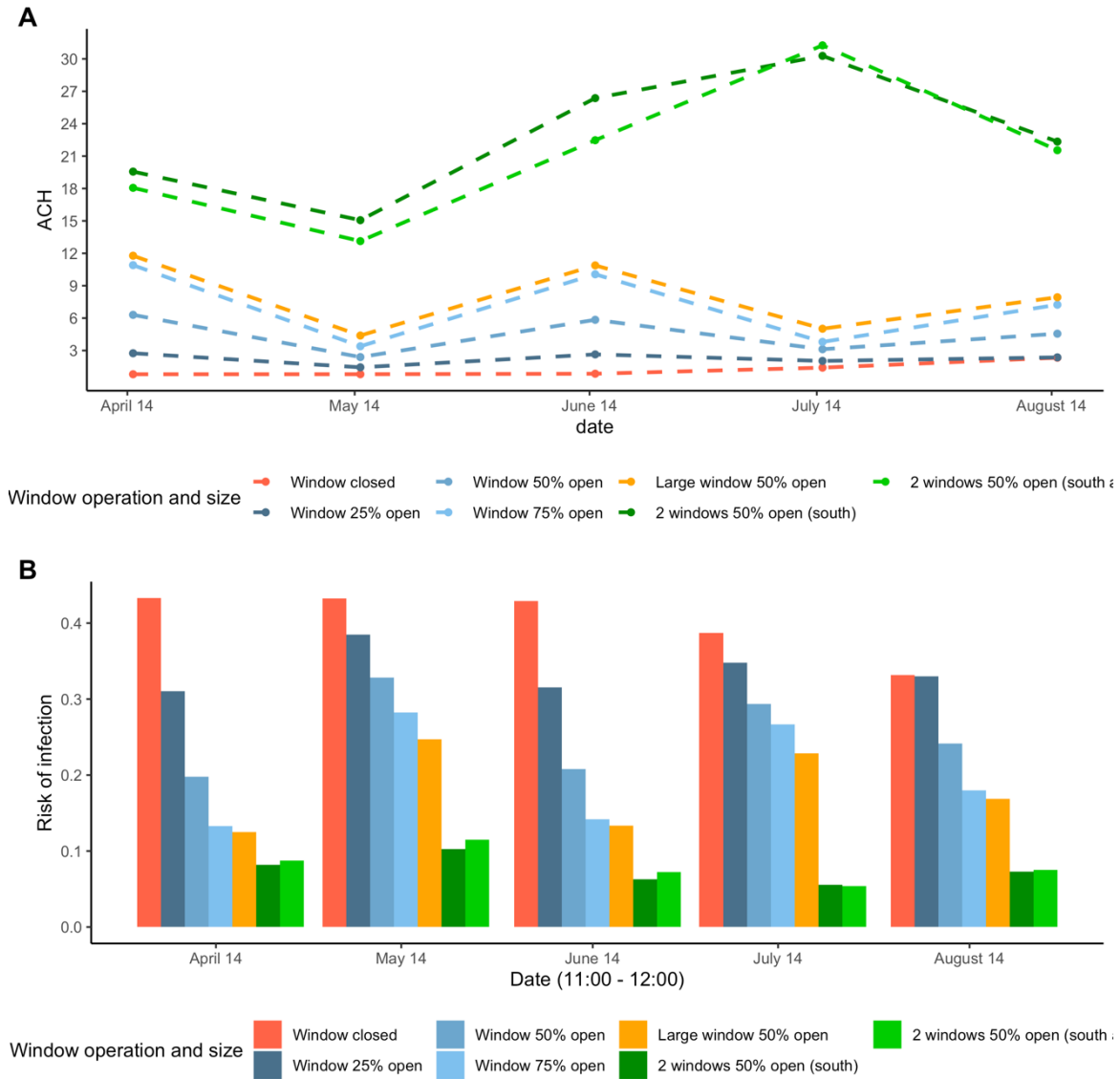
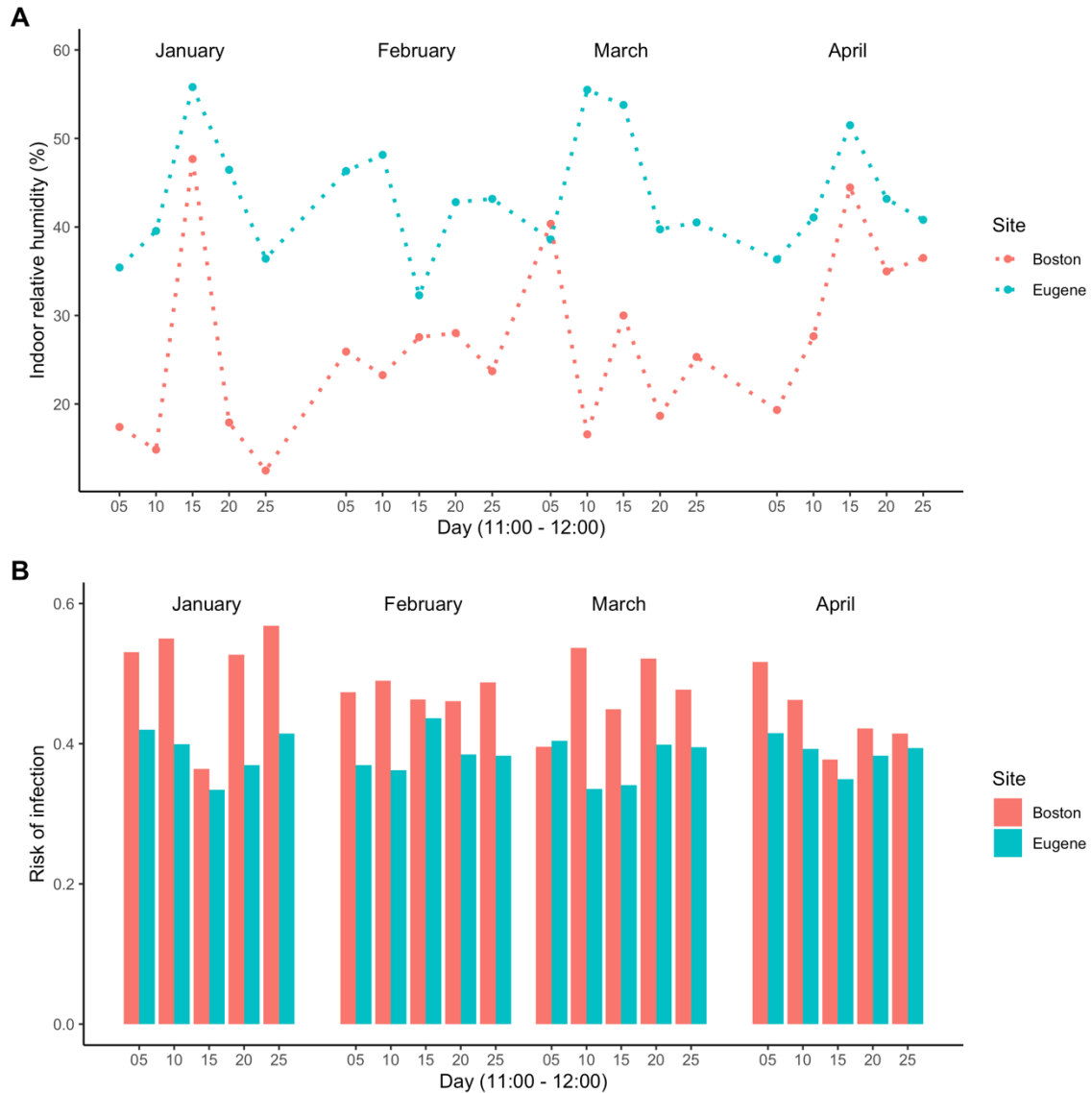


Figure V.3. The impact of relative humidity on risk of COVID-19 infection; A) Relative humidity levels associated with location’s climate during wintertime and B) Risk of infection for the city of Eugene and Boston.



V.3. Future Outlook

In this chapter, we demonstrated that simple decisions in architectural design process can result in alternate risk of infection. We presented a parametric approach to study disease transmission indoors, using data provided in our aerosol risk estimation platform (Chapter II) and experimental studies with human subjects (Chapter III & IV).

In addition to environmental and human factors addressed in this dissertation, future design will need to respond to many other architectural factors that will potentially influence the paradigm of healthy buildings. Previous articles conducted comprehensive literature reviews and concluded that human and spatial parameters such as occupant-introduced perturbations, opening and closing of interior apertures, interior objects, and indoor movements can change the steady-state conditions to a transient-flow system[190,191]. According to our understanding of disease transmission indoors, airflow patterns can induce additional momentum on virus-laden particles that can change the trajectory of aerosol transmission, all of which can be assessed during design phase. Moreover, building massing and spatial planning can significantly alter the environmental factors which consequently impact disease transmission in indoor spaces. Therefore, human health in buildings need to be considered in both initial conceptual phases as well as indoor microenvironments. Modeling of spatial and temporal analysis of indoor microenvironment is currently not feasible and tends to be expensive through CFD analysis. Therefore, our proposed methodology in Chapter IV can be used as a valuable experimental approach to quantify indoor microenvironment impact on dispersion and transport of airborne contaminants, including virus-laden particles in future studies.

VI. CONCLUSION

The global spread of COVID-19 disease in 2020 presented humankind with one of the most challenging times in recent history. Extensive damage to the health of millions of people, global restrictions, long-term health symptoms, travel restrictions, closure of schools and universities, economic burden, and most importantly, the loss of millions of lives only indicate a portion of devastating impacts. Studies of previous infectious disease demonstrated that pandemics are inevitable. Admitting this simple fact leads us to reevaluate our strategies for combating human-to-human transmission of pathogens in future and places architecture design and building operations at center-stage.

The outcome of thousands of scholarly books and research articles in the past few decades highlight the importance of buildings impacts on our health and well-being. Because we spend more than 90% of our lives indoors, the properties of indoor environments shape our health. The importance of “healthy buildings” became more explicit during COVID-19 pandemic. Mounting evidence confirms that indoor spaces are the primary vector where COVID-19 is transmitted, and that we must look beyond tidy 6 ft circles from the infected source emitter in indoor spaces to adequately mitigate transmission risk. Therefore, understanding the role of buildings parameters on the spread of pathogens is key to controlling the current pandemic and prepare for future outbreaks, especially since pharmaceutical interventions are not always available are never a universal solution. As a building designer, I am honored that I have had the chance to contribute to the mission of reimagining building design and operation practices amidst infectious disease transmission indoors. The interdisciplinary nature of this doctoral curriculum at Institute for Health in the Built Environment provided me an invaluable opportunity to

collaborate with some of the most outstanding scientists to answer a critical question: “what is the airborne viral exposure risk indoors and how can building design and operations help to effectively reduce the risk of disease transmission indoors during the COVID-19 pandemic?”

In chapter II, we developed a quantitative risk estimation model that calculates the risk of infection according to building related parameters, occupant density, and behavior according to best available information. The novelty of our model is related to the concept of inhaled and deposited dose in human’s respiratory system which bridges the gap between aerosol engineering, microbial risk assessments, and public health interventions. Surprisingly, the infectious dose estimated by our model is almost the same value that is recently reported in a study that quantified minimum viral dose to begin infection in human volunteers[192]. Most importantly, the modular and mechanistic nature of this approach allows for easy updates when new information is available regarding dose-response relationship for SARS-CoV-2 or other pathogens.

In chapter III, we conducted the first real-world study of measuring environmental mitigation strategies effectiveness for reducing SARS-CoV-2 viral load indoors with participants who were diagnosed with COVID-19. Our findings provided important quantitative relationships between the viral loads detected in humans and indoor environment (aerosol and surfaces). Moreover, our results confirm that environmental mitigation strategies such as ventilation, filtration, and humidification substantially reduce the concentration of virus in air. The amount of reduction in aerosol viral load in Chapter III are in perfect agreement with the estimated values from the quantitative risk estimation platform in Chapter II.

In Chapter IV, we used an environmentally controlled chamber to measure volatile organic compounds (VOCs) released from a healthy participant who consumed breath mints, which contained unique tracer compounds. Tracer measurements were made at 2.5 ft, 5 ft, 7.5 ft from a human emitter, as well as in the exhaust plenum of the chamber. We observed that 2.5 ft trials have relatively higher concentrations than other distances during the first 20 minutes of experiments, highlighting the importance of the near-field relative to the far-field before virus-laden respiratory aerosol plumes are continuously mixed into the far-field. However, for the conditions studied, the concentrations of human-sourced tracers during steady-state periods of 60 minute at 2.5 ft, 5 ft, and 7.5 ft were only ~18%, ~11%, and ~7.5% higher than volume-integrated background concentrations, respectively. Our findings highlight the importance of far-field transmission of airborne pathogens including SARS-CoV-2, which need to be considered in public health decision makings.

Chapter IV provides an evaluation of near-field and far-field exposure to emissions from a source in a quantitative way, which can be used to update SafeAirSpaces risk estimation platform's well-mixed assumption with magnifiers that determine risk of infection at alternate distances. Moreover, the ratios of near- and far-field magnifiers resulted from Chapter IV agree with the near- and far-field ratios of viral load, CO₂, and particles of 0.3-5 μm in the study of environmental mitigation strategies described in Chapter III.

In Chapter V, we demonstrated the application of this dissertation finding in an architectural design case study. We offer a parametric approach to evaluate the risk of disease transmission for based upon spatial parameters and design iterations.

VI.1. Moving Forward

My collaborative projects in this dissertation provided novel insights into the role of building design and operation on the risk of COVID-19 infection in indoor spaces. We introduced a mechanistic model with the ability of evaluating the risk of infection according to buildings and occupational parameters. We conducted the first real-world study on the effectiveness of environmental mitigation strategies and showed that building related interventions can effectively reduce the concentration of SARS-CoV-2 in indoor spaces. Our pilot project indicated that alternate distances have relatively small impact on the distribution of bioaerosols in indoor spaces, however, our resultant magnifiers can be used in future studies of indoor environmental modeling to improve the accuracy of estimation models with regards to well-mixed assumptions.

In this dissertation we propose knowledge that may impact the architectural design process to incorporate strategies to improve indoor air and lower health risks. Now we have tools to intentionally design and operate buildings such that they can combat disease transmission indoors and create healthier indoor spaces for the future. Since the beginning of the COVID-19 outbreak, we have learned so many lessons from the beginning of pandemic. Today, the technology can help us detect the virus in our environments before it is deposited in people's respiratory system. In this dissertation we present different types of data streams to help understand real-time risk profile. Information such as indoor risk level (Chapter II) and mitigation strategies (Chapter III) are essential to make these data actionable. I am hoping that our efforts in informing decision makers about the risk of transmission and effective pathways to combat the disease result in serious course of actions.

I am also hopeful that this piece of work paves the road for better resilience, healthier indoor environments, and thriving communities into the future.

هرگز نمیرد آنکه دلش زنده شد به عشق، ثبت است بر جریده عالم دوام ما

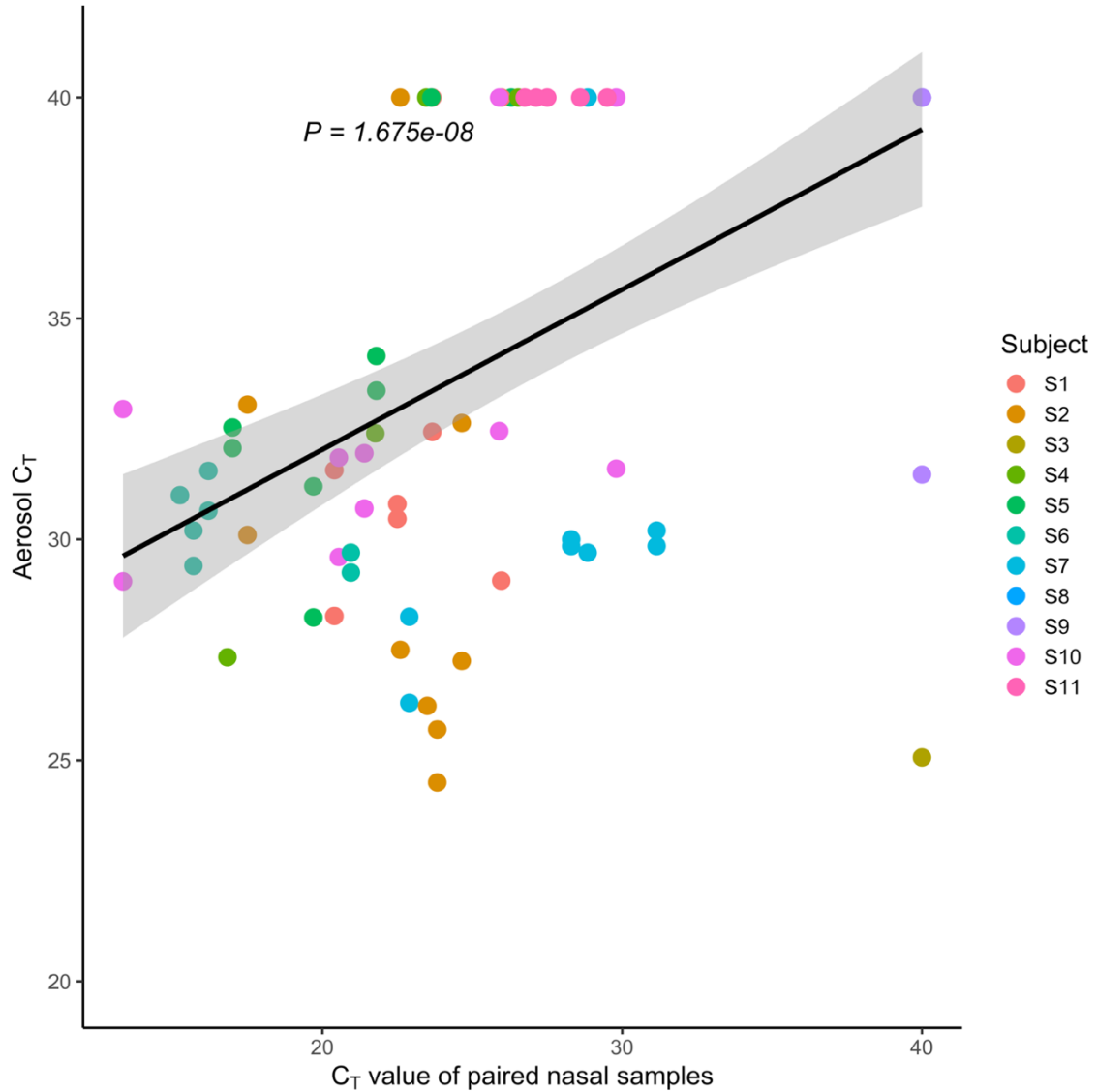
حافظ

The end.

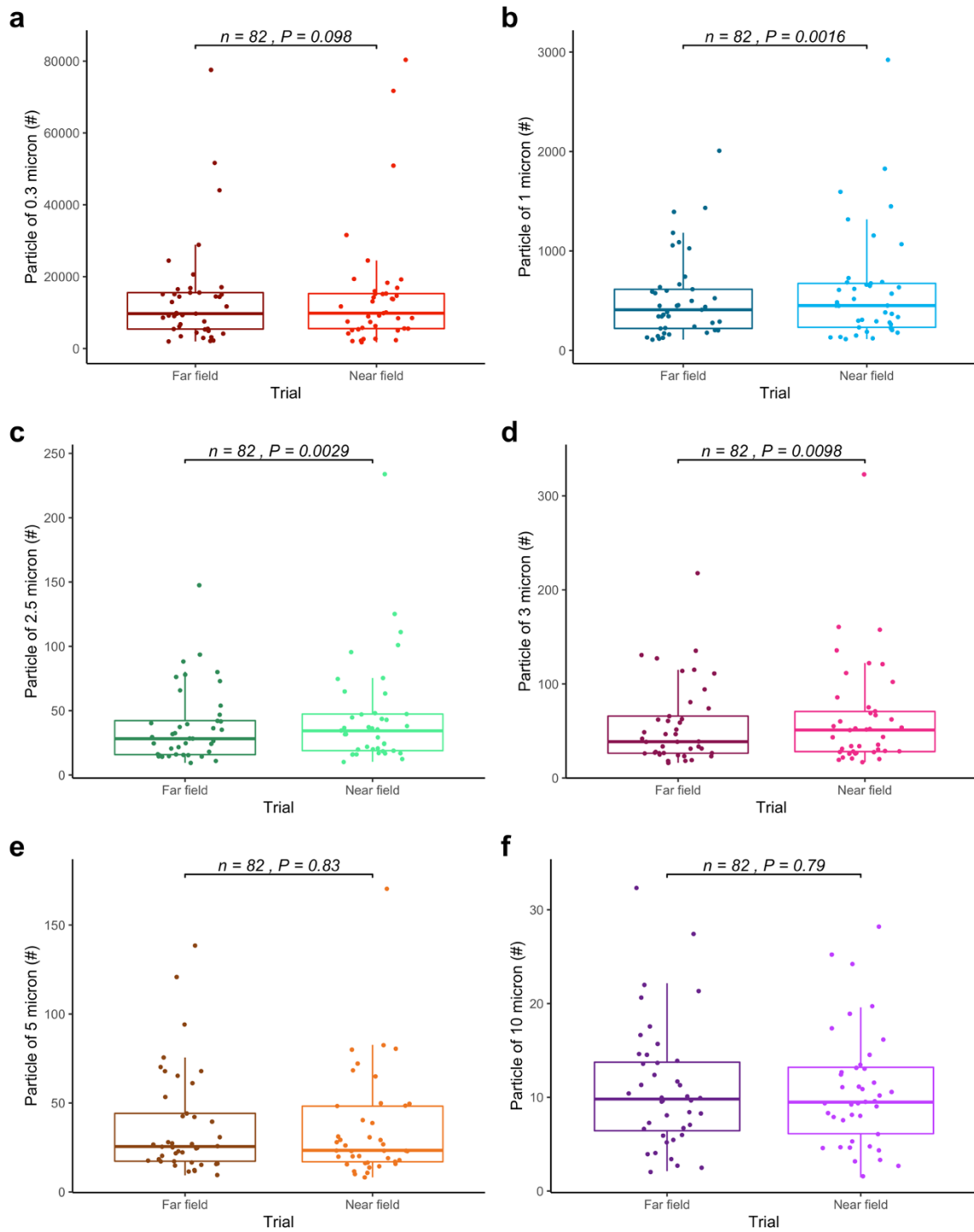
APPENDIX A

This Appendix contains the supplemental figures, supplemental tables, and supplemental paragraphs associated with Chapter III of this dissertation.

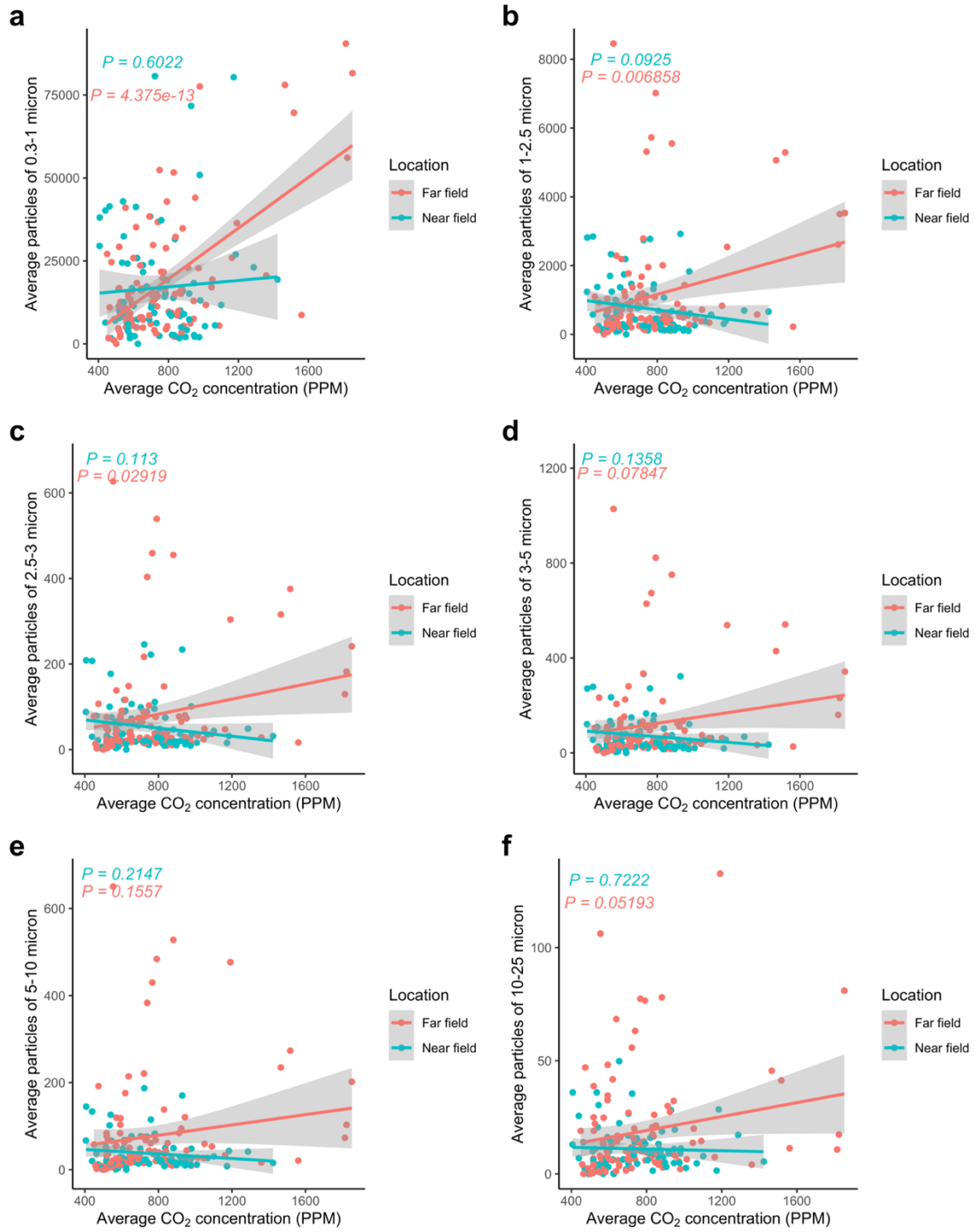
Supplemental figure III. 1. The correlation of both near field (1.2 m) and far field (3.5 m) aerosol viral loads (RNA) with corresponding human nasal samples during routine trials.



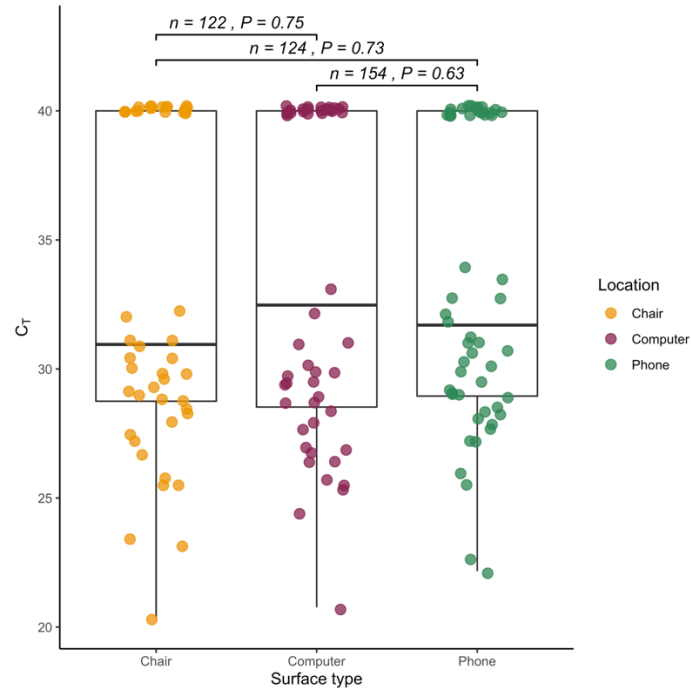
Supplemental figure III. 2. Difference between number of particles of difference sizes (0.3 μm -25 μm) for routine trials; a) 0.3 μm – 1 μm , b) 1 μm -2.5 μm , c) 2.5 μm -3 μm , d) 3 μm -5 μm , e) 5 μm -10 μm , f) 10 μm -25 μm .



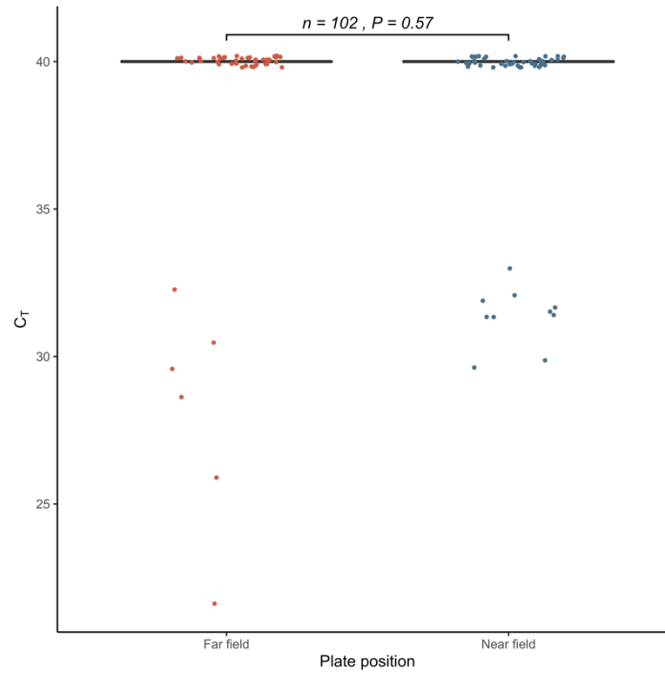
Supplemental figure III. 3. Correlation between aerosol particles of difference sizes (0.3-25) and average CO₂ concentration for routine trials at ~0 ACH; a) 0.3 μm -1 μm, b) 1 μm -2.5 μm, c) 2.5 μm -3 μm, d) 3 μm -5 μm, e) 5 μm -10 μm, f) 10 μm -25 μm.



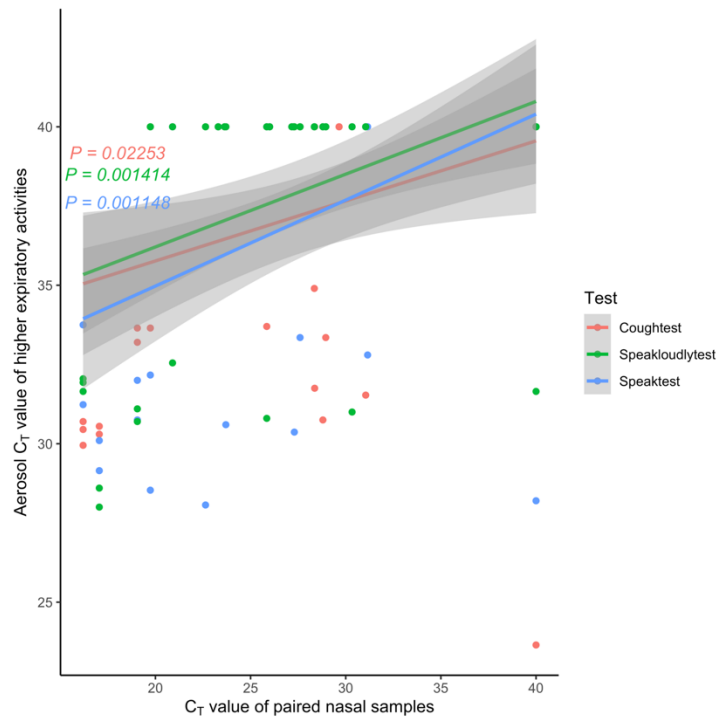
Supplemental figure III. 4. Comparison of surface viral load for three high touched surfaces.



Supplemental figure III. 5. Comparison of surface viral load for settling plates in near and far field.



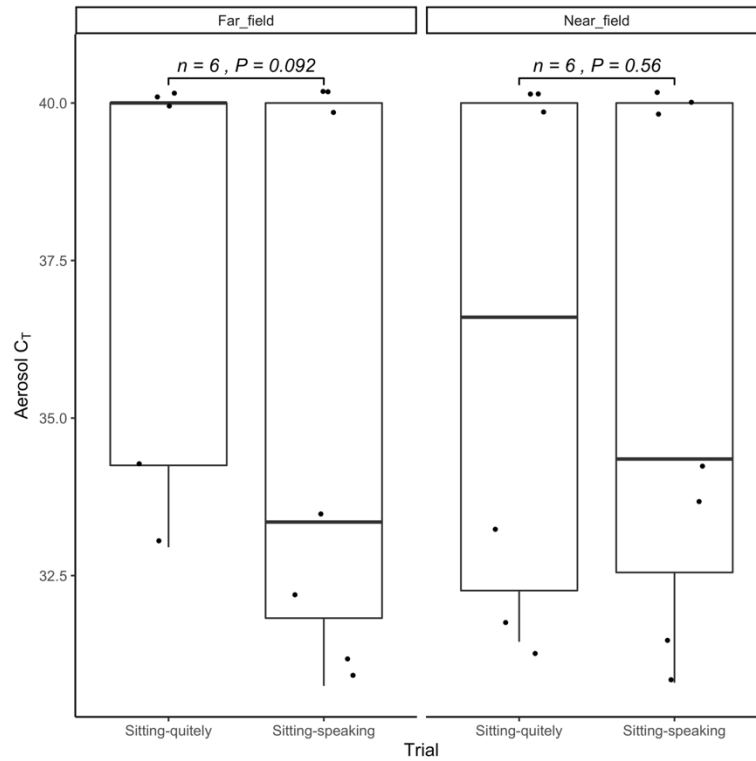
Supplemental figure III. 6. Correlation between aerosol and paired nasal vial load for higher expiratory rials.



Sitting Quietly and Speaking Trials

In addition to routine trials lasting one hour, we conducted a series of shorter trials (using Setup 2 with six participants) whereby participants were sitting silently for 30 minutes in one trial and then were speaking on a conference call or online meetings for 30 minutes. The mean difference of aerosol viral load for speaking trials was 1.957143 C_T and 0.242857 C_T lower than for silent trials in near field and far field aerosols, respectively; however, these results were not statistically significant (P = 0.09164 for far field and P = 0.5608 for near field). We hypothesize that the mean difference observed may be associated with higher concentrations of bioaerosols emitted during speaking trials, but the small sample size is a limitation.

Supplemental figure III. 7. Comparison of aerosol CT for sitting-speaking and sitting-quietly trials in near field and far field.



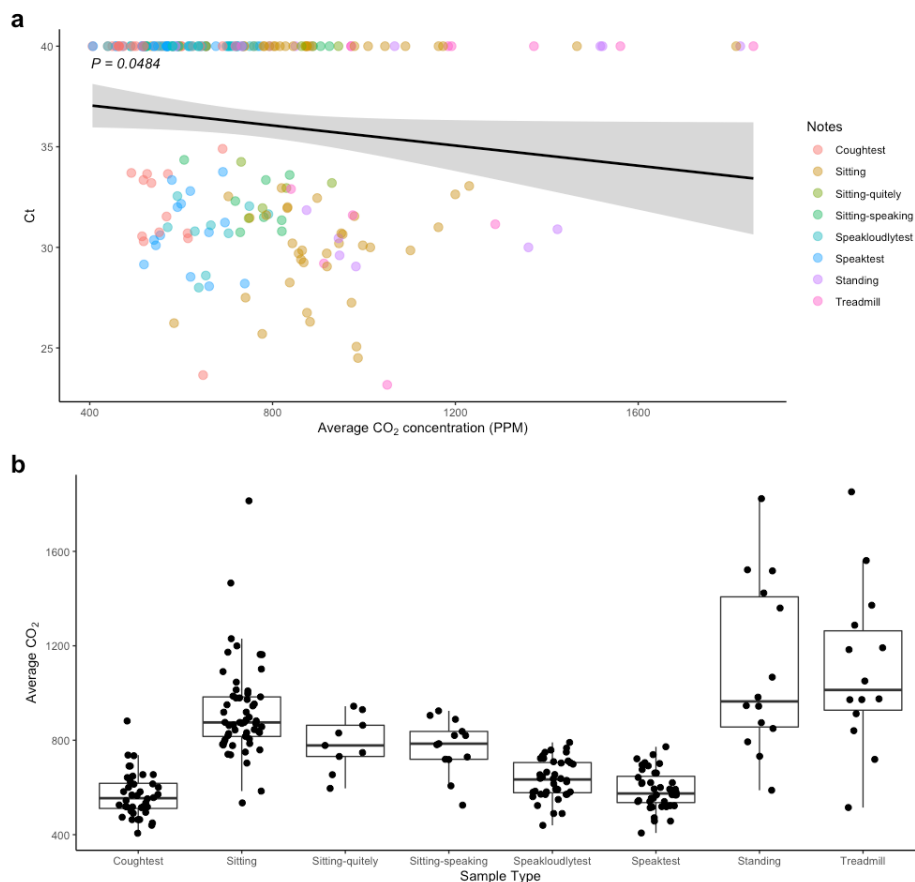
Physical Activity and Aerosol Viral Load

Human exhaled breath is the major source of viral pathogens[193–195]. Few measurements are available documenting the relationship between physical activity, viral shedding rate, and aerosol viral loads in realistic environments. Here we investigated this relationship by measuring room aerosol viral load and CO₂ concentrations during the following trials: coughing, speaking, sitting, standing, sitting silently, sitting while speaking, and walking on a treadmill.

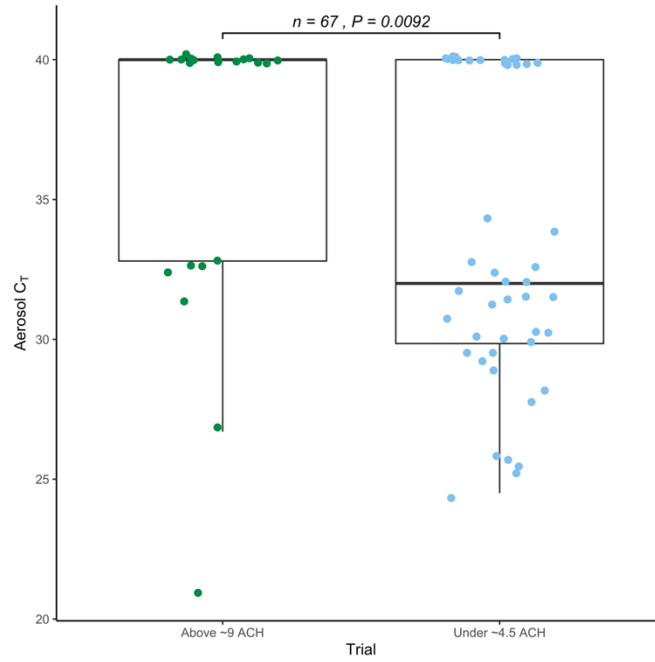
CO₂ is frequently used as a surrogate for human exhaled breath[196]. Models of disease transmission use CO₂ as an indicator of air exchange rate within a space[71,197]. However, here we monitored CO₂ with the aim of characterizing the degree of physical activity. Therefore, all physical activity trials were conducted at ~0 ACH and ambient

conditions. Supplemental figure III.3a shows the significant correlation between aerosol C_T value and average CO_2 concentration and Supplemental figure III.3b shows the relative difference in average CO_2 concentrations across physical activity trials. Among physical activity trials, we observed an increase in room aerosol viral load equivalent to $\sim 1 C_T$ to be associated with an average CO_2 concentration increase of 400 PPM ($P = 0.0484$). Moreover, increased CO_2 concentration as the result of increased physical activity level was associated with increased number of particles of 0.3-1, 1-2.5, and 2.5-3 micron (Supplemental figure III.4). Our study provides evidence that the level of physical activity is significantly correlated with the rate of viral shedding in indoor environments.

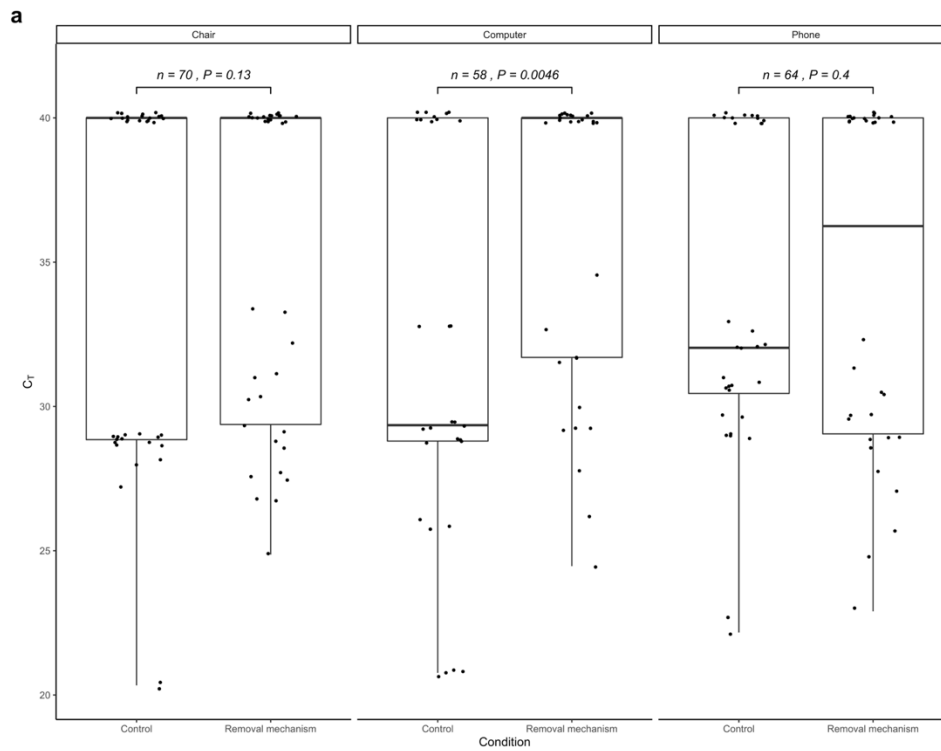
Supplemental figure III. 8. Physical activity correlations, a) paired C_T values and corresponding average concentration affected by only physical activity (~ 0 ACH), b) average CO_2 of different physical activities.



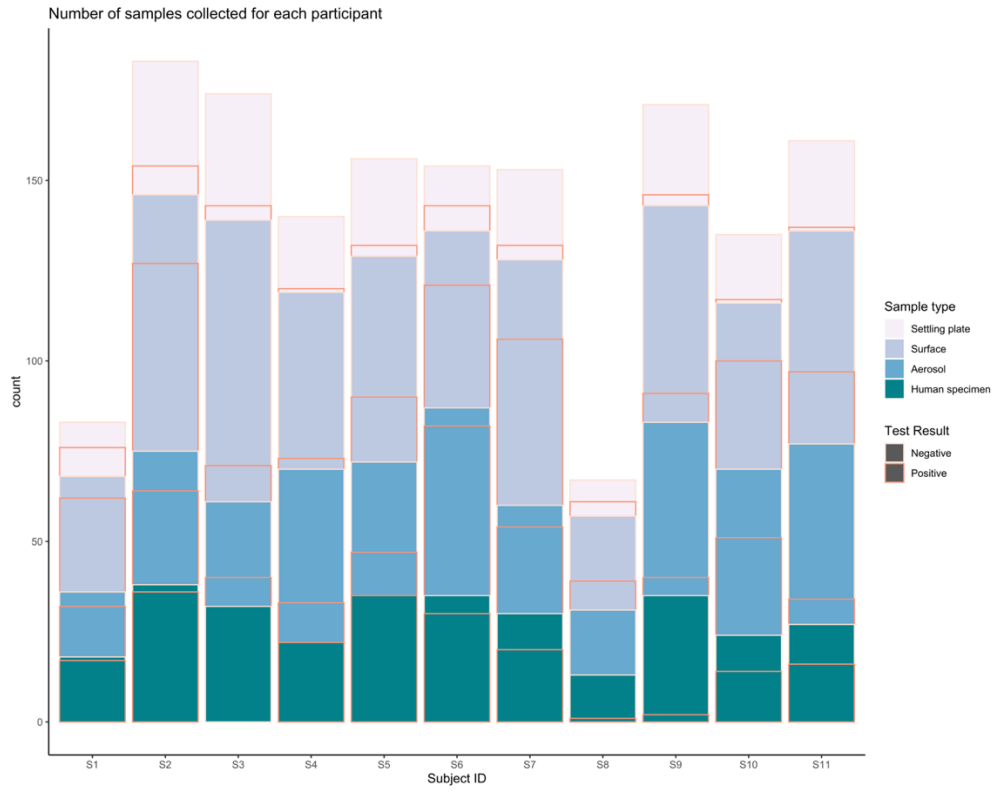
Supplemental figure III. 9. Comparison of aerosol CT for ventilation trials of under ~4.5 ACH and above ~9 ACH in near field and far field.



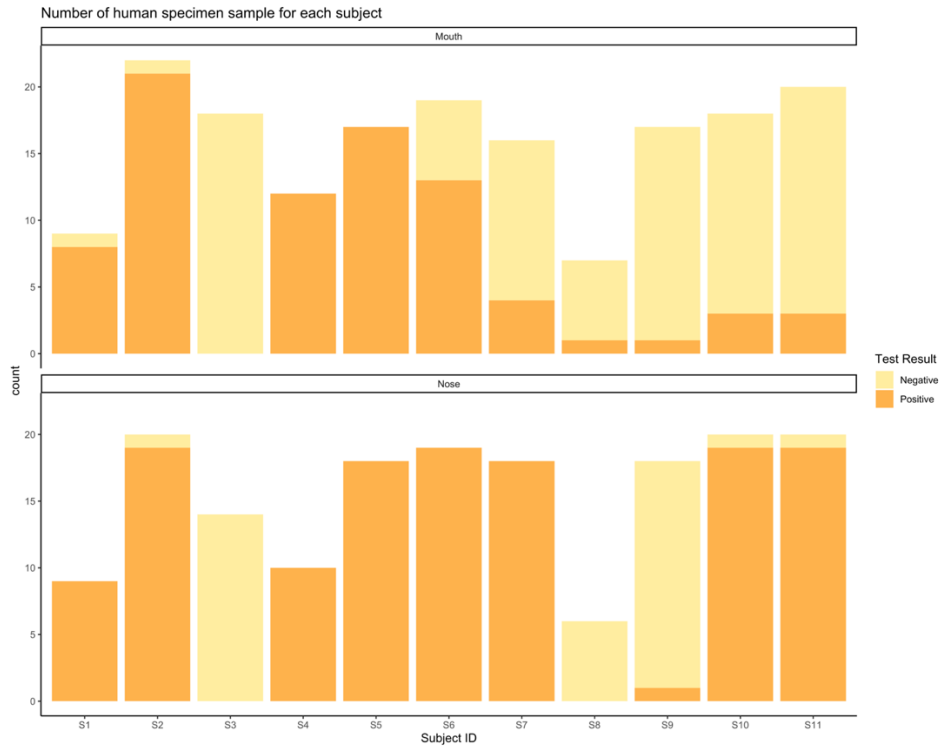
Supplemental figure III. 10. The impact of removal mechanism on high touched surface viral load.



Supplemental figure III. 11. Number and type of samples collected for each participant.



Supplemental figure III. 12. Number and proportion positive of nasal and saliva samples.



Supplemental table III. 1. Demographic data of the study participants.

Biological sex		<i>Percent(n)</i>
Male		36(4)
Female		63(7)
Ethnicity		Percent(n)
White		72(8)
Hispanic/Latino/Spanish		27(3)
Native Hawaiian / Pacific Islander		-
Black / African American		18(2)
Multiple		36(4)
Asian		9(1)

Supplemental table III. 2. The mean difference of removal mechanism trials and their paired control trials with ~ 0 ACH.

<i>Observation</i>	<i>~3 & 4.5 ACH~Control</i>	<i>~9ACH~Control</i>	<i>Filtration~Control</i>
<i>Near field C_T</i>	1.1409(P = 0.25)	2.5766(P = 0.07)	5.1462(P = 0.03)
<i>Far field C_T</i>	0.5125(P = 0.39)	0.8233(P = 0.32)	1.3351(P = 0.23)
<i>Near field CO₂</i>	-332.90 (P = 1.12e-08)	-398.46 (P = 1.11e-06)	87.41 (P = 0.37)
<i>Far field CO₂</i>	-320.08 (P = 1.4e-06)	-369.62 (P = 2.39e-05)	103.27 (P = 0.09)

APPENDIX B

Rainbow Passage[150]:

When the sunlight strikes raindrops in the air, they act as a prism and form a rainbow. The rainbow is a division of white light into many beautiful colors. These take the shape of a long round arch, with its path high above, and its two ends apparently beyond the horizon. There is, according to legend, a boiling pot of gold at one end. People look, but no one ever finds it. When a man looks for something beyond his reach, his friends say he is looking for the pot of gold at the end of the rainbow.

APPENDIX C

Institutional Approval and Data Availability

Biological protocols were reviewed and approved by Advarra Institutional Biosafety Committee (IBC) (Protocol #PROTO202000132). Advarra IBC is an authorized external IBC for the University of Oregon and is registered with the National Institute of Health (NIH). Human participant protocols were reviewed and approved by the University of Oregon Institutional Review Board (IRB) (Protocol #12292020).

Participant Recruitment

University of Oregon COVID-19 protocols require individuals living in the university residence halls to spend their isolation period at an off-campus quarantine dormitory room for 10 days. Individuals positive for COVID-19 were identified through the University of Oregon Monitoring and Assessment Program (MAP). Following transfer to the isolation dormitory, individuals were recruited into the program to conduct a 3-day study at the RDM which was located in the dormitory parking lot. All participants volunteered to conduct different activities involved with this study with no penalty associated with leaving the research at any time.

RDM layout

The interior space of the RDM measured 2.8 m (width), 4.3 m (length), and 2.13 – 2.4 m (height) with a total volume of 28,080 L. Interior temperature was maintained at 22°C +/-4 °C with three portable electric resistance heaters. Relative humidity was adjusted using two portable humidifiers and two dehumidifiers, respectively. Outdoor ACH of ~3 – 4.5 and ~9 were provided through a HEPA filtered (CleanShield HEPA 550, ALORAIR) exhaust air removal from the RDM with make-up air via infiltration and

an operable window that opened during maximum ventilation trials. Filtration was provided with two in-room HEPA filters with combined Clean Air Delivery Rate (CADR) of $\sim 1000 \text{ m}^3/\text{h}$ (600 Cubic Feet per Minute). Temperature, RH, and CO₂ were monitored and recorded using multiple data loggers (Onset HOBO MX1102A). Particles were measured at six cut point size bins as follows: 0.3 μm -1 μm , 1 μm -2.5 μm , 2.5 μm -3 μm , 3 μm -5 μm , 5.0 μm -10 μm and 10 μm -25 μm , using 3 particle counters (TSI Aerotrak 9306-V2). Exhaust air flow rate was confirmed using an anemometer (Omega HHF92A CFM Master II) and later through analysis of CO₂ concentration during routine and removal mechanism trials. After each experimental trial, air in the RDM was filtered at +30 ACH for 10+ minutes using a CleanShield HEPA 550 (AlorAir) fitted with a HEPA filter as well two in-room HEPA filters.

Sample Collection

Samples were collected 8-12 times throughout a day as described in Table III.1, as well as Supplemental figures III.11 & III.12. Participants were instructed to conduct speaking and speaking loudly activities in S1 (Figure III.1a) by reading from a standard passage (CDC approved, Supplemental document, appendix B)[150]. During activities listed in S2 (Figure III.1b), participants conducted routine office activities for all trials unless specified otherwise in Table III.1. Participants were invited to attend a video call meeting with their friends or family members during 30-min sitting and speaking trials listed in physical activity (Table III.1).

At the end of each trial, both a mouth and shallow nasal swab were self-collected by the study participant. Environmental samples were collected using flocced swabs (Harmony #P25-3506-H), passive air settling plates (Millipore Sigma #P5731-500EA),

and active air samplers (ThermoFisher #2900AA). The average sampling period according to each intervention were as follows: 57.6 minutes for routine trials, 60.5 minutes for outdoor air exchange trials, 60.4 minutes for filtration trials, and 59.7 minute for relative humidity trials. Environmental swabs were collected from the participant's cell phone, computer, chair, and exhaust inlet. For walking on treadmill trials, samples from treadmill handrail, front rail, and bottom were collected. Flocked nylon swabs pre-moistened with DNA/RNA Shield (Zymo Research, Catalog #R1100) were used to swab the sampling location in a zig-zag 'S' pattern for 15-20 seconds and then returned to a labeled 5 ml tube containing 1 ml of DNA/RNA Shield. Settling particles were captured using both components (base and lid) of standard Petri dishes. Following the sampling period, both sides of the Petri dish (sampling area ~110 cm²) were swabbed following the protocol described above for environmental swabs. Active air samples were collected using two AerosolSense samplers. The AerosolSense sampler works by drawing air into an accelerating slit impactor at a rate of 200 L/minute, causing particles to impact onto a collection substrate. Following the sampling period, the collection substrate was transferred to 1 ml of DNA/RNA Shield using flame-sterilized forceps and transported back to a BSL-2 laboratory. Upon return to the laboratory, the capture media was briefly vortexed, then centrifuged for 2-minutes at 1,500 x g to remove all liquid from the collection substrate. Following centrifugation, the collection substrate was placed into biohazard disposal bag and discarded appropriately.

Molecular Analysis

All protocols were performed in a Purifier Logic+ Class II, Type A2 biosafety cabinet (LabConco, Catalog #302420001). Total RNA was extracted using the Quick-

DNA/RNA Viral Magbead kit (Zymo Research, Catalog #R2141). Nucleic acids were stored at -80°C until downstream analysis could be performed. A 5 µl spike-in of *Escherichia coli* MS2 bacteriophage was added to each extraction well to confirm the success of each RNA extraction. Additionally, a sample of nuclease free water was included with each batch of samples during extraction to serve as an extraction control. Samples underwent quantitative reverse-transcription polymerase chain reaction (qRT-PCR) analysis using the TaqPath COVID-19 Combo Kit (Thermo Fisher Scientific, Catalog #A47814) targeting the spike (S), nucleocapsid (N), and RNA-dependent RNA polymerase (RdRP/ORF1ab) genomic regions. Additionally, the assay also targets the *Escherichia coli* MS2 bacteriophage as an internal process control. The reaction mixtures included 5 µl TaqPath 1-Step Multiplex Mastermix without ROX (Thermo Fisher Scientific, Catalog #A28521), 9 µl nuclease-free water (Invitrogen, Catalog #4387936), 1 µl COVID-19 Real Time PCR Assay Multiplex Mix (Thermo Fisher Scientific, Catalog #A47814), and 5 µl of template RNA. Thermocycling was performed with the QuantStudio5 (Applied Biosystems). Samples were considered positive if amplification was observed in two of three genome targets with a cycle threshold (C_T) value less than or equal to 35 ($C_T \leq 35$)[198]. Each qRT-PCR plate contained a positive RNA control and a no-template control (nuclease-free water) All controls performed as expected.

Statistical Analyses

Analyses were performed using the statistical programming environment R. The correlation between observed C_T values and other environmental parameters was conducted through the use of a generalized linear model. One-tailed paired t-test were

used to identify statistical differences between categorical variables such as mean C_T values and environmental parameters unless otherwise noted. Black solid horizontal line represents median in all box plots in this article. One tailed non-paired t-test was used to identify statistical differences for trials with outdoor air exchange rate of under ~ 4.5 ACH and above ~ 9 ACH.

APPENDIX D

This appendix presents further discussion on particles data in Figure III.4.

Interestingly in Figure III.4, the 0.3 μm -1 μm size bin indicates the highest correlation coefficient between immediate field particle counts and immediate field aerosol viral load. While the relationship between the particles of 1 μm -2.5 μm and immediate field viral load is significant, there is no significant relationship found for 2.5 μm -3 μm , 3 μm -5 μm and 5 μm -10 μm .

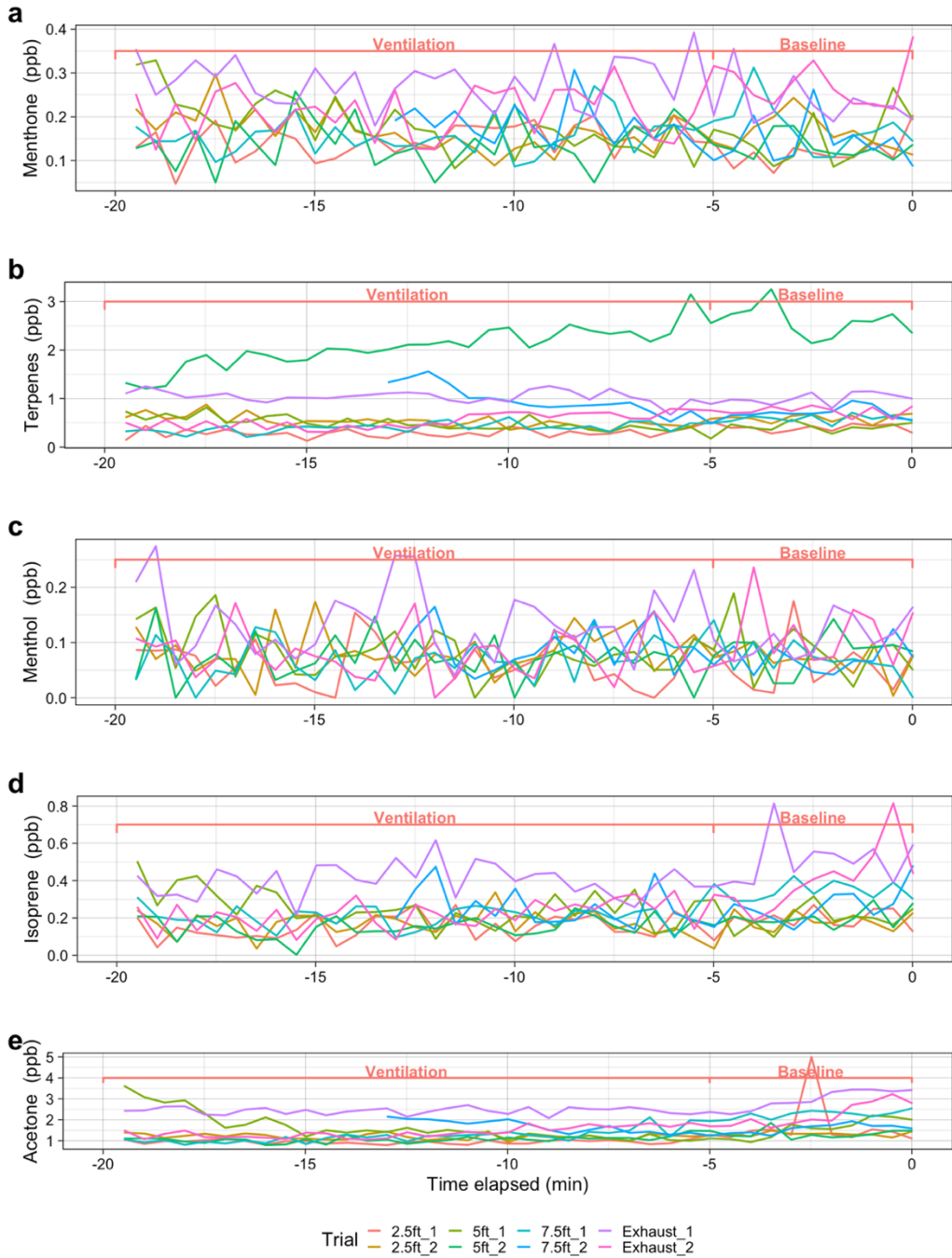
Among high expiratory trials, we observed an increase in immediate field viral load equivalent to -1 C_T to be associated with an increase of ~ 1000 particles of the size 0.3 μm -1 μm , and an increase in ~ 100 particles of the size 1 μm -2.5 μm , and \sim one particle of the size 10 μm -25 μm in the immediate field. It is important to stress that these results are relevant to immediate field particles dominated by bioaerosols.

Our findings for immediate field trials support previous research in which SARS-CoV-2 RNA was identified in fine particles[135]. While we did not find any statistically significant relationship between aerosol viral load and particle counts of 5 μm -25 μm during routine trials in the near field (1.2m) or the far field (3.5 m), during immediate field (<1m) high expiratory trials we identified a significant relationship for large particles (10 μm -25 μm) and immediate field aerosol viral load; we hypothesize that may be due to immediate field respiratory droplets prevalent in high expiratory activities[119,143,199].

APPENDIX E

This appendix presents supplemental figures associated with Chapter IV.

Supplemental figure IV. 1. Evaluating the impact of distance on bioaerosol exposure in a typical indoor environment.



Supplemental table IV. 1. Evaluating the impact of distance on bioaerosol exposure in a typical indoor environment.

INTERVALS	2.5 ft			5 ft			7.5 ft		
	Magnifier	Effect size	\pm EU ²	Magnifier	Effect size	\pm EU ²	Magnifier	Effect size	\pm EU ²
Min_0_60	1.2123	0.32 (s)	0.3496	1.0799	0.14 (N)	0.3265	1.0516	0.1 (N)	0.3094
Min_0_5	2.7476	0.57(M)	4.6822	1.7211	- 0.08(N)	3.4974	0.7354	- 0.58(M)	1.8898
Min_5_10	0.8995	-0.26(S)	0.507	0.6893	- 0.95(L)	0.51	0.6587	- 1.12(L)	0.4337
Min_10_15	1.3637	1.96(L)	0.4228	0.949	- 0.42(S)	0.3454	0.878	- 0.93(L)	0.3048
Min_15_20	1.4471	3.65(L)	0.3764	1.021	0.09(N)	0.3187	0.9731	-0.28(S)	0.2789
Min_20_25	1.2559	2.00(L)	0.3088	1.1754	1.32(L)	0.2948	1.1446	1.07(L)	0.2637
Min_25_30	1.1251	1.39(L)	0.2301	1.0277	0.23(S)	0.2242	1.1122	1.08(L)	0.2173
Min_30_35	1.1901	2.13(L)	0.251	1.162	1.78(L)	0.2595	1.1689	2.12(L)	0.2292
Min_35_40	1.1774	2.00(L)	0.2356	1.1293	1.35(L)	0.2131	1.1219	1.41(L)	0.2147
Min_40_45	1.1904	2.54(L)	0.2036	1.1633	2.27(L)	0.2108	1.1343	1.88(L)	0.1938
Min_45_50	1.1518	2.39(L)	0.1856	1.1082	1.71(L)	0.1826	1.0647	1.01(L)	0.1761
Min_50_55	1.2103	2.76(L)	0.2546	1.1452	2.01(L)	0.217	1.0662	0.92(L)	0.202
Min_55_60 ¹	1.1839	2.39(L)	0.2559	1.1121	1.49(L)	0.213	1.0775	1.03(L)	0.1793

* N = negligible effect size, S = small effect size, M = medium effect size, L = large effect size

¹ = Steady state period

² = Expanded uncertainty

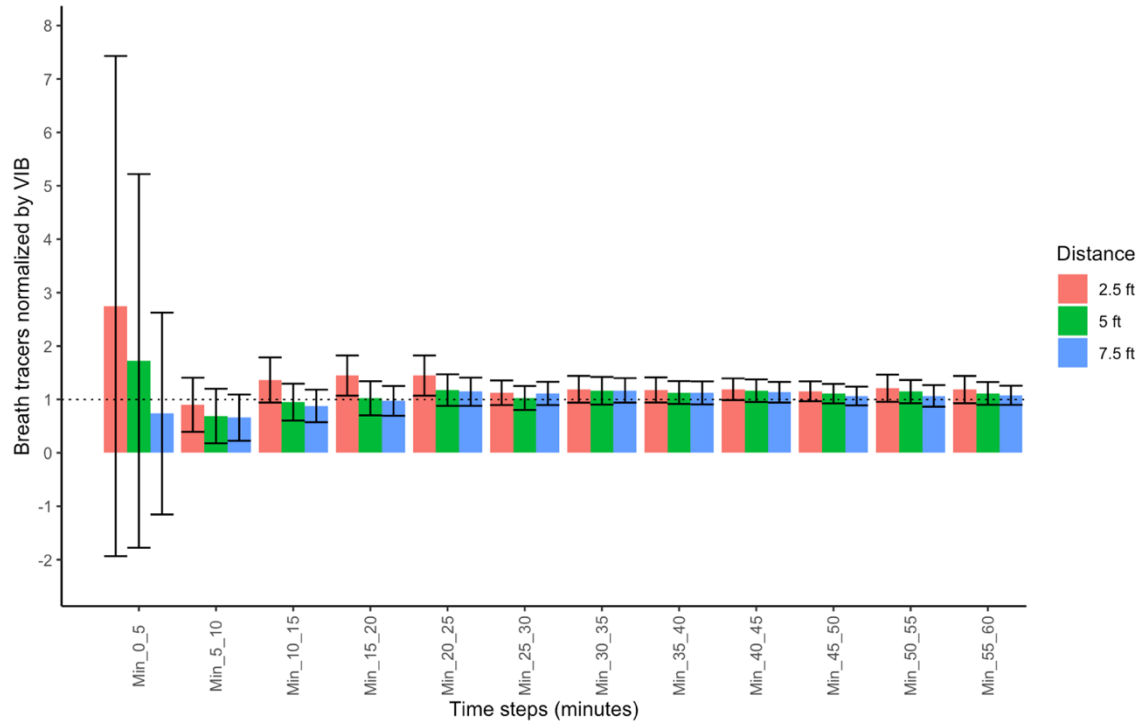
The implications of magnifiers in a real-world case study

The purpose of this section is to compare the results of near -field and far-field magnifiers for the present study and two recent relevant studies.[159,170]

In one study [170] the team measured near-field and far-field CO₂ concentrations to estimate magnifiers in patient rooms within a healthcare environment having 8-11 ACH. The study reported background (far-field) CO₂ levels of 580 ppm (mean across 7

patients) and reported near-field mean CO₂ levels of 605 ppm, thus 25 ppm higher than background, which equates to a near-field magnifier of 4.3%[170].

Supplemental figure IV. 2. Comparison of the concentrations of breath tracers for each distance to volume integrated background with expanded uncertainties.



A second study reports on bioaerosols emitted from individuals that were diagnosed with COVID-19 within a space having similar environmental conditions as the present study.[159] Near-field and far-field terms were used to report the concentration of SARS-CoV-2 viral RNA in room aerosols, room CO₂, and room particles in the range of 0.3-25 μm at 1.2 m (4 ft) and 3.5 m (11 ft). We translate their data into near-/far-field ratios to provide a comparison with the near-field magnifiers reported in Figure 3 of the present study. The near-/far-field ratios from the previous study (Supplemental table 3) ranged from ~8-12% for CO₂ and particles (1-2.5μm), which correspond reasonably well

with the near-field magnifiers of the present study (Figure 3) where the concentration of targeted VOCs in the near-field (2.5 ft) was ~10% higher than far-field (7.5ft) during steady-state periods.

Supplemental table IV. 2. Comparison of spatial parameters between the present and the controlled study with participants diagnosed with COVID-19[159].

Key variables	Breath tracer (present study)	Parhizkar, et al (2022)
Volume (m3)	27	28.04
Air exchange rate (1/h)	~ 3 ACH	~0
Duration (minutes)	60	60
Near- field distance (ft)	2.5	4
Far- field distance (ft)	7.5	11
Near/far fields ratio	3	2.75
Number of participants in the room for each trial	1	1

Supplemental table IV. 3. Comparison of near- field and far-field in a recent controlled study on participants that were diagnosed with COVID-19.[159]

Variable	<i>Near-field</i>	<i>Far-field</i>	Near-field / Far-field
CO2 (ppm)	937.724	862.4149	1.0836
Particles, 0.3 µm - 1µm	16454.36	15959.25	1.0305
Particles, 1 µm - 2.5 µm	559.5155	493.7172	1.1249
Particles, 2.5 µm - 3µm	37.61776	31.71535	1.1702
Particles, 3 µm - 5 µm	50.8684	45.12782	1.1196
Particles, 5 µm - 10 µm	26.47086	27.24334	N/A
Particles, 10 µm - 25 µm	8.85414	8.961011	N/A

REFERENCE CITED

1. World Health Organization [WHO]. WHO Coronavirus (COVID-19) Dashboard. 2021. Available at: <https://covid19.who.int/>. Accessed 18 June 2021.
2. Dietz L, Horve PF, Coil DA, Fretz M, Eisen JA, Van Den Wymelenberg K. 2019 novel Coronavirus (COVID-19) pandemic: Built environment considerations to reduce transmission. *mSystems* **2020**; 5. Available at: <http://dx.doi.org/10.1128/mSystems.00245-20>.
3. Bourgonje AR. SARS-CoV-2 and the pathophysiology of coronavirus disease 2019. *2*.
4. Sridhar S, Nicholls J. Pathophysiology of infection with SARS-CoV-2-What is known and what remains a mystery.
5. Chertow D, Stein S, Ramelli S, et al. SARS-CoV-2 infection and persistence throughout the human body and brain. *Research Square*. 2021; Available at: <https://www.researchsquare.com/article/rs-1139035/v1>. Accessed 1 February 2022.
6. Morens DM, Folkers GK, Fauci AS. What is a pandemic? *J Infect Dis* **2009**; 200:1018–1021.
7. View of history of pandemics in the twentieth and twenty-first century. Available at: <https://doisrpska.nub.rs/index.php/SNZ/article/view/7356/7143>. Accessed 10 February 2022.
8. Altman LK. Is this a pandemic? Define ‘pandemic.’ *NY Times*. 2009; Available at: <https://www.nytimes.com/2009/06/09/health/09docs.html>. Accessed 10 February 2022.
9. Shaw-Taylor L. An introduction to the history of infectious diseases, epidemics and the early phases of the long-run decline in mortality. *Econ Hist Rev* **2020**; 73:E1–E19.
10. History of smallpox. 2021. Available at: <https://www.cdc.gov/smallpox/history/history.html>. Accessed 14 February 2022.
11. History of 1918 flu pandemic. 2019. Available at: <https://www.cdc.gov/flu/pandemic-resources/1918-commemoration/1918-pandemic-history.htm>. Accessed 14 February 2022.
12. Smallpox. 2019. Available at: <https://www.cdc.gov/smallpox/index.html>. Accessed 14 February 2022.

13. SARS. 2021. Available at: <https://www.cdc.gov/sars/about/fs-sars.html>. Accessed 14 February 2022.
14. Kim S-H, Chang SY, Sung M, et al. Extensive viable Middle East respiratory syndrome (MERS) Coronavirus contamination in air and surrounding environment in MERS isolation wards. *Clin Infect Dis* **2016**; 63:363–369.
15. CDCGlobal. Global measles outbreaks. 2022. Available at: <https://www.cdc.gov/globalhealth/measles/data/global-measles-outbreaks.html>. Accessed 14 February 2022.
16. Available at: <https://www.washingtonpost.com/history/2020/09/01/1918-flu-pandemic-end/>. Accessed 14 February 2022.
17. Wang CC, Prather KA, Sznitman J, et al. Airborne transmission of respiratory viruses. *Science* **2021**; 373:eabd9149.
18. Chan HTH, Yanis B. The lancet covid-19 commission task force on safe work, safe school, and safe travel. Available at: <https://uvresources.com/wp-content/uploads/2021/05/SafeWorkTFDesigninginfectiousdiseaseresilienceApril2021.pdf>. Accessed 14 February 2022.
19. Coleman KK, Tay DJW, Sen Tan K, et al. Viral load of SARS-CoV-2 in respiratory aerosols emitted by COVID-19 patients while breathing, talking, and singing. *Clin Infect Dis* **2021**; Available at: <http://dx.doi.org/10.1093/cid/ciab691>.
20. Lednicky JA, Lauzardo M, Fan ZH, et al. Viable SARS-CoV-2 in the air of a hospital room with COVID-19 patients. *Int J Infect Dis* **2020**; 100:476–482.
21. Marr LC, Tang JW. A paradigm shift to align transmission routes with mechanisms. *Clin Infect Dis* **2021**; 73:1747–1749.
22. Samet JM, Prather K, Benjamin G, et al. Airborne transmission of SARS-CoV-2: What we know. *Clin Infect Dis* **2021**; Available at: <http://dx.doi.org/10.1093/cid/ciab039>.
23. Morawska L, Allen J, Bahnfleth W, et al. A paradigm shift to combat indoor respiratory infection. *Science* **2021**; 372:689–691.
24. CDC. Scientific brief: SARS-CoV-2 transmission. 2021. Available at: <https://www.cdc.gov/coronavirus/2019-ncov/science/science-briefs/sars-cov-2-transmission.html>. Accessed 1 February 2022.

25. Modes of transmission of virus causing COVID-19: implications for IPC precaution recommendations. Available at: <https://www.who.int/news-room/commentaries/detail/modes-of-transmission-of-virus-causing-covid-19-implications-for-ipc-precaution-recommendations>. Accessed 1 February 2022.
26. Allen JG, Waring MS. Harnessing the power of healthy buildings research to advance health for all. *J Expo Sci Environ Epidemiol* **2020**; 30:217–218.
27. Bayati M, Vu DC, Vo PH, et al. Health risk assessment of volatile organic compounds at daycare facilities. *Indoor Air* **2021**; Available at: <http://dx.doi.org/10.1111/ina.12801>.
28. Fahimipour AK, Hartmann EM, Siemens A, et al. Daylight exposure modulates bacterial communities associated with household dust. *Microbiome* **2018**; 6:175.
29. Nazaroff WW, Weschler CJ, Corsi RL. Indoor air chemistry and physics. *Atmos Environ (1994)* **2003**; 37:5451–5453.
30. Hongu T, Phillips GO, Takigami M. Frontier of health and comfort fibers. In: *New Millennium Fibers*. Elsevier, 2005: 173–217.
31. GBD Compare. Available at: <https://vizhub.healthdata.org/gbd-compare/>. Accessed 18 February 2022.
32. Farmer DK, Vance ME, Abbatt JPD, et al. Overview of HOMEChem: House Observations of Microbial and Environmental Chemistry. *Environ Sci Process Impacts* **2019**; 21:1280–1300.
33. Horve PF, Dietz LG, Ishaq SL, Kline J, Fretz M, Van Den Wymelenberg KG. Viable bacterial communities on hospital window components in patient rooms. *PeerJ* **2020**; 8:e9580.
34. Misztal PK, Lympelopoulou DS, Adams RI, et al. Emission factors of microbial volatile organic compounds from environmental bacteria and fungi. *Environ Sci Technol* **2018**; 52:8272–8282.
35. Williams J, Stöner C, Wicker J, et al. Cinema audiences reproducibly vary the chemical composition of air during films, by broadcasting scene specific emissions on breath. *Sci Rep* **2016**; 6:1–10.
36. Allen JG, MacNaughton P, Laurent JGC, Flanigan SS, Eitland ES, Spengler JD. Green Buildings and Health. *Curr Environ Health Rep* **2015**; 2:250–258.
37. Greenhalgh T, Jimenez JL, Prather KA, Tufekci Z, Fisman D, Schooley R. Ten scientific reasons in support of airborne transmission of SARS-CoV-2. *Lancet* **2021**; 397:1603–1605.

38. Bulfone TC, Malekinejad M, Rutherford GW, Razani N. Outdoor transmission of SARS-CoV-2 and other respiratory viruses: A systematic review. *J Infect Dis* **2021**; 223:550–561.
39. Morawska L, Cao J. Airborne transmission of SARS-CoV-2: The world should face the reality. *Environ Int* **2020**; 139:105730.
40. Lewis D. Superspreading drives the COVID pandemic - and could help to tame it. *Nature* **2021**; 590:544–546.
41. Eichler N, Thornley C, Swadi T, et al. Transmission of severe acute respiratory syndrome Coronavirus 2 during border quarantine and air travel, New Zealand (Aotearoa). *Emerg Infect Dis* **2021**; 27:1274–1278.
42. Sharma A, Clark E, McGlothlin JD, Mittal SK. Efficiency of Airborne Sample Analysis Platform (ASAP) bioaerosol sampler for pathogen detection. *Front Microbiol* **2015**; 6:512.
43. Li Y, Qian H, Hang J, et al. Probable airborne transmission of SARS-CoV-2 in a poorly ventilated restaurant. *Build Environ* **2021**; 196:107788.
44. Kwon KS, Park JI, Park YJ, Jung DM, Ryu KW, Lee JH. Evidence of long-distance droplet transmission of SARS-CoV-2 by direct air flow in a restaurant in Korea. *J Korean Med Sci* **2020**; 35:e415.
45. Hamner L, Dubbel P, Capron I, et al. High SARS-CoV-2 attack rate following exposure at a choir practice - Skagit County, Washington, March 2020. *MMWR Morb Mortal Wkly Rep* **2020**; 69:606–610.
46. Katelaris AL, Wells J, Clark P, et al. Epidemiologic evidence for airborne transmission of SARS-CoV-2 during church singing, Australia, 2020. *Emerg Infect Dis* **2021**; 27:1677–1680.
47. Shen Y, Li C, Dong H, et al. Community outbreak investigation of SARS-CoV-2 transmission among bus riders in eastern China. *JAMA Intern Med* **2020**; 180:1665.
48. Jang S, Han SH, Rhee J-Y. Cluster of Coronavirus disease associated with fitness dance classes, South Korea. *Emerg Infect Dis* **2020**; 26:1917–1920.
49. Khanh NC, Thai PQ, Quach H-L, et al. Transmission of SARS-CoV 2 during long-haul flight. *Emerg Infect Dis* **2020**; 26:2617–2624.
50. Horve PF, Dietz L, Northcutt D, Stenson J, Van Den Wymelenberg K. Evaluation of a bioaerosol sampler for indoor environmental surveillance of Severe Acute Respiratory Syndrome Coronavirus 2. *PLoS One* **2021**; 16:e0257689.

51. Hermesch AC, Horve PF, Edelman A, et al. Severe acute respiratory syndrome Coronavirus 2 (SARS-CoV-2) environmental contamination and childbirth. *Obstet Gynecol* **2020**; 136:827–829.
52. Pan J, Hawks SA, Prussin AJ II, Duggal NK, Marr LC. SARS-CoV-2 on surfaces and HVAC filters in dormitory rooms. *Environ Sci Technol Lett* **2022**; 9:71–76.
53. Horve P, Dietz L, Bowles G, et al. Longitudinal analysis of built environment and aerosol contamination associated with isolated COVID-19 positive individuals. 2021; Available at: https://assets.researchsquare.com/files/rs-861942/v1_covered.pdf?c=1630438371.
54. Borges JT, Nakada LYK, Maniero MG, Guimarães JR. SARS-CoV-2: a systematic review of indoor air sampling for virus detection. *Environ Sci Pollut Res Int* **2021**; 28:40460–40473.
55. Horve PF, Dietz LG, Fretz M, et al. Identification of SARS-CoV-2 RNA in healthcare heating, ventilation, and air conditioning units. *Indoor Air* **2021**; 31:1826–1832.
56. Chia PY, Coleman KK, Tan YK, et al. Detection of air and surface contamination by SARS-CoV-2 in hospital rooms of infected patients. *Nat Commun* **2020**; 11:2800.
57. Lednicky JA, Shankar SN, Elbadry MA, et al. Collection of SARS-CoV-2 virus from the air of a clinic within a university student health care center and analyses of the viral genomic sequence. *Aerosol Air Qual Res* **2020**; 20:1167–1171.
58. Liu Y, Ning Z, Chen Y, et al. Aerodynamic analysis of SARS-CoV-2 in two Wuhan hospitals. *Nature* **2020**; 582:557–560.
59. Doremalen N, T B, Dh M, et al. Aerosol and surface stability of SARS-CoV-2 as compared with SARS-CoV-1. 2020;
60. Lednicky JA, Lauzardo M, Alam MM, et al. Isolation of SARS-CoV-2 from the air in a car driven by a COVID patient with mild illness. *Int J Infect Dis* **2021**; Available at: <http://dx.doi.org/10.1016/j.ijid.2021.04.063>.
61. Available at: <http://assets.thermofisher.com/TFS-Assets/CAD/Technical-Notes/TS-AerosolSense-Tech-Comp.pdf>. Accessed 18 February 2022.
62. Caley E. How it works. 2021. Available at: <https://poppy.com/how-it-works/>. Accessed 18 February 2022.
63. Dai D, Prussin AJ II, Marr LC, Vikesland PJ, Edwards MA, Pruden A. Factors shaping the human exposome in the built environment: Opportunities for engineering control. *Environ Sci Technol* **2017**; 51:7759–7774.

64. McNeill VF, Corsi R, Huffman JA, et al. Room-level ventilation in schools and universities. *Atmospheric Environment: X* **2022**; 13:100152.
65. MacNaughton P, Spengler J, Vallarino J, Santanam S, Satish U, Allen J. Environmental perceptions and health before and after relocation to a green building. *Build Environ* **2016**; 104:138–144.
66. Guo H, Morawska L, He C, Gilbert D. Impact of ventilation scenario on air exchange rates and on indoor particle number concentrations in an air-conditioned classroom. *Atmos Environ (1994)* **2008**; 42:757–768.
67. Wargocki P, Porras-Salazar JA, Contreras-Espinoza S, Bahnfleth W. The relationships between classroom air quality and children’s performance in school. *Build Environ* **2020**; 173:106749.
68. Fisk WJ. The ventilation problem in schools: literature review. *Indoor Air* **2017**; 27:1039–1051.
69. Burrige HC, Bhagat RK, Stettler MEJ, et al. The ventilation of buildings and other mitigating measures for COVID-19: a focus on wintertime. *Proc Math Phys Eng Sci* **2021**; 477. Available at: <http://dx.doi.org/10.1098/rspa.2020.0855>.
70. Gettings J, Czarnik M, Morris E, et al. Mask use and ventilation improvements to reduce COVID-19 incidence in elementary schools - Georgia, November 16-December 11, 2020. *MMWR Morb Mortal Wkly Rep* **2021**; 70:779–784.
71. Rudnick SN, Milton DK. Risk of indoor airborne infection transmission estimated from carbon dioxide concentration. *Indoor Air* **2003**; 13:237–245.
72. Miller SL, Nazaroff WW, Jimenez JL, et al. Transmission of SARS-CoV-2 by inhalation of respiratory aerosol in the Skagit Valley Chorale superspreading event. *Indoor Air* **2020**; Available at: <http://dx.doi.org/10.1111/ina.12751>.
73. Waring MS, Wells JR. Volatile organic compound conversion by ozone, hydroxyl radicals, and nitrate radicals in residential indoor air: Magnitudes and impacts of oxidant sources. *Atmos Environ (1994)* **2015**; 106:382–391.
74. Zhang Y, Mo J, Li Y, et al. Can commonly-used fan-driven air cleaning technologies improve indoor air quality? A literature review. *Atmos Environ (1994)* **2011**; 45:4329–4343.
75. Darnell MER, Subbarao K, Feinstone SM, Taylor DR. Inactivation of the coronavirus that induces severe acute respiratory syndrome, SARS-CoV. *J Virol Methods* **2004**; 121:85–91.

76. Heilingloh CS, Aufderhorst UW, Schipper L, et al. Susceptibility of SARS-CoV-2 to UV irradiation. *Am J Infect Control* **2020**; 48:1273–1275.
77. Dols WS, Polidoro BJ, Poppendieck D, Emmerich SJ. A tool to model the Fate and Transport of Indoor Microbiological Aerosols (FaTIMA). Gaithersburg, MD: National Institute of Standards and Technology, 2020. Available at: <http://dx.doi.org/10.6028/nist.tn.2095>.
78. Batterman S, Godwin C, Jia C. Long duration tests of room air filters in cigarette smokers' homes. *Environ Sci Technol* **2005**; 39:7260–7268.
79. Cheng YS, Lu JC, Chen TR. Efficiency of a portable indoor air cleaner in removing pollens and fungal spores. *Aerosol Sci Technol* **1998**; 29:92–101.
80. Offermann FJ Iii, Loiselle SA, Sextro G. Performance of air cleaners in a residential forced air system. *ASHRAE J* **1992**; 34:51–57.
81. Davis WT, Cornell C. Dever Comparison of Experimental and Theoretical efficiencies of residential air filters. *TAPPI Journal* **1994**; 77:180–186.
82. Available at: https://assets.publishing.service.gov.uk/government/uploads/system/uploads/attachment_data/file/939173/S0867_EMG_Potential_application_of_air_cleaning_devices_and_personal_decontamination_to_manage_transmission_of_COVID-19.pdf. Accessed 2 February 2022.
83. Epa US, OAR. What is a HEPA filter? **2019**; Available at: <https://www.epa.gov/indoor-air-quality-iaq/what-hepa-filter-1>. Accessed 2 February 2022.
84. Pineda Rojas AL, Cordo SM, Saurral RI, Jimenez JL, Marr LC, Kropff E. Relative humidity predicts day-to-day variations in COVID-19 cases in the city of Buenos Aires. *Environ Sci Technol* **2021**; 55:11176–11182.
85. Ahlawat A, Wiedensohler A, Mishra SK. An overview on the role of relative humidity in airborne transmission of SARS-CoV-2 in indoor environments. *Aerosol Air Qual Res* **2020**; 20:1856–1861.
86. Jones B, Sharpe P, Iddon C, Hathway EA, Noakes CJ, Fitzgerald S. Modelling uncertainty in the relative risk of exposure to the SARS-CoV-2 virus by airborne aerosol transmission in well mixed indoor air. *Build Environ* **2021**; 191:107617.
87. Dabisch P, Schuit M, Herzog A, et al. The influence of temperature, humidity, and simulated sunlight on the infectivity of SARS-CoV-2 in aerosols. *Aerosol Sci Technol* **2021**; 55:142–153.

88. Lin K, Marr LC. Humidity-dependent decay of viruses, but not bacteria, in aerosols and droplets follows disinfection kinetics. *Environ Sci Technol* **2020**; 54:1024–1032.
89. Prussin AJ 2nd, Schwake DO, Lin K, Gallagher DL, Buttling L, Marr LC. Survival of the enveloped virus Phi6 in droplets as a function of relative humidity, absolute humidity, and temperature. *Appl Environ Microbiol* **2018**; 84. Available at: <http://dx.doi.org/10.1128/AEM.00551-18>.
90. Kormuth KA, Lin K, Qian Z, Myerburg MM, Marr LC, Lakdawala SS. Environmental persistence of influenza viruses is dependent upon virus type and host origin. *mSphere* **2019**; 4. Available at: <http://dx.doi.org/10.1128/mSphere.00552-19>.
91. Kormuth KA, Lin K, Prussin AJ 2nd, et al. Influenza virus infectivity is retained in aerosols and droplets independent of relative humidity. *J Infect Dis* **2018**; 218:739–747.
92. Chan KH, Peiris JSM, Lam SY, Poon LLM, Yuen KY, Seto WH. The effects of temperature and relative humidity on the viability of the SARS Coronavirus. *Adv Virol* **2011**; 2011:734690.
93. Biryukov J, Boydston JA, Dunning RA, et al. Increasing temperature and relative humidity accelerates inactivation of SARS-CoV-2 on surfaces. *mSphere* **2020**; 5. Available at: <http://dx.doi.org/10.1128/mSphere.00441-20>.
94. Schuit M, Ratnesar-Shumate S, Yolitz J, et al. Airborne SARS-CoV-2 is rapidly inactivated by simulated sunlight. *J Infect Dis* **2020**; 222:564–571.
95. Chaudhuri S, Basu S, Saha A. Analyzing the dominant SARS-CoV-2 transmission routes toward an ab initio disease spread model. *Phys Fluids (1994)* **2020**; 32:123306.
96. Parhizkar H, Van Den Wymelenberg KG, Haas CN, Corsi RL. A quantitative risk estimation platform for indoor aerosol transmission of COVID-19. *Risk Anal* **2021**; Available at: <http://dx.doi.org/10.1111/risa.13844>.
97. Tellier R, Li Y, Cowling BJ, Tang JW. Recognition of aerosol transmission of infectious agents: a commentary. *BMC Infect Dis* **2019**; 19:101.
98. Lu J, Gu J, Li K, et al. COVID-19 outbreak associated with air conditioning in restaurant, Guangzhou, China, 2020. *Emerg Infect Dis* **2020**; 26:1628–1631.
99. Hwang SE, Chang JH, Bumjo O, Heo J. Possible aerosol transmission of COVID-19 associated with an outbreak in an apartment in Seoul, South Korea, 2020. *Int J Infect Dis* **2020**; Available at: <http://dx.doi.org/10.1016/j.ijid.2020.12.035>.

100. Nissen K, Krambrich J, Akaberi D, et al. Long-distance airborne dispersal of SARS-CoV-2 in COVID-19 wards. Research Square. 2020; Available at: <http://dx.doi.org/10.21203/rs.3.rs-34643/v1>.
101. CDC. Scientific Brief: SARS-CoV-2 Transmission. 2021. Available at: <https://www.cdc.gov/coronavirus/2019-ncov/science/science-briefs/sars-cov-2-transmission.html>. Accessed 20 June 2021.
102. Morawska L, Milton DK. It is time to address airborne transmission of Coronavirus disease 2019 (COVID-19). *Clin Infect Dis* **2020**; 71:2311–2313.
103. Hadei M, Hopke PK, Jonidi A, Shahsavani A. A letter about the airborne transmission of SARS-CoV-2 based on the current evidence. *Aerosol Air Qual Res* **2020**; 20:911–914.
104. Riley EC, Murphy G, Riley RL. Airborne spread of measles in a suburban elementary school. *Am J Epidemiol* **1978**; 107:421–432.
105. Leung NHL, Chu DKW, Shiu EYC, et al. Author Correction: Respiratory virus shedding in exhaled breath and efficacy of face masks. *Nat Med* **2020**; 26:981.
106. Drewnick F, Pikmann J, Fachinger F, Moormann L, Sprang F, Borrmann S. Aerosol filtration efficiency of household materials for homemade face masks: Influence of material properties, particle size, particle electrical charge, face velocity, and leaks. *Aerosol Sci Technol* **2021**; 55:63–79.
107. Li L, Niu M, Zhu Y. Assessing the effectiveness of using various face coverings to mitigate the transport of airborne particles produced by coughing indoors. *Aerosol Sci Technol* **2020**; :1–12.
108. Gandhi M, Marr LC. Uniting infectious disease and physical science principles on the importance of face masks for COVID-19. *Med* **2020**; Available at: <http://dx.doi.org/10.1016/j.medj.2020.12.008>.
109. Milton DK, Fabian MP, Cowling BJ, Grantham ML, McDevitt JJ. Influenza virus aerosols in human exhaled breath: particle size, culturability, and effect of surgical masks. *PLoS Pathog* **2013**; 9:e1003205.
110. Murray DM, Burmaster DE. Residential air exchange rates in the United States: Empirical and estimated parametric distributions by season and climatic region. *Risk Anal* **1995**; 15:459–465.
111. Persily AK, Gorfain J, Brunner G. Survey of ventilation rates in office buildings. *Build Res Inf* **2006**; 34:459–466.

112. K. Lai AC, Nazaroff WW. Modeling indoor particle deposition from turbulent flow onto smooth surfaces. *J Aerosol Sci* **2000**; 31:463–476.
113. Hussein T, Kulmala M. Indoor aerosol modeling: Basic principles and practical applications. *Water Air Soil Pollut Focus* **2008**; 8:23–34.
114. Waring MS, Siegel JA, Corsi RL. Ultrafine particle removal and generation by portable air cleaners. *Atmos Environ (1994)* **2008**; 42:5003–5014.
115. Hinds WC. *Aerosol technology: Properties, behavior, and measurement of airborne particles*. Wiley-Interscience, 2012.
116. Epa US, ORD. *Exposure Factors Handbook chapter 6*. **2015**; Available at: <https://www.epa.gov/expobox/exposure-factors-handbook-chapter-6>. Accessed 2 January 2021.
117. Guha S, Hariharan P, Myers MR. Enhancement of ICRP’s lung deposition model for pathogenic bioaerosols. *Aerosol Sci Technol* **2014**; 48:1226–1235.
118. Sturm R. Bioaerosols in the lungs of subjects with different ages-part 1: deposition modeling. *Ann Transl Med* **2016**; 4:211.
119. Asadi S, Wexler AS, Cappa CD, Barreda S, Bouvier NM, Ristenpart WD. Aerosol emission and superemission during human speech increase with voice loudness. *Sci Rep* **2019**; 9:2348.
120. Lindsley WG, Pearce TA, Hudnall JB, et al. Quantity and size distribution of cough-generated aerosol particles produced by influenza patients during and after illness. *J Occup Environ Hyg* **2012**; 9:443–449.
121. Moses FW, Gonzalez-Rothi R, Schmidt G. COVID-19 outbreak associated with air conditioning in restaurant, Guangzhou, China, 2020. *Emerg. Infect. Dis.* 2020; 26:2298–2298.
122. ICRP. Human respiratory tract model for radiological protection. A report of a Task Group of the International Commission on Radiological Protection. *Ann ICRP* **1994**; 24:1–482.
123. Watanabe T, Bartrand TA, Weir MH, Omura T, Haas CN. Development of a dose-response model for SARS coronavirus. *Risk Anal* **2010**; 30:1129–1138.
124. Miliotis M, Dennis S, Buchanan R, Potter M. Role of epidemiology in microbial risk assessment. *Food Addit Contam Part A Chem Anal Control Expo Risk Assess* **2008**; 25:1052–1057.

125. Haas CN. Action levels for SARS-CoV-2 in air: Preliminary approach. *Risk Anal* **2021**; 41:705–709.
126. Alford RH, Kasel JA, Gerone PJ, Knight V. Human influenza resulting from aerosol inhalation. *Proc Soc Exp Biol Med* **1966**; 122:800–804.
127. Rim D, Siegel J, Spinhirne J, Webb A, McDonald-Buller E. Characteristics of cabin air quality in school buses in Central Texas. *Atmos Environ (1994)* **2008**; 42:6453–6464.
128. Miller SL, Nazaroff WW, Jimenez JL, et al. Transmission of SARS-CoV-2 by inhalation of respiratory aerosol in the Skagit Valley Chorale superspreading event. *Indoor Air* **2020**; :0–2.
129. Cevik M, Tate M, Lloyd O, Maraolo AE, Schafers J, Ho A. SARS-CoV-2, SARS-CoV, and MERS-CoV viral load dynamics, duration of viral shedding, and infectiousness: a systematic review and meta-analysis. *Lancet Microbe* **2021**; 2:e13–e22.
130. Gendreau M. Book review: Tuberculosis and air travel: Guidelines for prevention and control, 3rd edition by the world health organization. Published by WHO press, 2008. Paperback 43pp. Price \$10.00. ISBN 978 92 4 154750 5. *Perspect Public Health* **2010**; 130:191–191.
131. Coronavirus disease (COVID-19) – World Health Organization. Available at: https://www.who.int/emergencies/diseases/novel-coronavirus-2019?adgroupsurvey={adgroupsurvey}&gclid=CjwKCAjw7--KBhAMEiwAxfpkWI8fJtpz2fXY5q0AxUIIXLGFRSC9pYblemoXwCtoieyEPtBtOWcRmBoCKmsQAvD_BwE. Accessed 5 October 2021.
132. Anderson EL, Turnham P, Griffin JR, Clarke CC. Consideration of the aerosol transmission for COVID-19 and public health. *Risk Anal* **2020**; 40:902–907.
133. Ma J, Qi X, Chen H, et al. Coronavirus disease 2019 patients in earlier stages exhaled millions of severe acute respiratory syndrome Coronavirus 2 per hour. *Clin Infect Dis* **2021**; 72:e652–e654.
134. Zhou L, Yao M, Zhang X, et al. Breath-, air- and surface-borne SARS-CoV-2 in hospitals. *J Aerosol Sci* **2021**; 152:105693.
135. Santarpia JL, Herrera VL, Rivera DN, et al. The size and culturability of patient-generated SARS-CoV-2 aerosol. *J Expo Sci Environ Epidemiol* **2021**; :1–6.
136. Tang JW, Bahnfleth WP, Bluysen PM, et al. Dismantling myths on the airborne transmission of severe acute respiratory syndrome coronavirus-2 (SARS-CoV-2). *J Hosp Infect* **2021**; 110:89–96.

137. Hoffmann M, Kleine-Weber H, Schroeder S, et al. SARS-CoV-2 cell entry depends on ACE2 and TMPRSS2 and is blocked by a clinically proven protease inhibitor. *Cell* **2020**; 181:271-280.e8.
138. Prather KA, Marr LC, Schooley RT, McDiarmid MA, Wilson ME, Milton DK. Airborne transmission of SARS-CoV-2. *Science* **2020**; 370:303–304.
139. Flaxman S, Mishra S, Gandy A, et al. Estimating the effects of non-pharmaceutical interventions on COVID-19 in Europe. *Nature* **2020**; 584:257–261.
140. Azimi P, Keshavarz Z, Cedeno Laurent JG, Stephens B, Allen JG. Mechanistic transmission modeling of COVID-19 on the Diamond Princess cruise ship demonstrates the importance of aerosol transmission. *Proc Natl Acad Sci U S A* **2021**; 118:e2015482118.
141. Pei S, Kandula S, Shaman J. Differential effects of intervention timing on COVID-19 spread in the United States. *Sci Adv* **2020**; 6:eabd6370.
142. Mathai V, Das A, Bailey JA, Breuer K. Airflows inside passenger cars and implications for airborne disease transmission. *Sci Adv* **2021**; 7:eabe0166.
143. Qian H. Indoor transmission of SARS-CoV-2. *Indoor Air* **2020**; :12766.
144. Zhang R, Li Y, Zhang AL, Wang Y, Molina MJ. Identifying airborne transmission as the dominant route for the spread of COVID-19. *Proc Natl Acad Sci U S A* **2020**; 117:14857–14863.
145. Bazant MZ, Bush JWM. A guideline to limit indoor airborne transmission of COVID-19. *Proc Natl Acad Sci U S A* **2021**; 118. Available at: <https://www.pnas.org/content/118/17/e2018995118>. Accessed 20 October 2021.
146. Edwards DA, Ausiello D, Salzman J, et al. Exhaled aerosol increases with COVID-19 infection, age, and obesity. *Proc Natl Acad Sci U S A* **2021**; 118:e2021830118.
147. Kim SW, Ramakrishnan MA, Raynor PC, Goyal SM. Effects of humidity and other factors on the generation and sampling of a coronavirus aerosol. *Aerobiologia (Bologna)* **2007**; 23:239–248.
148. Li Y, Leung GM, Tang JW, et al. Role of ventilation in airborne transmission of infectious agents in the built environment - a multidisciplinary systematic review. *Indoor Air* **2007**; 17:2–18.

149. de Man P, Paltansing S, Ong DSY, Vaessen N, van Nielen G, Koeleman JGM. Outbreak of Coronavirus disease 2019 (COVID-19) in a nursing home associated with aerosol transmission as a result of inadequate ventilation. *Clin. Infect. Dis.* **2021**; 73:170–171.
150. Available at: <https://www.cdc.gov/niosh/npptl/stps/pdfs/RCT-APR-0067-508.pdf>. Accessed 11 September 2021.
151. Fairbanks G. Voice and Articulation Drillbook. *Laryngoscope* **1941**; 51:1141.
152. Jia Y. Real-Time PCR. In: Conn PM, ed. *Methods in Cell Biology*. San Diego, CA: Elsevier, 2012: 55–68.
153. Allen JG, Ibrahim AM. Indoor air changes and potential implications for SARS-CoV-2 transmission. *JAMA* **2021**; 325:2112–2113.
154. Dietz L, Horve PF, Coil DA, Fretz M, Eisen JA, Van Den Wymelenberg K. Correction for Dietz et al., “2019 Novel Coronavirus (COVID-19) Pandemic: Built Environment Considerations To Reduce Transmission.” *mSystems* **2020**; 5. Available at: <http://dx.doi.org/10.1128/mSystems.00375-20>.
155. Klompas M, Baker MA, Rhee C. Airborne transmission of SARS-CoV-2: Theoretical considerations and available evidence. *JAMA* **2020**; 324:441–442.
156. Hänel G. Humidity effects on gravitational settling and Brownian diffusion of atmospheric aerosol particles. *Pure Appl Geophys* **1977**; 115:775–797.
157. Rocha ALS, Pinheiro JR, Nakamura TC, et al. Fomites and the environment did not have an important role in COVID-19 transmission in a Brazilian mid-sized city. *Sci Rep* **2021**; 11:15960.
158. Adenaiye OO, Lai J, de Mesquita PJB, et al. Infectious SARS-CoV-2 in exhaled aerosols and efficacy of masks during early mild infection. *Clin Infect Dis* **2021**; Available at: <https://academic.oup.com/cid/advance-article/doi/10.1093/cid/ciab797/6370149>. Accessed 24 November 2021.
159. Parhizkar H, Dietz L, Olsen-Martinez A, et al. Quantifying environmental mitigation of aerosol viral load in a controlled chamber with participants diagnosed with COVID-19. *Clin Infect Dis* **2022**; Available at: <https://academic.oup.com/cid/advance-article/doi/10.1093/cid/ciac006/6498295>. Accessed 17 January 2022.
160. Li Y, Cheng P, Jia W. Poor ventilation worsens short-range airborne transmission of respiratory infection. *Indoor Air* **2021**; Available at: <http://dx.doi.org/10.1111/ina.12946>.

161. Nazaroff WW, Gadgil AJ, Weschler CJ. Modeling of Indoor Air Quality and Exposure. ASTM International, 1993.
162. National Research Council (US) Committee on Indoor Pollutants. Monitoring and modeling of indoor air pollution. Washington, D.C., DC: National Academies Press, 1981.
163. Mahyuddin N, Awbi H. The spatial distribution of carbon dioxide in an environmental test chamber. *Build Environ* **2010**; 45:1993–2001.
164. Bhagat RK, Davies Wykes MS, Dalziel SB, Linden PF. Effects of ventilation on the indoor spread of COVID-19. *J Fluid Mech* **2020**; 903:F1.
165. Shen G, Ainiwaer S, Zhu Y, et al. Quantifying source contributions for indoor CO₂ and gas pollutants based on the highly resolved sensor data. *Environ Pollut* **2020**; 267:115493.
166. Qiu Y, Tao S, Yun X, et al. Indoor PM_{2.5} profiling with a novel side-scatter indoor lidar. *Environ Sci Technol Lett* **2019**; 6:612–616.
167. Sagona JA, Shalat SL, Wang Z, et al. Evaluation of particle resuspension in young children's breathing zone using stationary and robotic (PIPER) aerosol samplers. *J Aerosol Sci* **2015**; 85:30–41.
168. Micallef A, Caldwell J, Colls JJ. The influence of human activity on the vertical distribution of airborne particle concentration in confined environments: Preliminary results. *Indoor Air* **1998**; 8:131–136.
169. Lakey PSJ, Won Y, Shaw D, et al. Spatial and temporal scales of variability for indoor air constituents. *Commun Chem* **2021**; 4:1–7.
170. Gall ET, Laguerre A, Noelck M, Van Meurs A, Austin JP, Foster BA. Near-field airborne particle concentrations in young children undergoing high-flow nasal cannula therapy: a pilot study. *J Hosp Infect* **2021**; 113:14–21.
171. Haahr A-M, Bardow A, Thomsen CE, et al. Release of peppermint flavour compounds from chewing gum: effect of oral functions. *Physiol Behav* **2004**; 82:531–540.
172. Ampollini L, Katz EF, Bourne S, et al. Observations and contributions of real-time indoor ammonia concentrations during HOMEChem. *Environ Sci Technol* **2019**; 53:8591–8598.

173. Lindinger W, Hansel A, Jordan A. On-line monitoring of volatile organic compounds at pptv levels by means of proton-transfer-reaction mass spectrometry (PTR-MS) medical applications, food control and environmental research. *Int J Mass Spectrom Ion Process* **1998**; 173:191–241.
174. de Gouw JA, Goldan PD, Warneke C, et al. Validation of proton transfer reaction-mass spectrometry (PTR-MS) measurements of gas-phase organic compounds in the atmosphere during the New England Air Quality Study (NEAQS) in 2002. *J Geophys Res* **2003**; 108. Available at: <http://dx.doi.org/10.1029/2003jd003863>.
175. Jordan C, Fitz E, Hagan T, et al. Long-term study of VOCs measured with PTR-MS at a rural site in New Hampshire with urban influences. *Atmos Chem Phys* **2009**; 9:4677–4697.
176. Guideline 2-2005 ; Engineering Analysis of experimental data. Available at: https://www.techstreet.com/ashrae/standards/guideline-2-2005-engineering-analysis-of-experimental-data?gateway_code=ashrae&product_id=1644049. Accessed 24 November 2021.
177. Carlo M. Package “propagate.” 2018. Available at: <https://cran.r-project.org/web/packages/propagate/propagate.pdf>. Accessed 18 January 2022.
178. Lachenbruch PA, Cohen J. *Statistical Power Analysis for the Behavioral Sciences* (2nd ed.). *J Am Stat Assoc* **1989**; 84:1096.
179. CohensD function - RDocumentation. Available at: <https://www.rdocumentation.org/packages/lsr/versions/0.5.2/topics/cohensD>. Accessed 18 January 2022.
180. Dunne E, Galbally IE, Cheng M, Selleck P, Molloy SB, Lawson SJ. Comparison of VOC measurements made by PTR-MS, adsorbent tubes–GC-FID-MS and DNPH derivatization–HPLC during the Sydney Particle Study, 2012: a contribution to the assessment of uncertainty in routine atmospheric VOC measurements. *Atmos Meas Tech* **2018**; 11:141–159.
181. Cohen J. Statistical power analysis. *Curr Dir Psychol Sci* **1992**; 1:98–101.
182. Aflaki A, Mahyuddin N, Al-Cheikh Mahmoud Z, Baharum MR. A review on natural ventilation applications through building façade components and ventilation openings in tropical climates. *Energy Build* **2015**; 101:153–162.
183. Barbosa S, Ip K, Southall R. Thermal comfort in naturally ventilated buildings with double skin façade under tropical climate conditions: The influence of key design parameters. *Energy Build* **2015**; 109:397–406.

184. de Gracia A, Navarro L, Castell A, Cabeza LF. Energy performance of a ventilated double skin facade with PCM under different climates. *Energy Build* **2015**; 91:37–42.
185. Parhizkar H, Khoraskani RA, Tahbaz M. Double skin façade with Azolla; ventilation, Indoor Air Quality and Thermal Performance Assessment. *J Clean Prod* **2020**; 249:119313.
186. Aviv D, Chen KW, Teitelbaum E, et al. A fresh (air) look at ventilation for COVID-19: Estimating the global energy savings potential of coupling natural ventilation with novel radiant cooling strategies. *Appl Energy* **2021**; 292:116848.
187. Ladybug Tools. Available at: <https://www.ladybug.tools/>. Accessed 14 February 2022.
188. Morris DH, Yinda KC, Gamble A, et al. Mechanistic theory predicts the effects of temperature and humidity on inactivation of SARS-CoV-2 and other enveloped viruses. *Elife* **2021**; 10. Available at: <http://dx.doi.org/10.7554/eLife.65902>.
189. Health risk in winter: modern buildings often leads to a desert-like environment in living spaces. Available at: <https://www.condairgroup.com/news/health-risk-in-winter-modern-buildings-often-leads-to-a-desert-like-environment-in-living-spaces>. Accessed 14 February 2022.
190. Mousavi E, Bhattacharya A. Event based approach for modeling indoor airflow patterns. *J Build Eng* **2022**; 51:104244.
191. Shih Y-C, Chiu C-C, Wang O. Dynamic airflow simulation within an isolation room. *Build Environ* **2007**; 42:3194–3209.
192. Killingley B, Mann A, Kalinova M, et al. Safety, tolerability and viral kinetics during SARS-CoV-2 human challenge. *Research Square*. 2022; Available at: <http://dx.doi.org/10.21203/rs.3.rs-1121993/v1>.
193. Tellier R. Aerosol transmission of influenza A virus: a review of new studies. *J R Soc Interface* **2009**; 6 Suppl 6:S783-90.
194. Gralton J, Tovey E, McLaws M-L, Rawlinson WD. The role of particle size in aerosolised pathogen transmission: a review. *J Infect* **2011**; 62:1–13.
195. Tang JW. Investigating the airborne transmission pathway - different approaches with the same objectives. *Indoor Air* **2015**; 25:119–124.
196. Yang L, Wang X, Li M, et al. Carbon dioxide generation rates of different age and gender under various activity levels. *Build Environ* **2020**; 186:107317.

197. Blocken B, van Druenen T, Ricci A, et al. Ventilation and air cleaning to limit aerosol particle concentrations in a gym during the COVID-19 pandemic. *Build Environ* **2021**; 193:107659.
198. Available at: <https://www.fda.gov/media/136112/download>. Accessed 24 September 2021.
199. Coleman KK, Wen Tay DJ, Tan KS, et al. Viral load of SARS-CoV-2 in respiratory aerosols emitted by COVID-19 patients while breathing, talking, and singing. *bioRxiv*. 2021; :2021.07.15.21260561. Available at: <https://www.medrxiv.org/content/10.1101/2021.07.15.21260561v1>. Accessed 28 July 2021.